Title
Cardiac Magnetic Resonance Imaging-Guided Therapies for Chronic Hemorrhagic Myocardial Infarction

Author
Johnson, Eric

Publication Date
2021

Peer reviewed|Thesis/dissertation

UNIVERSITY OF CALIFORNIA

Los Angeles

Cardiac Magnetic Resonance Imaging-Guided Therapies for Chronic Hemorrhagic Myocardial Infarction

A dissertation submitted in partial satisfaction of the

requirements for the degree Doctor of Philosophy

in Bioengineering

by

Eric Andrew Johnson

2021

ABSTRACT OF THE DISSERTATION

Cardiac Magnetic Resonance Imaging-Guided Therapies for Chronic Hemorrhagic Myocardial Infarction

by

Eric Andrew Johnson

Doctor of Philosophy in Bioengineering

University of California, Los Angeles, 2021

Professor Rohan Dharmakumar, Co-Chair

Professor Holden H Wu, Co-Chair

This dissertation aims to evaluate therapies that have the potential to improve the recovery of the left ventricle (LV) following myocardial infarction (MI) burdened with intramyocardial hemorrhage (IMH). Prior studies have shown that hemorrhagic MI results in the deposition of chronic iron in the myocardium, which induces cytotoxic effects as well as impacts the normal function of the microvasculature. In order to characterize the content of intramyocardial iron, T2* magnetic resonance imaging (MRI) was used as the gold standard in non-invasive detection of cardiac iron, and therefore acts as a diagnostic guidance tool informing the efficacy of the therapies. The dissertation may be broken down into three phases, all performed with MRI guidance to elucidate: 1) mechanistic understanding of the microvascular environment in chronic

MI subjects; 2) effects of iron chelation therapy via Deferiprone (DFP) administration; and 3) effects of therapeutic hypothermia (TH) induced post reperfusion.

The first phase investigated the long-term changes in myocardial perfusion assessed via MRI, in patients with reperfused myocardial infarction and an animal model of ischemia reperfusion (I/R) injury. From animal studies, histology, immunohistochemistry (IHC), and western blotting analysis were performed to elucidate the mechanistic underpinnings of MRI observations. The outcomes of this study led to the discovery that hemorrhagic MI results in reduced myocardial perfusion within hemorrhagic, but not non-hemorrhagic, MI territories. Further, the protein expression investigations enabled the proposal of a mechanistic pathway to examine the role chronic iron deposition plays in the perfusion defects observed in hemorrhagic MI.

The subsequent study in a canine model of hemorrhagic MI to remove iron from within chronic infarction regions using the small-molecule iron chelator deferiprone (DFP), is the first to show the potential to abrogate resting perfusion defects observed in the hemorrhagic MI setting. Furthermore, the study showed that the recovery of rest perfusion did not persist following termination of the DFP therapy, indicating the potential need for continuous, or extended, iron chelation in this population to maintain persistent benefits. Lastly, the study showed the potential beneficial impact of DFP therapy on LV remodeling by resulting in reduced end-diastolic mass, suggesting a possible role of iron in LV hypertrophy and diastolic dysfunction.

Finally, a study of post-reperfusion localized therapeutic hypothermia was conducted in a pig model to evaluate the potential impact of hypothermia therapy on IMH and chronic iron deposition. This is the first study to show the capability of therapeutic hypothermia to reduce chronic iron deposition in hemorrhagic MI. The results of this study showed that post-reperfusion

hypothermia did not impact acute infarct size and did not affect hemorrhage in the acute phase (day 3 post-MI). However, by 1 month hypothermia-treated animals showed significantly reduced T2*-derived iron deposition volume, which held when normalized by infarct size. By 2 months post-MI, absolute T2* values were also indicative of decreased myocardial iron content, with significantly increased T2* values (lower iron content) in hypothermia-treated animals. Furthermore, LV ejection fraction (LVEF) was significantly elevated at 2 months in the hypothermia group, suggesting a positive effect of therapeutic hypothermia on chronic LV function.

In summary, this dissertation used animal models of hemorrhagic MI to investigate two promising therapeutic methods for alleviating the adverse remodeling in hemorrhagic MI subjects, showing promising results that will aid the future development of adjunctive clinical therapies for advancing treatment in MI and ischemia reperfusion injury.

The dissertation of Eric Andrew Johnson is approved.

Kim-Lien Nguyen

Michael Albert Thomas

Behzad Sharif

Holden H Wu, Committee Co-Chair

Rohan Dharmakumar, Committee Co-Chair

University of California, Los Angeles

2021

To my parents and brother, my wife and daughter …

for your support, love, and encouragement

Table of Contents

List of Figures

List of Tables

List of Symbols and Acronyms

AAR	Area-at-Risk
AIF	Arterial Input Function
ANOVA	Analysis of Variance
ASL	Arterial Spin Labeling
ATP	Adenosine Triphosphate
AU	Arbitrary Units
BCA	Bicinchoninic Acid
BID	Bis In Die (twice daily)
BSA	Bovine Serum Albumin
CAD	Coronary Artery Disease
CD31	Cluster Of Differentiation 31 (also known as PECAM-1)
CHF	Congestive Heart Failure
CMR	Cardiac Magnetic Resonance
CO	Carbon Monoxide
CO_2	Carbon Dioxide
CT	Computed Tomography

CTA	Computed Tomography Angiography
CTP	Computed Tomography Perfusion
CVD	Cardiovascular Disease
DCE	Dynamic Contrast Enhanced
DFO	Deferoxamine
DFP	Deferiprone
DFX	Deferasirox
DL	Deep Learning
DNA	Deoxyribonucleic acid
ECG	Electrocardiogram
ECL	Enhanced Chemiluminescence
ECM	Extracellular matrix
EF	Ejection Fraction
eNOS	Endothelial Nitric Oxide Synthase
FDA	Food and Drug Administration
Fe	Iron
FFR	Fractional Flow Reserve
FPP	First-pass Perfusion

GAPDH	Glyceraldehyde-3-phosphate dehydrogenase, a western blot normalization enzyme
GBCA	Gadolinium-Based Contrast Agents
Gd	Gadolinium
GRE	Gradient-Recalled Echo
HCP-1	Heme Carrier Protein 1
HF	Heart Failure
HIF-1α	Hypoxia-Inducible Factor 1-alpha
hMI-	Non-hemorrhagic Myocardial Infarction
hMI+	Hemorrhagic Myocardial Infarction
HO-1	Heme Oxygenase 1
I/R injury	Ischemia Reperfusion Injury
IACUC	Institutional Animal Use and Care Committee
ICD	Implantable Cardioverter Defibrillator
IHC	Immunohistochemistry
IMH	Intramyocardial Hemorrhage
iNOS	Inducible Nitric Oxide Synthase
IQR	Interquartile Range

IV	Intravenous
LGE	Late Gadolinium Enhancement
L-NMMA	A nitric oxide synthase inhibitor enzyme
LV	Left Ventricle
LVEDV	Left Ventricular End-Diastolic Volume
LVEF	Left Ventricular Ejection Fraction
LVESV	Left Ventricular End-Systolic Volume
MACE	Major Adverse Cardiovascular Events
MaR	Myocardium-at-Risk
MBF	Myocardial Blood Flow
MCE	Myocardial Contrast Echocardiography
MI	Myocardial Infarction
MPI	Myocardial Perfusion Index
MRI	Magnetic Resonance Imaging
MVO	Microvascular Obstruction
NIH	National Institute of Health
NO	Nitric Oxide
NOS	Nitric Oxide Synthase

OHCA	Out-of-Hospital Cardiac Arrest
PB	Prussian Blue
PCI	Percutaneous Coronary Intervention
PECAM-1	Platelet Endothelial Cell Adhesion Molecule-1 (also known as CD31)
PET	Positron Emission Tomography
PO	Oral administration
PSIR	Phase Sensitive Inversion Recovery
PVC	Premature Ventricular Contraction
RBC	Red Blood Cell
RF	Radiofrequency
RIPA	Radio-Immunoprecipitation Assay
ROI	Region-of-Interest
ROS	Reactive Oxygen Species
R-R Interval	Interval between heart beats (identified by R-wave) on ECG waveform
SCD	Sudden Cardiac Death
SD	Standard Deviation
SDS-PAGE	Sodium Dodecyl Sulphate–Polyacrylamide Gel Electrophoresis
SEM	Standard Error of the Mean

SI	Signal Intensity
SNR	Signal-to-Noise ratio
SPECT	Single-Photon Emission Computed Tomography
SPGR	Spoiled Gradient-Recalled Echo
SR	Saturation Recovery
SSO_2	Super-Saturated Oxygen
STEMI	ST-Elevated Myocardial Infarction
T1	T1 relaxation time
T2	T2 relaxation time
T2*	T2* relaxation time
TE	Echo Time
TH	Therapeutic Hypothermia
TI	Inversion Time
TIMI	Thrombolysis In Myocardial Infarction
TR	Repetition Time
VEGF	Vascular Endothelial Growth Factor

Acknowledgements

I would like to thank my advisor, Dr. Rohan Dharmakumar, for his guidance, expertise, and resources to complete my PhD at UCLA. His individual attention has been a great benefit during my graduate research, and I will continue to use the lessons learned throughout my career. I also deeply thank Anand Nair for his mentorship, collaboration, and support of my research projects. My graduate colleagues, Xingmin and Xinheng, I thank for their friendship, generous help, and brainstorming sessions. I would also like to thank the surgeons at the Heart Institute, Adrian Glenn and Edgardo Paredes, for the countless hours troubleshooting and perfecting our animal models. This work would not have been possible without the contributions of our many collaborators at Cedars Sinai, Northern Ontario School of Medicine, University of Calgary, and Lawson Health Research Institute. Particularly, Drs. Andreas Kumar, Andrew Howarth, and Stefanie Marek-Iannucci, provided invaluable insight into the experimental design, animal model subtleties, and physiology of hemorrhagic MI that significantly improved the quality of the research. I would also like to thank Yi Zhang from the Biobank at Cedars Sinai for her assistance with histological and immunohistochemical experiments, and Dhirendra Singh at Louisiana State University for his assistance with western blotting studies.

I would not be here if not for the nurturing support and encouragement of my parents, who always believed in me and pushed me to be better. My wife, Hannah, has always provided necessary encouragement when things were not going well, and shared in my victories during the good times – her ambition, dedication, love, and support have been an inspiration.

Vita

2018	Master of Science, Bioengineering, University of California, Los Angeles, Los Angeles, CA
2012-2015	Biomedical Engineer, Farus LLC, Vista, CA
2011	Bachelor of Science, Bioengineering, University of California, Berkeley, Berkeley, CA

PUBLICATIONS AND PRESENTATIONS

Johnson, E. A., Nair A. R., Singh, D. P., Yang, H. J., Zhang, Y., Sharif, B., Kumar, A., Francis, J., Dharmakumar, R. (2021). Rest Perfusion Defects in Chronic Hemorrhagic Myocardial Infarction: From Observations in Patients to Mechanistic Insights in Canines. *In Preparation.*

Johnson E. A., Nair A. R., Tang, R., Iannucci, S. M., Wang, G., Sharif, B., Gottlieb, R., Kumar, A., Dharmakumar, R. (2021). Cardioprotective Effects of Mild Therapeutic Hypothermia in Hemorrhagic Myocardial Infarctions: Findings in a Swine Model of Chronic Reperfused Myocardial Infarction. *In Preparation.*

Spivak NM, Korb AS, Reyes SD, Bych BP, Schafer SF, Khanlou N, **Johnson EA**, Schafer ME, Cohen MS, Kuhn T, & Bystritsky A. (2021). Histological Examination of Transcranial Focused Ultrasound Effects on Human Brain Tissue. *Brain Stimulation,* 14(6):1486-8. DOI: 10.1016/j.brs.2021.09.015.

Johnson EA, Nair A, Cokic I, Yang HJ, Kumar A, Dharmakumar R. (2020) Chronic Myocardial Infarcts with Iron Deposits Exhibit Lower Rest Perfusion and Elevated Nitric Oxide Synthase Activity. *Proceedings of the International Society for Magnetic Resonance in Medicine.* Oral abstract presented. (ISMRM 29th Annual Meeting, Virtual).

Nair, A. R., **Johnson, E. A.**, Yang, H. J., Cokic, I., Francis, J., & Dharmakumar, R. (2020). Reperfused hemorrhagic myocardial infarction in rats. *Plos one*, *15*(12), e0243207.

Johnson EA, Nair A, Cokic I, Yang HJ, Kumar A, Dharmakumar R. (2020) Impaired Rest Perfusion in Iron-Laden Myocardial Infarct Regions with Histological Insights. *Proceedings of the Society for Cardiovascular Magnetic Resonance.* Oral abstract presented. (SCMR 9th Annual Meeting, Orlando, FL).

Johnson EA, Wang G, Tang R, Sharif B, Cokic I, Kumar A, Dharmakumar R. (2019) Cardioprotective Effects of Mild Therapeutic Hypothermia in Hemorrhagic Myocardial Infarctions: Early Findings in a Swine Model of Acute Reperfused Myocardial Infarction. *Proceedings of the International Society for Magnetic Resonance in Medicine.* Abstract presented. (ISMRM 28th Annual Meeting, Montreal, QC, Canada).

Johnson EA, Yang HJ, Cokic I, Sykes J, Prato FS, Kumar A, Dharmakumar R. (2019) Iron-Rich Chronic Myocardial Infarct Territories are Associated with Reduced Resting Perfusion: Early Findings in Patients with Multi-Modal Validation in a Canine Model of Reperfused Infarction. *Proceedings of the Society for Cardiovascular Magnetic Resonance.* Abstract presented. (SCMR 8th Annual Meeting, Seattle, WA).

Johnson EA, Wang G, Tang LQ, Marek Iannucci S, Sharif B, Cokic I, Gottlieb R, Dharmakumar R. (2019) Therapeutic Hypothermia for Hemorrhagic Myocardial Infarction: Early Findings in a Swine Model. *Proceedings of the Society for Cardiovascular Magnetic Resonance.* Oral presentation, nominee for Early Career Award in Translational Science. (SCMR 8th Annual Meeting, Seattle, WA).

Johnson EA, Kumar A, Dharmakumar R. (2018) Rest Perfusion within Chronic Infarctions Depends on Type of Acute Myocardial Infarction: Insights from a Serial MRI Study in Patients. *Proceedings of the International Society for Magnetic Resonance in Medicine.* Abstract presented. (ISMRM 27th Annual Meeting, Paris, France).

Johnson EA, Kumar A, Dharmakumar R. (2018) Rest Perfusion Characteristics in Patients with Chronic Hemorrhagic Myocardial Infarctions: Early Findings. *Proceedings of the Society for Cardiovascular Magnetic Resonance.* Abstract presented. (SCMR 7th Annual Meeting, Barcelona, Spain).

B. Medema, **E. Johnson,** M. Culjat, R. Singh, M. Choi, S. White. (2014) Ultrasound Imagery for Endodontic Diagnosis and Treatment Planning in a Porcine Model. *Journal of Endodontics, Vol. 40, No. 3.* [Abstract] Presented at American Association of Endodontists Annual Session.

Chapter 1: Introduction

1.1 Background: From Development of Coronary Artery Disease to Myocardial Infarction

Atherosclerosis is a chronic condition consisting of fatty deposits building up in the endothelial lining of the arteries. As additional material accumulates in the endothelium, atherosclerotic plaques form from the enlarging lesions. These plaques cause narrowing of the vascular lumen and may limit the blood flow capacity of that artery. When atherosclerotic lesions occur in the coronary arteries the condition is referred to as coronary artery disease (CAD). If the lesion becomes severe enough that blood flow is limited beyond a critical point or occluded completely, heart muscle (myocardium) downstream from the blockage becomes starved of oxygen (ischemia) and nutrients needed to maintain function. Additionally, a thrombus (blood clot) may form at the plaque site, occluding the vessel and potentially rupturing and sending a clot downstream to smaller arteries, potentially occluding a critical coronary artery. In either of these scenarios the blood supply to the myocardium distal to the occlusion is in danger of severe damage or cell death (necrosis). Initially, the starved myocardium switches from oxidative phosphorylation to anaerobic glycolysis, which is a less efficient and oxygen-free method of energy production. As the ischemia progresses the affected myocardium loses its ability to produce ATP and the nutrient starvation leads to ultimate cell death, or necrosis (*1, 2*).

Atherosclerosis, which may ultimately develop atheromatous plaques leading to plaque-induced myocardial infarctions (MI) (*3*), is highly prevalent in many adults and young adults without visible symptoms (*4-6*), and presents an early clinical risk profile for long term outcomes. Jarett et al. investigated the extent and prognostic impact of subclinical atherosclerosis in adults under 50,

finding that while 10-year risk remained low, the lifetime risk was elevated for individuals with greater atherosclerotic burden (*7*). A heart attack, or MI, is the process in which an imbalance in the oxygen supply and demand in the heart muscle (myocardium) causes the cells to die off in an expanding wave of necrosis (*8*). Myocardial infarctions can generally be divided into two categories: Type 1 MI and Type 2 MI. Type 1 MI involves an acute atherothrombotic event in which a ruptured plaque leads to occlusion of the coronary arteries, limiting the flow of blood to distal myocardium and causing myocardial necrosis (*3, 9*). Type 2 MI is less common and involves oxygen deprivation caused by an acute stressor other than a ruptured plaque (*10*). Treatment for Type 1 MI focuses on acute restoration of the occluded blood flow via pharmacological or surgical intervention, whereas Type 2 MI treatment attempts to target the underlying etiology. Since the majority of MIs fall into the Type 1 category and closely parallel animal models of acute ischemia/reperfusion, the rest of this dissertation will focus on Type 1 MI.

1.2 Clinical Diagnosis and Treatment of CAD and MI

Up until the early 1900s, acute coronary artery occlusion and subsequent MI was thought to be a universally fatal event (*11*). Several clinicians at that time challenged the prevailing notion that an acute MI was not survivable, initiating the concept of treating MI patients to improve their recovery (*12*). However, it was not until the 1980s that the largest gains in therapy were made, when fibrinolytics came into use as a mainline pharmacological agent for the early treatment of acute MI, drastically reducing patient mortality (*13-15*). Aided by the animal work of Reimer and Jennings in the 1950s and 1960s, the primary objective of emergency and cardiology units became minimizing the time to reperfusion in order to limit infarct size, and therefore improve

patient outcomes (*2*). According to the American Heart Association 2021 update, approximately 800,000 heart attacks occur in the US each year, with the direct and indirect economic burden of heart disease in the US exceeding $220 billion, due to extensive healthcare costs and the impact of lost productivity (*16*) . The estimated number of people in the US that will be living with heart failure (HF) by 2030 is 8 million *(17)*. The standard of care for patients suffering an acute MI includes a variety of therapies encompassing fibrinolytics, pharmacotherapy, primary percutaneous intervention (PCI), and surgical intervention. Advances in technology and biomedical understanding have greatly increased the effectiveness of treatment and therefore the lifespan and quality of life for these patients (*18, 19*).

1.3 Physiological Characteristics of Myocardial Infarction

Identifying the physiological characteristics in acute and chronic myocardial infarction is highly significant for the development of targeted imaging protocols and subsequent risk stratification for adverse outcomes such as LV remodeling or heart failure (HF). The extent of the necrotic wave and resultant microvascular dysfunction that develop during acute and chronic MI are key indicators of long-term outcomes in MI patients (*20-27*). Below, the key features are discussed in relation to MI physiology: myocardial viability, microvascular obstruction (MVO), intramyocardial hemorrhage (IMH), and myocardial blood flow (MBF).

1.3.1 Myocardial Viability

The primary measure of efficacy for reperfusion therapies has long been the extent of myocardial necrosis, and to some level the degree to which myocardium-at-risk is salvaged. Therefore, segregating irreversibly damaged myocardium from viable tissue is of utmost importance.

Secondarily, identifying ischemic areas that risk progressing to necrosis has emerged as a major biomarker for treatment efficacy. However, studies show that the primary MRI feature utilized to characterize area-at-risk (AAR), T2-weighted imaging, does not accurately depict the AAR (*28, 29*), and may be confounded by the presence of IMH (*30*). Another study by Bulluck et al. found excellent correlation between T1-weighted MRI and T2-weighted MRI for delineating the AAR (*31*). Interestingly, T1 mapping is also a leading method for non-contrast infarct imaging (*32, 33*). It becomes possible then to hypothesize that for studies utilizing AAR as an outcome measure, treatment outcomes may be confounded by using this reference measure.

Myocardial viability is an important prognostic indicator of future adverse events. Myocardial viability assessment has progressed from characterization of CAD patients to disorders of the heart valves and even non-ischemic cardiomyopathies, driving treatment decision-making (*34*). In a retrospective multicenter study of 154 patients with severe ischemic cardiomyopathy, Doukas et al. showed a 47% reduction in composite events in patients with >50% myocardial viability (*20*). The Surgical Treatment for Ischemic Heart Failure (STICH) trial initially failed to show a mortality benefit based on viability in the 5-year follow-up (*35*). However, the 10-year (STICH extended study) follow-up demonstrated improved survival for patients with severe LV dysfunction who underwent revascularization (*36*).

Several methods exist to non-invasively characterize myocardial viability including echocardiography (*37-39*), single photon emission computed tomography (SPECT) (*40-43*), positron emission tomography (PET) (*44-46*), computed tomography (CT) (*47-49*), and cardiac magnetic resonance (CMR) (*50-52*). Among these, CMR using Gadolinium-based contrast agents

(GBCAs) has emerged as the reference standard for viability imaging due to its high resolution, use of non-ionizing radiation, high prognostic value, and lower cost relative to SPECT/PET (*34*).

1.3.2 Microvascular Obstruction

Rapid coronary reperfusion is the primary goal of clinical treatment for patients with acute MI, reducing the extent of the infarcted myocardium and improving outcomes vs. non-reperfused MI. However, the process of re-opening the occluded artery frequently results in additional damage and microvascular dysfunction, which can be classified into microvascular obstruction (MVO) and intramyocardial hemorrhage (IMH). The adverse occurrence of MVO has been termed "no-reflow" due to the continued obstruction of the coronary microvasculature despite restoration of epicardial blood flow (*53*) in the previously occluded artery. There have been several mechanisms suggested to explain the development of MVO in acute post-reperfusion MI, including distal embolization of the occlusive thrombus, vasospasm of the microvessels, platelet and leukocyte plugging, radical oxygen species (ROS) generation, luminal protrusions, and endothelial and myocyte swelling (*1, 53, 54*). The presence of MVO has been shown to be independently prognostic for the development of major adverse events (*55-57*). A pooled analysis by de Waha et al. found both the presence and extent of acute MVO to be associated with all-cause mortality and heart failure (HF) (*56*).

Cardiac MRI is the gold standard for detection and quantification of MVO using the contrast-enhanced technique of late gadolinium enhancement (LGE) (*58, 59*), which is discussed in more detail in section 1.4. MVO is easily visualized as a hypointense core within the hyperintense infarct region of the myocardium.

1.3.3 Intramyocardial Hemorrhage

Severe microvascular injury resulting from the rapid restoration of oxygenated blood flow to ischemic coronaries culminates in the extravasation of RBCs into the interstitial spaces of the myocardium. The escalating deterioration of the endothelial wall and gap junctions in reperfused infarctions lead to constituent leakage, causing pressure build-up and RBC breakdown products (i.e., heme, iron) to collect in the extracellular matrix (ECM). IMH is closely related to the phenomenon known as "no-reflow" or microvascular obstruction (MVO), which has been shown to provide additive prognostic value for the occurrence of adverse events (*53, 55-57, 60, 61*). IMH has been characterized as independently prognostic for future adverse events in MI patients including hospital readmission, MACE and death (*22-24*), to a greater extent than MI size or MVO presence (*62*). However, a study by Beek et al. did not find IMH to have prognostic significance beyond MVO in a 45-patient study using T2-weighted CMR to characterize IMH presence (*21*). The controversy in the discussion of MVO vs. IMH may be caused by the nonuniform characterization of IMH, aided by the potential for T2-wighted MRI to underestimate or obscure IMH in the presence of edema or small hemorrhagic lesions (*63, 64*).

Hemorrhage is a paradoxical consequence of reperfusion therapy, occurring in cases of both surgical and pharmacological reperfusion (*65-68*), and is largely dependent on the length of ischemia. Capone and Most showed in pigs that 15 minutes of LAD occlusion followed by reperfusion did not result in IMH, whereas 60 minutes of occlusion led to extensive IMH (*69*). The same study also demonstrated the relative absence of IMH in non-reperfused control pigs. A separate study in dogs similarly demonstrated gross hemorrhage in reperfused animals, but not in those with permanently clamped coronary arteries (*70*).

1.3.4 Myocardial Blood Flow

1.3.4.1 Physiology

The heart has a dedicated blood vessel circulatory system that supplies the myocardium with oxygenated blood and nutrients for the muscle to function optimally. The heart consumes more oxygen per gram of tissue than any other organ in the human body, and the level of oxygen that is extracted from the delivered blood flow, at ~70-80%, is roughly double that of skeletal muscle outside the heart (*71*). Therefore, in order to maintain normal function, the heart is heavily dependent on adequate blood flow through the coronary circulation. Blood from the left ventricle is driven through the aorta to the rest of the body, while the coronary arteries are supplied via two main coronary arteries that branch from the aorta and supply the entire heart. These main arteries branch into smaller arterioles and capillaries that supply the myocardial tissue with oxygen and nutrients. In a healthy state, the myocardial blood flow is carefully maintained in order to match oxygen supply with metabolic demand. This is achieved through autoregulatory mechanisms that allow the coronary circulation to dynamically respond to changes in myocardial demand by altering coronary resistance vessel dilatation to modify myocardial blood flow (*72*). The complex control over coronary flow involves external tissue pressure, coronary perfusion pressure, sympathetic stimulation, local vasodilators, and myogenic mechanisms, among others (*71*). The primary site of action for coronary autoregulation is the coronary resistance vessels, or the small arterioles that control downstream access to the capillary beds. Constriction or dilation of these vessels alters the vascular resistance, which is inversely proportional to blood flow, allowing critical control over the flow through the coronary circulation. Proper vascular resistance is achieved by a balance of vasoconstrictive and

vasodilatory forces, with nitric oxide (NO) acting as a prominent vasoactive agent, released by the coronary endothelium to promote vasodilatory influence (*72*). Given the highly impactful nature of the myocardial blood flow, diagnostic assessment of the health of this system is of high significance across a variety of disease states.

1.3.4.2 Myocardial Blood Flow in Diseased States

During acute myocardial infarction, the requisite blood flow to a portion of the coronary vasculature is impeded or cutoff entirely. Following the standard of care, the patient receives thrombolytics and potentially additional catheter-based or surgical intervention to remove the offending blockage, which rapidly restores the flow of highly oxygenated blood to the ischemic territories. As discussed, this rapid restoration of oxygen-rich blood has the potential to inflict microvascular injury including MVO and hemorrhage. In the case of MVO, capillaries may continue to exhibit significant perfusion defects due to inflammation and edema (*21, 73, 74*), platelet plugging, or vascular spasm (*1, 23, 75, 76*). This phenomenon is easily observed via LGE MRI images as a hypointense core within the hyperintense zone of infarction (*75*). Hemorrhaging may also occur as the coronary vessels become destroyed or sufficiently damaged to allow the extravasation of RBCs. Initially, IMH was overshadowed by MVO as a potential therapeutic target in the case of I/R injury (*77*). However, recent studied have suggested an expanded role of IMH as a major contributing factor in post-reperfusion microvascular dysfunction. As we will show, the presence of hemorrhage in acute myocardial infarction, among other negative remodeling characteristics (*22, 24, 78*), is associated with perfusion defects visualized with first-pass perfusion MRI, a technique that tracks contrast-enhanced blood as it flows through the LV and into the myocardium.

Impaired coronary blood flow or flow reserve is an important finding in a variety of morbidities with cardiovascular complications. While cigarette smoking is a well-known risk factor for CVD, Czernin et al. identified MBF abnormalities only from acute smoking subjects, while long-term smokers avoided MBF alterations, potentially indicating a pathway for the increased risk of sudden cardiac death by lowering the ischemic threshold (*79*). In the type II diabetes population, CVD is a primary concern given that the main cause of mortality in this group stems from complications thereof (*80-82*). Iltis et al. showed that myocardial blood flow in nonobese type II diabetic rats compared with normal controls was diminished along with decreased ejection fraction, indicating a reduction in LV function which may be a contributing factor driving the CVD complications (*83*). The same group found similar results with a rat model of type I diabetes and hypertension (*84*), while Pop-Busui et al. suggested that impaired MBF in type I diabetics may be related to augmented cardiac sympathetic tone (*85*). Hypothyroidism has been linked to heart failure, and Tang et al. showed in a rat model of hypothyroidism that systolic dysfunction and impaired MBF were associated with the disease (*86*). The inflammatory disease cardiac sarcoidosis is characterized by inflammation of the myocardium and has been shown to be associated with regionally-impaired myocardial flow (*87*). Similarly, the Dharmakumar lab and others have shown previously elevated levels of cardiac inflammation in chronic hemorrhagic infarction (*88, 89*). In chapter 2, regional deficits in resting perfusion will also be shown in patients and animals with IMH and chronic iron deposition.

Studies investigating the diagnostic potential for resting perfusion measurements have indicated a benefit in triaging symptomatic diabetic patients (*90*), as well as serving as a highly prognostic indicator of CAD events (e.g., MI, heart failure, sudden cardiac death) (*91*). Additionally, in 64 ST-

elevated MI (STEMI) patients Borlotti et al. showed acute resting myocardial perfusion has significant predictive value for infarct size and LV remodeling (i.e., wall thickening) at 6 months and correlated with EF (*92*). Morishima et al. investigated the potential for myocardial single-photon emission computed tomography (SPECT) perfusion at rest to predict future arrhythmic events and sudden cardiac death (SCD) in patients with prior MI, showing that rest perfusion was the strongest predictor of fatal events (*93*). Similarly, a study by Nishisato et al. in patients without recent acute ischemic events identified impaired resting myocardial SPECT perfusion to be associated with arrhythmic events preceding SCD, which when combined with assessment of impaired sympathetic innervation may best stratify patients who stand to benefit most from prophylactic implantable cardioverter defibrillator (ICD) use (*94*). Finally, the myocardial perfusion SPECT study by Shaw et al. identified the highly predictive value of perfusion defects for adverse cardiovascular events in outpatients with suspected or known CAD, with results showing a 3% increase in risk of major adverse events for every 1% of the myocardium with resting perfusion defects (*91*). These informative studies exemplify the importance of resting myocardial perfusion as a prognostic indicator of cardiac health and support its usefulness in measuring LV dysfunction in the post-MI setting.

Rest perfusion images can also be acquired along with a stress perfusion scan in order to ascertain the blood flow reserve in the myocardial vessels. The ability for the coronary vasculature to elicit a vasodilatory response that lowers resistance and consequently increases blood flow is an important hyperemic mechanism when oxygen demand increases. Experimentally, this can be achieved via an exercise stress test or with pharmacological vasodilator or inotropic agents (e.g., adenosine, dobutamine). While differences exist between these two mechanisms, exercise-

induced stress may actually produce a decrease in vessel lumen diameter, differentiating from vasodilator or inotropic stress testing and possibly producing enhanced perfusion defects (*72, 95*). The absence of perfusion defects at rest that subsequently appear on stress perfusion images are indicative of inducible perfusion defects. Clinically, these stress-induced perfusion defects, measured as the coronary flow reserve, are a useful parameter to identify a patient's risk of future cardiac events (*96, 97*).

Leading up to an acute MI event, both the rest and exercise-induced perfusion of the myocardium may be compromised due to a significant narrowing of the coronaries. As the blood flow slows and ultimately drops below an ischemic threshold, the supply of oxygen and nutrients no longer meets the high demand of the myocardium. The precursor flow level is predictive of future MI risk and is often measured via invasive fractional flow reserve (FFR) or computed tomography (CT)-based FFR, in addition to other imaging modalities (e.g., MRI, PET) (*98-103*). In the acute post-MI setting following primary PCI, MBF should be restored with the re-opening of the occluded artery. However, microvascular dysfunction evidenced by MVO and IMH frequently interrupts the normal resolution of blood flow, causing defects in the rest perfusion that may persist chronically as the infarct matures and remodels. These alterations in MBF can be identified and measured with a variety of invasive (e.g., infused microspheres) and non-invasive (i.e., imaging-based) modalities. The prognostic importance of these measurements lies in the opportunity to stratify patients into varying categories of risk, as well as enabling the potential for differential treatment based on myocardial perfusion state (*92*), thereby improving outcomes.

1.4 Imaging Myocardial Infarction with Magnetic Resonance Imaging

Imaging the myocardium in the acute phase after a myocardial infarction is critical to determine the extent of irreversibly injured myocardium, and as an evaluation marker to identify the potential efficacy of adjuvant treatments in the early stage of MI (*104-106*). The image quality has greatly improved along with developments in MRI sequences, allowing for enhanced prognostic capabilities. This dissertation will focus on three primary MRI sequences – LGE, T2*-weighted, and first-pass perfusion MRI – used for the detection of myocardial infarction, myocardial hemorrhage, and myocardial blood flow. The following sections will give a brief overview of these MRI sequences.

1.4.1 Late Gadolinium Enhancement MRI

Late gadolinium enhancement (LGE) imaging is a technique utilizing Gadolinium (Gd)-based contrast injection to non-invasively characterize irreversibly damaged myocardium. Free Gd is highly toxic, and therefore requires a chelator to maintain safe use as a clinical contrast agent. Gd is naturally cleared from the body by the kidneys, though patients with impaired kidney function may experience toxicity due to prolonged exposure and are therefore contraindicated for the use of GBCAs. While recent studies have raised concerns over chronic Gd deposition in otherwise healthy subjects, it remains a safe and effective agent in patients with normal kidney function referred for MRI, and no adverse effects have been documented as a result of these findings (*107-111*).

Gadolinium is an extracellular contrast agent that imparts a T1-shortening effect on MRI images. In infarcted myocardium, Gd collects in higher volumes, as well as having impaired wash-out

kinetics, causing the contrast agent to remain in the tissue longer than in healthy regions (*112-114*). The excess accumulation of Gd in regions affected by irreversibly damaged myocardium causes an alteration in the T1 relaxation time of the area. During an imaging protocol including LGE, a contrast bolus of 0.2 mmol/kg Gd is typically injected intravenously (IV), followed by an optimal waiting period of 10-15 minutes. This quiescent waiting period allows optimal contrast to develop between healthy and infarcted myocardial tissues. By utilizing an inversion-recovery sequence, and selecting an optimal inversion time (TI), healthy (remote) non-infarcted myocardium can be nulled to appear dark leaving the infarcted myocardium to appear bright on the LGE image, as shown in Figure 1.1. Typically, a TI scout will be implemented to identify the optimal TI for nulling of the myocardium. This TI is then set and adjusted over time to account for the dynamic contrast agent kinetics.

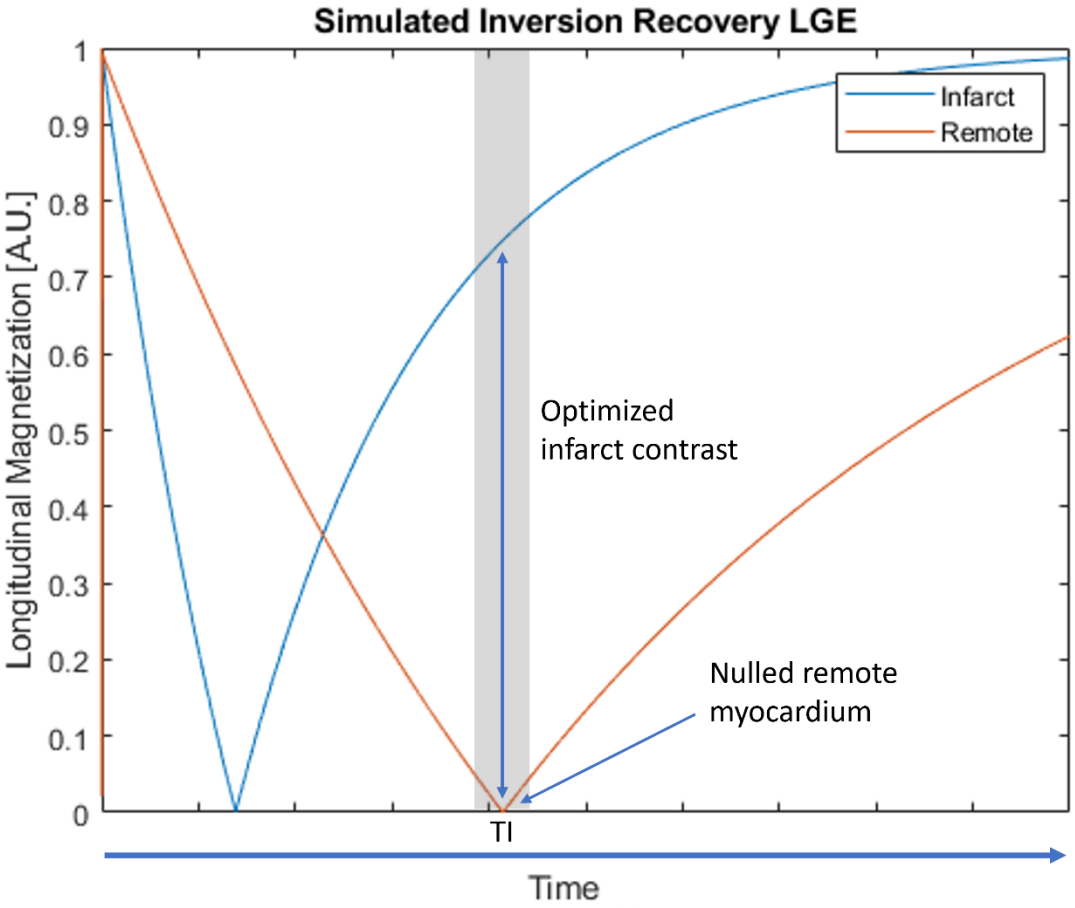

Figure 1.1: Simulated inversion recovery sequence showing longitudinal magnetization as a function of time in remote (orange) and infarcted (blue) myocardium. Optimal selection of the inversion time (TI) when the remote myocardium is nulled (0 longitudinal magnetization) allows maximum contrast development between remote and infarcted myocardium.

1.4.2 T2-Weighted MRI*

The T2* relaxation of tissues is a consequence of susceptibility-induced field inhomogeneities causing enhanced spin-spin decoupling, as well as chemical shift and spatial encoding gradients (*115*). It is directly related to the T2 relaxation time, and strictly faster than inherent T2 decay. T2* relaxation can be expressed by adding an additional term to the native T2 relaxation constant:

$$\frac{1}{T2^*} = \frac{1}{T2} + \frac{1}{T2'} \qquad \text{Equation 1.1}$$

in which T2' is added to capture the additional spin-spin relaxation caused by field inhomogeneities. In order to impart T2*-weighted contrast in MRI sequences, careful selection of flip angle, repetition time (TR), and echo time (TE) is required. Low flip angles limit T1 effects by minimizing the addition of longitudinal magnetization, while TE can be lengthened to impart T2*-weighted contrast (*115*). Practical limitations exist in both TE and TR that limit the length of both periods. For TR, maintaining a reasonable scan time while still limiting T1 weighting, and allowing a steady state to develop and sufficient magnetization recovery to occur keep TR relatively short, below ~25 ms (*33, 116, 117*). T2*-weighted MRI can suffer from significant artifacts, particularly at increasing TEs, so optimizing the balance between developing sufficient T2*-weighted contrast and limiting image artifacts needs to be considered (*118, 119*). Frequently, T2* mapping sequences employ a multi-echo protocol encompassing very short TEs (~1ms) to longer TEs (~13ms), from which a T2* map can be derived (*120*).

In the setting of MI, there are two primary sources for T2*-weighted contrast – hemorrhaging (i.e., deoxyhemoglobin) and blood breakdown products (i.e., iron deposition) (*115*). In acute MI, reperfusion-induced microvascular injury, as discussed previously, involves the extravasation of RBCs, which become degraded and release cellular constituents. Initially, oxyhemoglobin, which is diamagnetic is not visible on MRI. However, oxyhemoglobin is quickly reduced to deoxyhemoglobin, which is paramagnetic and visualized as dark regions on T2*-weighted MRI. As the RBCs become further degraded into heme and biliverdin, iron is released from heme and is stored as hemosiderin in the myocardium (*88*). Hemosiderin acts as a macrovascular source of

inhomogeneity (*115*), promoting T2*-weighted contrast and enabling the visualization of chronic iron deposition in hemorrhagic MI patients via T2*-weighted MRI and T2* mapping.

The development of T2*-weighted MRI and T2* mapping has provided a unique ability to non-invasively characterize IMH and myocardial iron deposition. Occasionally, the hypointensity is obvious enough to be apparent by visual assessment. More frequently, however, quantitative measures are used to assess the volume and extent of IMH or iron in T2*-weighted images and T2* maps. There are two primary methods by which this is achieved – relative hypointensity vs. a remote region-of-interest (ROI) or using absolute T2* values from a T2* map. Studies have identified a threshold of mean-2SD as the standard measurement for relative assessment. When analyzing T2* maps acquired at 1.5T, a threshold of 20ms is commonly used to delineate significant iron deposition, a point below which significant declines in LVEF and worsening LV remodeling are observed (*121*). T2* values have been validated against mass spectrometry measurements of [Fe] content (*88*) and the mean-2SD threshold has been validated against an *ex-vivo* gold standard (*122*).

1.4.3 First-Pass Perfusion MRI

First-pass perfusion (FPP) MRI is a technique that tracks the wash-in wash-out kinetics of blood as it flows through the heart. Primarily, first-pass sequences are contrast-enhanced, using the same GBCAs as LGE imaging. A lower dose of contrast than used for LGE, generally between 0.025-0.05mmol/kg, limits plateauing of the signal-intensity (SI) time curve (*92, 123*). While non-contrast sequences are being developed and investigated, such as arterial spin labeling (ASL), they suffer from SNR and contrast obstacles, and the standard protocols continue to use Gd

contrast (*124*). Additionally, clinical FPP sequences typically allow the collection of only a limited set of LV slices, given the requirement of fitting all slices within a single R-R interval while limiting breath hold lengths. Therefore, FPP sequences do not provide full coverage of the ventricle and select slices must be carefully chosen in the region of interest. Advances in FPP sequences enabling whole-heart coverage are being developed but are not yet clinically available (*125, 126*). It is common for studies to capture one short-axis slice in each of the apical, mid-ventricular, and basal regions, as well as a long-axis slice if possible. While this approach maximizes LV coverage, albeit sparsely, a more targeted technique that concentrates short axis slices in the area of infarction or hemorrhage may be more useful in applications of post-MI perfusion imaging.

The standard FPP sequence requires both breath holding and prospective electrocardiogram

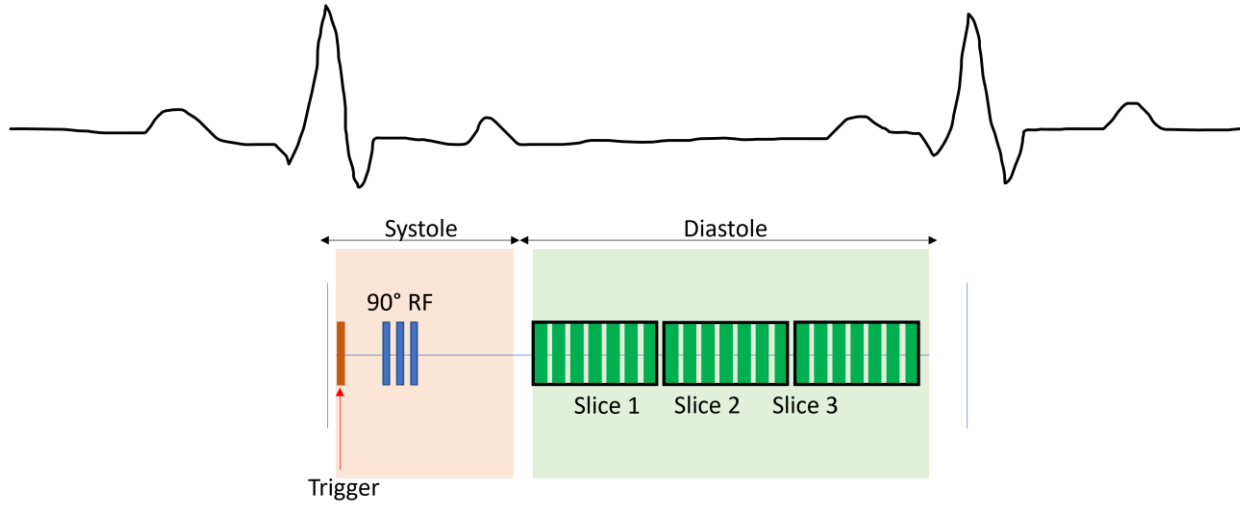

Figure 1.2: Example ECG-triggered first-pass perfusion MRI sequence. The QRS complex of the ECG triggers initiation of the sequence. Any RF preparation pulses (blue) are performed after the trigger, followed by the readout pulses (green). In this diagram, the sequence is designed to collect 3 myocardial slices during the diastolic phase of the cardiac cycle.

(ECG)-gating to limit respiratory motion artifacts and properly register the slices within the cardiac cycle. Detection of the QRS wave on the ECG initiates the sequence, which begins with radiofrequency (RF) preparation pulse(s) such as saturation recovery (SR) followed by readout

gradient pulses (e.g., spoiled gradient-recalled echo, SPGR) to capture the set of slices during diastole. The sequence produces a T1-weighted dynamic contrast-enhanced (DCE) cine series that tracks the flow of blood, allowing for the detection of perfusion deficits in areas that appear dark on first pass, suggesting impairment of the natural flow of blood through the myocardium. Myocardial perfusion imaging is discussed more extensively in the following section.

1.5 Assessing Myocardial Perfusion

1.5.1 Methods

There are numerous methods for measuring myocardial blood flow, encompassing both invasive and noninvasive techniques. The following sections will briefly describe these techniques and imaging modalities in the measurement of myocardial perfusion.

1.5.1.1 Invasive

1.5.1.1.1 Microspheres

Microspheres act as the gold standard for myocardial blood flow quantification and is used to validate other non-invasive perfusion imaging methods (*127*). The use of injectable small particles to study the blood flow through the coronary circulation of fetal pigs dates back to the early 20th century (*128*). The use of actual microspheres in the human heart came about in the mid-1940s in which investigators studied the collateral circulation via glass spheres injected into the left main coronary artery (*129*). Developments in radioactive labeling and new materials for the microspheres brought about the ability to measure absolute blood flow, which was not possible via early methods (*130*). The optimal method to reduce the unnecessary use of

radioactive particles in blood flow measurement is the use of fluorescent dye-labeled microspheres (*131*), which additionally enables the possibility for blood flow measurement in chronic studies (*132*).

1.5.1.1.2 Fractional Flow Reserve

Fractional flow reserve (FFR) is another invasive method for assessing the extent to which maximal hyperemic myocardial blood flow through a stenotic artery compares to maximal hyperemic blood flow through a healthy artery and can be measured by a ratio of pressures using catheter-based guidewire sensors (*133*). FFR was shown to correlate well with post-PCI MBF assessed via Positron Emission Tomography (PET) (*134*).

1.5.1.2 Non-invasive

1.5.1.2.1 SPECT

Single-photon emission computed tomography (SPECT) myocardial perfusion imaging involves the use of a radiotracer for detection of blood flow and is commonly used in patients with CAD. While SPECT has been used as a non-invasive imaging method, its clinical utility has been limited by the presence of artifacts (*135*), underestimation of ischemic extent (*136*), and lack of attenuation correction relative to PET (*137*). Recent advances in camera and collimator architecture have greatly improved radiation dose and imaging time, which have led to improvements in sensitivity and resolution (*138*). SPECT imaging is often combined with other imaging modalities (e.g., X-ray CT) and there have been recent developments toward a SPECT/MRI system similar to simultaneous PET/MRI scanners, although with additional obstacles in terms of ensuring MRI-compatibility (*139*).

1.5.1.2.2 PET

Positron Emission Tomography (PET) perfusion imaging allows the absolute quantification of coronary blood flow and is considered the gold standard for measuring MBF in humans (*140, 141*). Two promising tracers: ^{15}O-water and ^{13}N-ammonia have been tested in animal models against microsphere validation (*142*). Nitzsche et al. quantified myocardial blood flow in humans with ^{13}N-ammonia using ^{15}O-water as the validation, showing comparable results between the two tracers. Additionally, Prior et al. showed promising results for the measurement of MBF across the range of blood flow rates using ^{82}Rb validated against ^{15}O-water (*141*). Byrne et al. examined the association between myocardial perfusion impairment, assessed via ^{82}Rb PET/CT, and increasing LV dilatation in non-ischemic HF patients, implicating the potential role of microvascular dysfunction in the development of HF and adverse events (*143*). PET perfusion, while more costly and with a longer scan time than SPECT, has the advantage of decreased artifacts due to the implementation of attenuation correction (*137*).

1.5.1.2.3 CT

Computed tomography angiography (CTA) is the primary diagnostic test in lower risk patients with suspected CAD (*144*), given its high negative predictive value in detecting major stenoses (*145*). Recent advancements in CT technology have extended the use beyond angiography, enabling the detection of flow-limiting stenoses in the LV myocardium via computed tomography myocardial perfusion (CTP) (*144, 146*). The CT-based imaging protocol shares many similarities with MRI perfusion, by utilizing a contrast agent to produce an intensity-time curve that is used to estimate myocardial perfusion by measuring the curve's upslope. Additionally, CTP may be

performed both at rest and stress, allowing for the detection of exercise-induced burdens in myocardial flow. Dynamic CTP imaging allows for the quantification of blood flow and may be combined with CTA for optimal efficiency (*147*). However, prospective diagnosis when combined with CTA imaging exposes the patient to unnecessary radiation doses, given the propensity of conventional CTA to rule out CAD in most patients (*144, 146, 147*). Therefore, selective CTP following a CTA exam is most logical, limiting the potential use-case as a combination scan with angiography (*147*).

1.5.1.2.4 Ultrasound

Ultrasonic quantification of myocardial blood flow can be accomplished via IV administration of microbubbles that are destroyed by ultrasonic stimulation, providing a contrast-enhanced mechanism for measuring blood flow. Wei et al. showed the potential for myocardial contrast echo (MCE) measurement of MBF using a microbubble infusion method in canines (*148*). While the low cost and ease of use of ultrasonic blood flow measurement are promising, MRI remains the gold standard among non-ionizing perfusion modalities, due to its superior anatomical image quality and utility for detecting myriad cardiac abnormalities (*149*).

1.5.1.2.5 MRI

Myocardial blood flow imaging via MRI provides a noninvasive, non-ionizing method for assessing the perfusion in localized regions of the myocardium by capturing the first pass of contrast as it flows through the LV. The technique, referred to as first-pass perfusion, is typically performed as the initial scan in a late gadolinium enhancement (LGE) protocol as the contrast agent can then be utilized for both sequences. As discussed in Chapter 1, FPP defects detected via MRI carry

highly significant prognostic value for the risk of adverse LV remodeling, LV dysfunction, and development of major adverse cardiac events (MACE).

1.5.2 MRI Perfusion

1.5.2.1 Techniques

First-pass perfusion MRI may be acquired using either a dynamic contrast-enhanced (DCE) sequence or a non-contrast arterial spin labeling (ASL) sequence. ASL sequences have been developed to accommodate the subset of patients in whom Gd contrast in contraindicated, as well as enable repeated perfusion scans that would not be possible with contrast-enhanced imaging. Briefly, the ASL technique encompasses radiofrequency-labeled arterial blood containing a decaying signal related to the T1 relaxation, which is then allowed to flow into the target tissue. Additionally an unlabeled image is captured, from which the difference is extracted to produce the final image which proportionally reflects the flow of blood through the region of interest (*124*). However, ASL is still under development and suffers from significant obstacles such as largely decreased contrast and sensitivity compared to first-pass perfusion with Gd contrast.

First-pass DCE MRI perfusion is widely accepted clinically and has shown superiority to SPECT in the detection of CAD in the CE-MARK and MR-IMPACT multi-center trials (*150-152*). Further, FPP MRI has shown strong correlation with PET (gold standard in quantitative perfusion) using various radiotracers, with strong advantages over PET perfusion such as higher resolution and the use of non-ionizing radiation (*153-155*).

1.5.2.2 Analysis

The rest perfusion MRI sequence produces a signal intensity-time curve, from which various analytical techniques may be used for further assessment. A sample signal intensity-time curve is shown in Figure 1.3, produced using the cardiac MRI analysis software package CVI[42] (Calgary, Alberta, Canada). Using the raw signal intensity, which is assumed to be linearly correlated with contrast concentration, without further modification is referred to as qualitative perfusion. Combining the signal intensity values with the change over time enables a semi-quantitative measure of perfusion, which is often taken as a normalized value compared to the LV blood pool. Several parameters may be used for semi-quantitative analysis, including maximum upslope, time-to-peak, and upslope integral. Lastly, quantitative perfusion involves extraction of the absolute myocardial blood flow via complex mathematical deconvolution and requires a more complicated setup involving multiple contrast boluses or multiple sequences (*123, 156, 157*).

Clinical implementation of quantitative MRI perfusion remains limited, instead relying primarily on expert observers performing qualitative visual assessments (*158*).

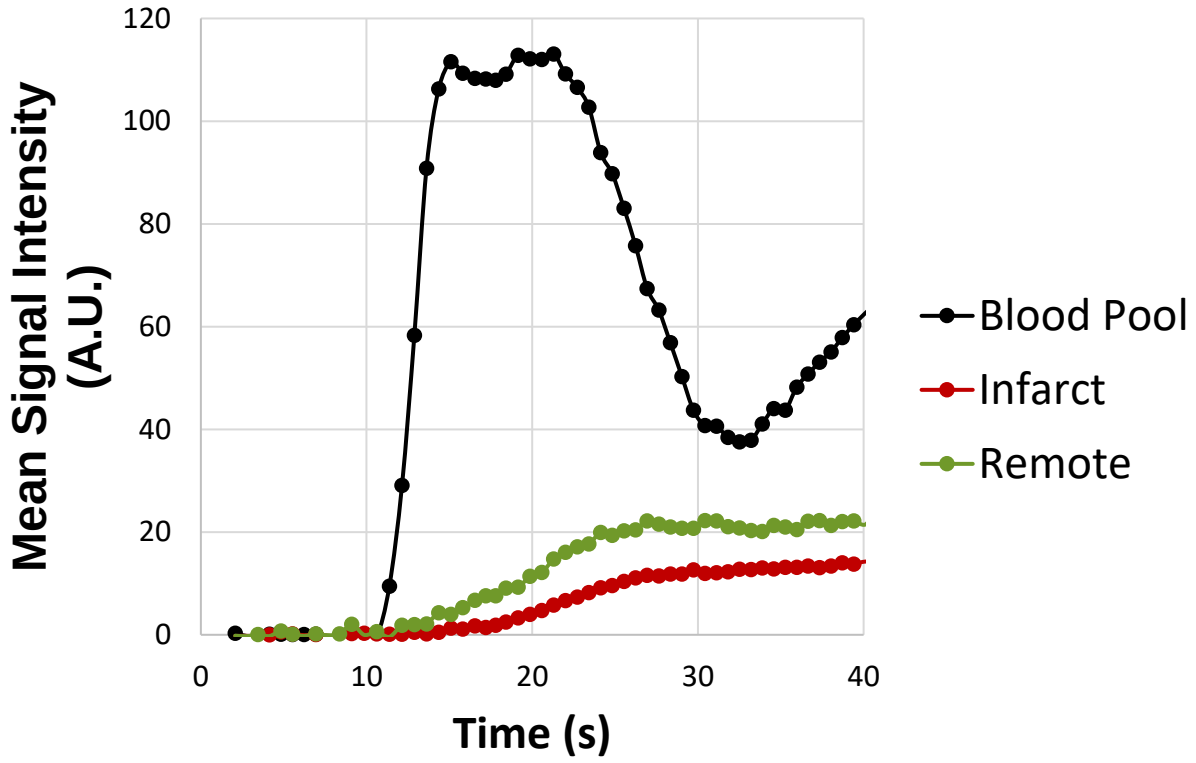

Figure 1.3: Example first-pass perfusion (FPP) curve with Gd contrast from CVI[42] cardiac MRI analysis software. The blood pool (yellow) is used as the basis for normalization. Remote (green) and infarct (red) ROIs are contoured to produce the regional curves shown.

1.5.2.2.1 Qualitative Perfusion Assessment

Myocardial perfusion analysis that involves only visual assessment or strictly changes in signal intensity without considering the rate of change are considered qualitative (*123*). Naturally, qualitative perfusion is useful when the perfusion defect is clearly apparent upon visual inspection. Currently, clinical perfusion MRI relies on qualitative assessment by expert observers due to the manual processing and sequence complexities involved in quantitative or semi-

quantitative perfusion (*158*). However, a study by Mordini et al. showed the diagnostic accuracy superiority of quantitative perfusion measures over qualitative assessment in the detection of significant coronary artery stenosis (*159*), indicating the importance of clinical transition from qualitative perfusion assessment to a quantitative measure of myocardial perfusion.

1.5.2.2.2 Semi-Quantitative Perfusion

A standard method for semi-quantitative myocardial perfusion analysis involves capturing the maximum upslope of the signal-intensity time curve in the ROI and dividing by that of the blood pool, thereby producing an output measure called the myocardial perfusion index (MPI). The measurement window is manually constrained to between the baseline and contrast washout, and a 5-point fitting is used to measure the maximal slope (see Figure 1.4).

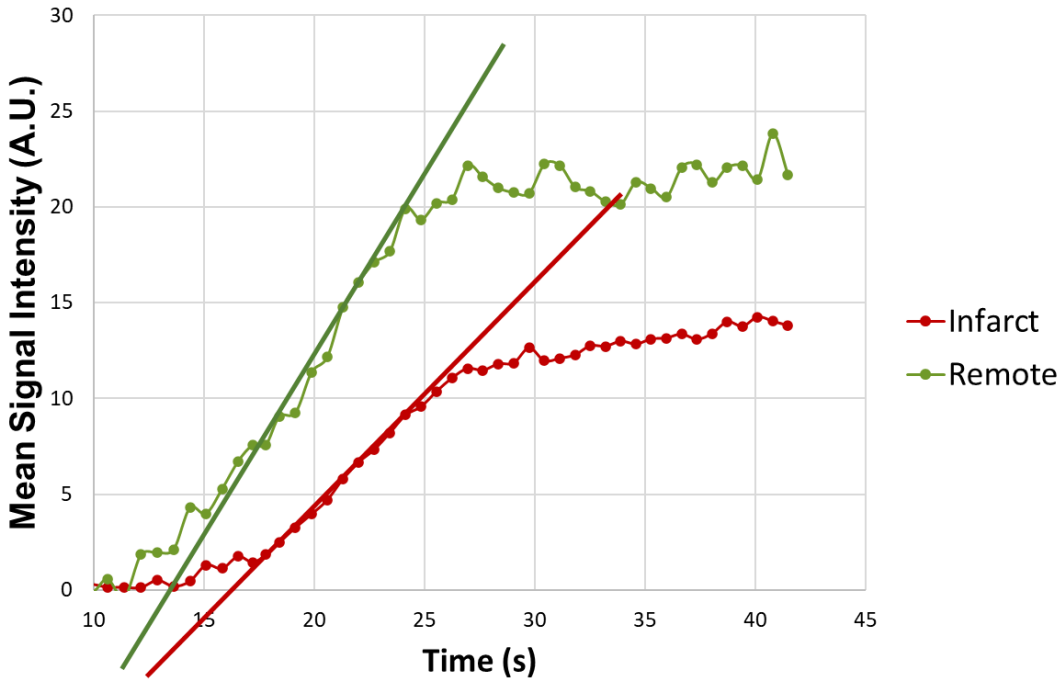

Figure 1.4: Maximum upslope measurement of the signal-intensity time curve using 5-point fitting.

Schwitter et al. showed strong correlation between FPP and ^{13}N-ammonia PET during hyperemic flow using the signal intensity upslope method as a semi-quantitative measure of MBF (*154*). In a myocardial perfusion study of 16 canines, Christian et al. compared quantitative, semi-quantitative, and qualitative FPP MRI to fluorescent microspheres (*123*). Although quantitative myocardial perfusion correlated most strongly with microsphere measurements, semi-quantitative assessment was accurate up to a level of ~3.0 mL/min/g (*123*), a level far greater than average resting MBF values of 0.6-1.3 mL/min/g (*160*). The MBF underestimation observed at higher blood flow rates (i.e., during hyperemia or stress perfusion) is not a concern in resting myocardial perfusion imaging as this occurs at blood flow rates within the accurate range of estimation for myocardial-to-LV upslope ratio (*123, 159*). Interestingly, in a healthy volunteer study Larghat et al. showed semiquantitative perfusion analysis using the maximum upslope method to have higher reproducibility than quantitative perfusion using a Fermi-constrained deconvolution method (*161*). A recent study by Seitz et al. investigated the impact of two baseline corrections methods to account for surface coil inhomogeneity effects on semiquantitative analysis of myocardial perfusion reserve index (MPRI) in patients without obstructed coronaries. In the study, the investigators found that dispersion of peak signal intensity and maximum upslope were corrected by baseline division, however this also resulted in paradoxically low MPRI and rest perfusion indices (*162*).

1.5.2.2.3 Absolute Quantitative Perfusion

Absolute quantification of myocardial perfusion is the most direct comparison to quantitative PET perfusion and has shown good concordance in multiple studies. Quantitative MRI perfusion requires complex sequence design and post-processing in order to derive the absolute MBF

values using the arterial input function (AIF) as a basis, and currently requires either a dual-bolus (*123*) or dual-sequence (*163*) technique. Novel MRI perfusion protocols are under development and aim to simplify the quantitative MRI protocol by removing the manual processing required for quantitative perfusion assessment. A recent study by Scannell et al. used a deep learning (DL) approach to compare MBF values derived automatically to manual processing, showing high accuracy for their DL-based perfusion quantification (*164*). Another recent study by Knott et al. investigated the prognostic significance of quantitative perfusion utilizing an inline perfusion mapping technique with automated segmentation and analysis, showing a strong correlation between reduced MBF and MACE (*165*).

1.6 Advances in Cardiac Imaging Enable Further Characterization of Myocardial Infarction

The process of primary percutaneous intervention (PCI), restoring blood flow to the blocked myocardial vasculature, leads to a paradoxical event of additional injury, which has been termed ischemia/reperfusion (I/R) injury. A number of mechanisms are involved in the development of I/R injury occurring in the acute reperfused infarction setting including a pro-inflammatory response, platelet aggregation, microvascular spasms, increased production of cytotoxic reactive oxygen species (ROS), destruction of the mitochondrial membranes, loss of Ca^{2+} control, and ultimately endothelial dysfunction and destruction leading to nitric oxide (NO) imbalance and erythrocyte extravasation (*166-171*). Additionally, the wave of cell death is able to hop between gap junctions in cardiomyocytes, spreading the cytotoxic environment throughout the myocardium (*172*). The extent of these microvascular injuries are primarily determined by the length of the ischemic period prior to reperfusion, as the deterioration of the vascular wall

structures causes a progression of vascular leakage from proteins and other macromolecules to eventual leakage of red blood cells (RBCs) (*173*), although additional predictive factors have been implicated in some studies such as per-PCI glycemia, platelet inhibition, glycoprotein IIa/IIIb inhibition, and infarct location (*23, 76, 174*). This differentiation leads to a continuum of infarct severity that can be harnessed for greater impact of MI therapies.

While limited success has been achieved in limiting I/R injury clinically (*172*), treatment of MI patients continues to be agnostic to the deeper segmentation, particularly considering effects on hemorrhagic patients. Utilizing advanced imaging techniques allows the early segregation of patients into categories of infarct severity. Importantly, CMR imaging, along with gadolinium-based contrast agents and advances in imaging sequences such as T2*-weighted MRI have enabled the discrimination of various types of infarctions. Namely, the mildest MI types show isolated hyperintensity on late gadolinium-enhancement (LGE) imaging, whereas a hypointense core on LGE is indicative of an acute phenomenon of "no-reflow," or microvascular obstruction (MVO), a more severe level of infarct. Finally, utilizing T2*-weighted MRI and T2* maps, the detection of intramyocardial hemorrhage (IMH) is possible by observing hypointense regions within the infarct zone. Infarct patients displaying this type of characteristic have the most severe type of MI and worse outcomes. This enables a deeper segmentation of the MI patient population into those without microvascular complications, those with only microvascular obstruction (MVO), and those with IMH. Adverse left ventricular (LV) remodeling has been associated with conditions of microvascular injury and consists of excess LV dilatation and scar expansion and thinning. While patients with MVO have been shown to have increased risk of negative outcomes over those without (*55, 56*), patients with IMH have been shown to have greater susceptibility to

adverse remodeling and have increased incidence of major adverse cardiovascular events (MACE) when compared with patients without IMH (*22-24, 169*).

1.7 Impact of Iron Deposition in Myocardial Infarction

Iron is an essential element for most living organisms as a necessary component in erythrocyte synthesis for oxygen transport and is additionally involved in widespread biological processes such as synthesis of DNA, electron transport, cellular respiration, and metabolism (*175-178*). Both iron deficiency and excess can have toxic effects on the normal function of most organ systems, given its biological necessity and its ability to form free radicals (*175, 177*). Therefore, the balance of physiological iron in the human body is a tightly controlled mechanism with dedicated absorption, storage, and transport agents (*175, 179*). Consequences of iron deficiency range from neurologic impairment to immune dysfunction (*180, 181*), and further compromises cardiac contractility (*182*). Further, Das De et al. found transferrin saturation to be negatively associated with CAD and MI (*183*), indicating the impact of iron deficiency on cardiac function and health. Likewise, iron overload can significantly impair physiological function of body organs and has been associated with increased cancer risk (*184*). Elevated iron levels are found in patients with chronic liver disease, hereditary hemochromatosis, and hepatitis C infection (*185*). Specifically, iron dysregulation may negatively impact most body organs, including the brain, heart, hepatic, renal, and pulmonary systems (*182, 183, 185-196*).

Recent studies have shown that acute IMH in MI patients resolves into iron deposits in the myocardium persisting chronically as the infarct matures (*88, 197*). Advances in MRI technology have expanded the capacity to non-invasively probe iron content that had previously only been

possible via blood analysis of ferritin, transferrin, or biopsy (e.g., of the liver) (*175, 198*). As discussed, susceptibility-induced magnetic field inhomogeneities from deoxyhemoglobin and iron lead to enhanced T2* decay and appear as hypointense regions on T2*-weighted images (*115*), providing the basis for myocardial iron detection via MRI.

The role of iron in the angiogenic state of tumors has been well-studied in the field of breast cancer (*199-202*), in which iron deficiency confers a pro-angiogenic response and stimulates tumorigenesis. Similarly, iron overload also contributes to elevated incidence of breast cancer by increasing oxidative stress (*199, 201*). While pro-angiogenic properties have been hypothesized as a therapeutic target in acute MI (*203*), the role iron plays in the angiogenic state of chronic MI patients has not been characterized. Likewise, further research is warranted on the potential impact of iron deposition on resting perfusion in chronic MI patients.

Studies investigating the role of iron in MI have shown a confluence of adverse effects including inflammation, electrical system anomalies, and adverse remodeling (*88, 89, 204, 205*). However, the connection between iron's role in microvascular dysfunction and these adverse events remain unclear. Microvascular function is a prominent factor in cardiac remodeling and cardiovascular events (*206*). Iron is also known to scavenge nitric oxide (NO) in the myocardium (*207*), which, as a common mechanism for control of endothelial function and vascular homeostasis, may potentiate a reduction in the bioavailability of NO and lead to endothelial dysfunction. Lastly, a persistent pro-inflammatory environment in the post-MI chronic myocardium may further contribute to adverse LV remodeling and poor outcomes (*208, 209*). Together, chronic iron deposition has the potential to drive an environment of hemorrhagic MI culminating in NO imbalance and adverse LV remodeling.

1.8 Therapeutic Interventions

In an effort to improve clinical outcomes for patients suffering an MI, investigators have proposed and tested numerous interventional treatments targeting various aspects of the pathophysiology. Pharmacological treatments such as adenosine, glycoprotein IIa/IIIb inhibitors, nitric oxide pathway modulation, cyclosporine, and calcium channel blockers, among many others, have potential as adjunctive therapies in limiting I/R injury and improving therapeutic outcomes (*166*). In particular, glycoprotein IIa/IIIb inhibitors have been shown to be independently associated with IMH based on multivariate analysis (*76*), an indication that unexpected adverse consequences may derive from these treatments.

Ischemic conditioning has shown promise as a mechanical stimulus to confer cardioprotection. Several variations of conditioning have been studied, including ischemic pre-conditioning in which intermittent ischemia is applied prior to the prolonged occlusion, post-conditioning which involved periodic reperfusion as opposed to instantaneous one-off blockage removal, as well as remote conditioning that involves applied ischemia to a peripheral limb as a global whole-body approach.

Additional mechanical approaches aimed at preventing proximal or distal embolization during the standard PCI treatment were theoretically plausible, but results were conflicting (*166*). Oxygen modulation therapy (i.e., hyperoxemia) has similarly been met with a lack of positive clinical outcomes, despite promising preclinical findings (*210*), which is unsurprising given the controversy over the role of oxygen administration in the acute MI setting (*211*). However, the FDA has recently approved a super-saturated oxygen (SSO2) therapy for use in this setting, which

stands as the only FDA-approved adjunctive therapy in myocardial infarction and has shown promising results in reducing infarct size in canine, pig, and clinical studies (*212-216*).

Therapeutic hypothermia, a treatment that has had long success in supporting neurological recovery in cardiac arrest patients, has shown promise in animal studies but has yet to make a significant clinical impact following disappointing randomized clinical trial results. By targeting a multitude of independent pathways (*217*), therapeutic hypothermia has the potential to confer significant benefits to acute MI patients. Briefly, the aim of the treatment is to lower the myocardial temperature to 32-35 °C and maintain mild-to-moderate hypothermia for a period of time during reperfusion prior to rewarming the heart to normal body temperature.

1.9 Therapeutic Hypothermia

1.9.1 Clinical History

Therapeutic hypothermia (TH) came into clinical practice in the 1950s based on the finding that hypothermia-treated hearts fared better during cardiac surgery than under normothermic conditions (*218, 219*). Furthermore, patients suffering brain injuries had improved neurologic outcomes when treated with TH, and hypothermia has been shown to be effective in protecting the neurovasculature in cardiac arrest patients (*220*). The effectiveness of treatment in patients suffering an out-of-hospital cardiac arrest (OHCA) caused by an acute MI who received therapeutic hypothermia led to the hypothesis that cardioprotective benefits may be achievable in addition to the neuroprotection conferred under current clinical practice (*217*).

Initial therapeutic hypothermia efforts to effect cardioprotection were laden with complications such as fibrillation and infection (*217, 221*). The treatment started gaining traction again by the

early 2000s with the improvement of temperature control and targeting a milder degree of hypothermia (*222-224*). There have been numerous studies and clinical trials looking at the effects of hypothermia on myocardial infarction in small and large animals as well as patients (*225-238*). Investigations have studied therapeutic hypothermia's effect on modulating the action of other pharmaceutical agents, cellular signaling pathways, and ultimately its gross effect on resulting infarct size (*229, 239-255*). Varying induction methods have been used, including surface cooling, intravenous catheter cooling, peritoneal lavage, and intranasal cooling (*223, 256-259*). To date, the clinical use of therapeutic hypothermia for cardioprotection remains a research problem to be solved following mixed clinical trial results, even though pre-clinical animal studies have resulted in promising outcomes.

1.9.2 Challenges in Clinical Translation

Most investigators have looked at the impact of TH in limiting overall infarct size and adverse event outcomes, albeit with extensive variability in hypothermia protocol (i.e., target temperature, duration of hypothermia, initiation of hypothermic intervention, and method of application). The safety and feasibility multi-center study by Dixon et al. used endovascular cooling targeting 33°C for 3 hours post-reperfusion in acute MI patients, with primary study endpoints of infarct size and adverse events at 30 days (*233*). The study resulted in non-significant decreases in MI size and adverse outcomes, and the use of SPECT for MI size assessment may have resulted in the lack of significant findings due to its lower sensitivity compared to MRI (*260-262*). Similarly, the COOL-MI trial showed no difference in infarct size measured with SPECT at 30 days, however most patients did not reach the target temperature of 35°C (*263*). The ICE-IT trial followed patients for 1 year post-MI, and also had limitations regarding successful target

temperature, though a retrospective pooled analysis did show a significant decrease in infarct size in successfully-cooled patients (*225*). The RAPID MI-ICE trial showed successful reduction in infarct size normalized to myocardium at risk assessed via LGE and T2-weighted MRI in patients that reached target temperatures of <35°C at the time of reperfusion (maintained for 3 hours), with only non-significant delay in door-to-balloon time (*237*). However, as discussed, the use of T2-weighted MRI to assess area at risk may be inaccurate and confound the results in the presence of hemorrhage. In the CHILL-MI trial, investigators assessed infarct size at 4 days post-MI using LGE normalized to area at risk in patients receiving 1 hour of therapeutic hypothermia via endovascular cooling but found no significant differences (*232*). However, in that study heart failure incidence at 45 days was significantly decreased in the hypothermia group. The randomized multi-center VELOCITY trial assessed acute infarct size in relation to T2-based area at risk (3-5 days) and composite event rate at 30 days in patients treated with peritoneal hypothermia for 3 hours post-reperfusion, resulting in increased event rates in the hypothermia group with no reduction in infarct size (*235*). The recent COOL AMI EU randomized multi-center trial used intravascular cooling to assess infarct size at 30-days post-MI, with non-significant reductions in MI size (reported as % of LV mass) (*234*). However, limitations of that study include being underpowered to detect study endpoints and lengthened ischemia time relative to other randomized control trials, with an intra-study delay bias against the hypothermia group. Clearly, there have been many mixed results and a wide variety of hypothermia protocols with nonuniform study endpoints, along with difficulties in achieving target hypothermia temperatures and delays in door-to-balloon and ischemic time. For these reasons, TH in the acute MI setting has not had the same impact and uptake clinically as it has for neuroprotection

following cardiac arrest (*220, 224*). However, with expanded therapeutic efficacies as detailed in Chapter 4, along with continued development and specific optimization of the hypothermia protocol for myocardial infarction, I/R injury, and microvascular dysfunction, these obstacles in clinical acceptance can be overcome.

Many of the clinical studies discussed above observed primary safety endpoints at 30-45 days post-MI, which is relatively early in the infarct maturation process (*264*), potentially leading to a lack of chronic insights (*232-235, 237, 265*). Additionally, the investigations often observe a set of outcome measures (e.g., infarct size, cumulative event rate) that may inadvertently exclude key benefits outside the scope of those parameters (i.e., hemorrhage).

Currently, the prevailing theory is that TH is optimized when initiated prior to, or at the time of, reperfusion in order to effect cardioprotective benefit. However, it remains plausible that effects outside the outcome measure scope of existing studies are achievable via post-reperfusion hypothermia. While the study by Shi et al. investigating post-reperfusion TH in a rat model of MI failed to show LV remodeling and functional benefits in the hypothermia group (*266*), a recent study by Marek-Iannucci et al. showed significant molecular pathway and functional benefits in a swine model of post-reperfusion hypothermia (*230*).

1.9.3 New Insights in Autophagy

Building on the mechanistic understanding of the cardioprotective action of TH is an important step in successful clinical translation of this therapy. A recent study in a swine model of MI by Marek-Iannucci et al. uncovered benefits of TH in the cellular renewal pathways autophagy and mitophagy, processes that may have large ramifications on the heart's recovery from acute MI

(*230*). While the study did not consider IMH, the results showed numerous beneficial differences in molecular markers of cell cycling and renewal in the TH-treated group, as well as improved ejection fraction (EF) measured via transthoracic echocardiography. As important processes in LV remodeling, upregulated autophagy and mitophagy may promote homeostasis of the myocardium in the post-MI setting by increasing mitochondrial function (*267*). These new insights provide an important baseline into the potential effects of TH in acute MI, particularly the potential for TH to effect both cellular and LV functional benefits as a post-reperfusion therapy, which has largely been disregarded in recent studies.

1.10 Current Gaps in Knowledge: Hemorrhagic MI and Therapeutic Hypothermia

So far, this chapter has discussed the current state of knowledge surrounding IMH and TH. While significant progress has been made in each of these fields, there remains much to discover in terms of mechanistic action and therapeutic potential. Recent studies have elucidated the potential for acute IMH to predict chronic LV function, as well as linking IMH to increased risk of MACE, yet the mechanisms of chronic hemorrhage and its effects on the cardiac microvascular environment are not well understood. The association between IMH, iron, and myocardial perfusion are likewise areas for potential therapeutic advancement. Stress perfusion has been extensively studied in relation to impaired myocardial perfusion reserve and its impacts on myocardial function. Resting perfusion, on the other hand, has not been well-characterized, particularly in the chronic phase of MI, and with its potential implications for LV function is an important target for MI research.

Therapeutic hypothermia has shown significant promise in pre-clinical studies, particularly in highly translational large animal models, but remains inconclusive based on the outcomes from randomized clinical trials. Understanding of the therapeutic pathways affected by TH has been a hot topic of research, although a critical aspect of this promising therapy has been largely overlooked: its impact on IMH and the downstream sequelae of chronic myocardial hemorrhage and iron deposition. By studying an optimized animal model of I/R injury treated with TH, we may be able to overcome obstacles faced by previous clinical trials and expand the efficacy profile for TH in MI patients.

This dissertation will dive deep into these topics, uncovering new insights and opportunities for future research. The mechanisms of IMH and its impacts on LV function and chronic resting perfusion were investigated in a comprehensive study covering clinical patient data, large animal model analysis, and molecular insights. Furthermore, we show evidence that by correcting the imbalance in iron homeostasis, LV dysfunction can be rectified, bring resting perfusion to levels similar to non-hemorrhagic MIs. Our therapeutic hypothermia study is the first to our knowledge to show the treatment's benefit on IMH and chronic iron in the myocardium, building a launchpad for expansion of TH into a new area of research.

1.11 Overview of the Dissertation

The core of this dissertation will describe the results of the 3 major large animal studies conducted to investigate the therapeutic impacts of iron modulation in chronic MI. Chapter 2 tests the hypothesis that resting myocardial perfusion is preferentially decreased in chronic hemorrhagic MI territories. We tested this in a clinical patient cohort and an animal model of I/R

injury, resulting in the detection of chronic resting perfusion defects in hemorrhagic subjects using T2*-weighted and first-pass perfusion MRI. Additionally, a mechanistic model is proposed showing the impact of myocardial iron on NO, VEGF, and resting perfusion defects. The following chapter (chapter 3) presents a study of iron chelation in a canine model of I/R injury, to evaluate the hypothesis that the iron chelator, Deferiprone (DFP), may alleviate chronic resting perfusion defects in hemorrhagic MI animals. This study concludes that control of myocardial iron via chelation with DFP provides significant benefits on resting perfusion in the chronic phase of MI in hemorrhagic animals, which dissipate upon termination of the DFP therapy. Chapter 4 presents a study on therapeutic hypothermia (TH) in a swine model of I/R injury that tests the hypothesis that mild hypothermia may reduce intramyocardial hemorrhage and chronic iron deposition. The results show the reduction of chronic myocardial iron and LV functional improvement in hypothermia-treated pigs at 2 months post-MI. Finally, chapter 5 provides a summary of the dissertation and describes the future directions and potential extensions of the work presented herein.

Chapter 2: Rest Perfusion Defects in Chronic Hemorrhagic MI

2.1 Abstract

Background: Hemorrhagic myocardial infarction (MI) is a strong independent predictor of adverse events. Chronic iron deposition in hemorrhagic MI may lead to significant microvascular dysfunction, which may be observed as deficits in resting myocardial perfusion on first-pass perfusion (FPP) MRI. The objective of this study was to develop and characterize a microenvironmental model of chronic hemorrhagic MI, assessed in a clinical trial pilot study and validated with a canine model of ischemia reperfusion (I/R) injury and protein expression analysis.

Methods and Results: 14 patients with ST-elevated MI (STEMI) and 22 canines were serially studied into the chronic phase of MI (6 months and 8 weeks, respectively). MRI scans were performed during acute (3-7 days) and chronic (8 weeks – 6 months) MI. Following completion of the animal studies, hearts were excised and analyzed for protein expression. Infarct ROIs were drawn on FPP images and normalized by remote ROIs to extract a normalized myocardial perfusion index (MPI). Resting perfusion was significantly decreased in the hemorrhagic groups of both patient (0.72 ± 0.03 vs. 0.83 ± 0.02; p=0.002) and canine (0.62 ± 0.02 vs. 0.85 ± 0.04, $p < 0.001$) studies. Phosphorylated endothelial nitric oxide synthase (eNOS) was significantly elevated in hemorrhagic animals compared to controls (1.23 ± 0.11 vs. 0.83 ± 0.08, respectively; p = 0.038). Similarly, vascular endothelial growth factor (VEGF) was significantly elevated compared to controls (0.95 ± 0.09 vs. 0.68 ± 0.07, respectively; p = 0.009).

Conclusion: Chronic resting perfusion defects in hemorrhagic MI subjects are associated with iron deposition and NO imbalance, even though neovascularization and eNOS stimulation is activated. Chronic iron deposition and myocardial microvascular homeostasis may be critical therapeutic targets for future studies in hemorrhagic MI populations.

2.2 Introduction

Despite the major advances in the treatment and outcomes over the decades, myocardial infarction (MI) remains the leading cause of death worldwide. Importantly, advances in reperfusion have led to significant reductions in mortality and recurrence of MI. However, at the same time, the incidence of chronic heart failure has increased (*268*). One negative consequence of reperfusion therapy is linked with microvascular damage including microvascular obstruction (MVO) and hemorrhage. It has been shown that MVO adds additional risk for the development of major adverse cardiovascular events (MACE) (*55-57, 269*) and the presence of hemorrhage, the most severe form of microvascular damage, further augments the risk for MACE (*56, 269*). In fact, intramyocardial hemorrhage has been shown to be an even stronger predictor of adverse events than MVO alone (*56*). Nonetheless, the means by which hemorrhage promotes negative outcomes is not well understood.

Microvascular function can play an important role in cardiac remodeling and cardiovascular events (*57, 206*). However, the link between these events and the physiological underpinnings of microvascular dysfunction are unclear. Iron deposition has been shown to be prevalent in chronic hemorrhagic infarctions (hMI+) in both humans and canine models, potentially implicating a new target for therapeutic intervention. Aside from the implications of iron in abnormal brain (*194,*

270, 271), renal (*187, 188*), hepatic (*185, 186*), and pulmonary function (*189-193*), iron is also known to scavenge nitric oxide in the myocardium (*207*). Further, nitric oxide (NO) is a known regulator of endothelial function and vascular homeostasis (*71, 72*). Thus, iron-induced scavenging may potentiate a reduction in the bioavailability of NO and impair endothelial function and lead to disruption of homeostatic mechanisms. Studies have also suggested the negative impact of chronic iron deposition on the cardiac electrical signaling pathway, providing a locus for arrythmias, which may additionally help explain the impact of hemorrhage on outcomes (*204*). Additionally, iron has been shown to drive a persistent pro-inflammatory response in the post-MI chronic myocardium (*208*). Understood to be a consequence of hemorrhagic infarction - the presence of a prolonged pro-inflammatory response in the infarction territory (*208, 209*) - may be a key driver of adverse left-ventricular remodeling and poor outcomes. Collectively, these factors implicate an environment of hemorrhagic MI that drives poor ventricular function, impaired hemostasis, and undesirable ventricular remodeling.

Based on these observations in the literature, we developed a hemorrhagic MI microenvironmental model encompassing the process from reperfusion-hemorrhage to impaired perfusion. The heme and iron deposits known to exist in hemorrhagic infarctions have a multifaceted influence on the microenvironment: stimulating reactive oxygen species (ROS), as well as the heme regulators heme-carrier-protein-1 (HCP-1) and heme-oxygenase-1 (HO-1). Heme and ROS are known to scavenge NO, which lays at the center of our hypothesis, acting as the driving force for the reduced perfusion. Additionally, HO-1 may impact perfusion through vasospastic actions of heme breakdown products (*272*). The perfusion state may then trigger

reactive mechanisms in an attempt to recover the microcirculatory capacity, namely nitric oxide synthases (NOS) and vascular endothelial growth factors (VEGF).

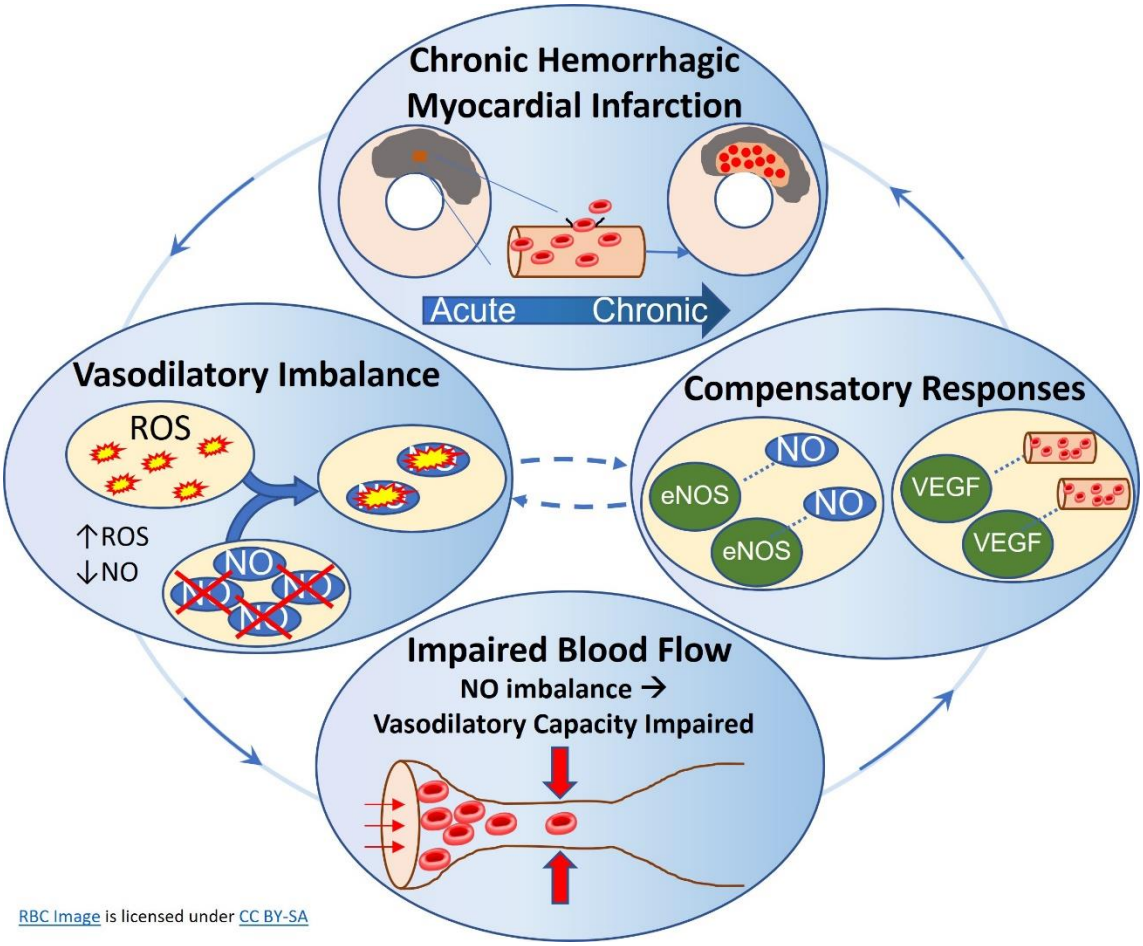

Figure 2.1: Proposed Mechanism for Iron-Induced Blood Flow Impairment in Hemorrhagic MI.

Hemorrhagic MI leads to vessel breakdown and RBC leakage & breakdown. This results in free heme and iron deposits in the myocardium, driving several responses. Elevated HCP-1 is observed in response to the increase in heme, but a commensurate elevation in HO-1 that could mediate appropriate heme dissolution was not detected, and in fact trended lower in hemorrhagic tissue regions. Additionally, the heme and iron may drive increased ROS generation, which together provide a stimulus to react with nitric oxide, lowering its bioavailability for vessel dilatation. A compensatory increase in eNOS was also shown and is hypothesized to be an unsuccessful attempt to recover the NO balance. Such an imbalance in NO homeostasis leads to a reduction in regional myocardial perfusion, which may also additionally stimulate VEGF to drive neovascularization (which has been activated throughout the MI recovery process). However, VEGF also has the ability to increase vascular permeability, which may instigate a positive feedback cycle, causing more leakage of RBCs and heme from the struggling vessels.
Pill Image is licensed under CC BY-NC

Therefore, we hypothesized that the rest perfusion in chronic hemorrhagic myocardial infarctions compared to non-hemorrhagic counterparts is significantly lower and that such

differences are based on the altered vascular microenvironment and state of nitric oxide constituents. We tested our hypothesis in chronic hemorrhagic MI patients and validated our observations in a clinically relevant animal model of hemorrhagic MI with the goal of ascertaining mechanistic details to gain insight into our observations in patients. In our patient cohort, we studied the presence of a hemorrhagic infarct-related impairment in local resting perfusion using CMR. We validated our findings in patients using a canine model of hemorrhagic infarction. The animal models allowed us to investigate the vascular microenvironment through correlative histological analyses of iron, nitric oxide, and endothelial cells to further elucidate the potential impact of iron-laden infarctions on vascular homeostasis. Our studies demonstrated that the perfusion within chronic hemorrhagic infarct zones were markedly reduced compared to non-hemorrhagic (hMI-) counterparts in patients, which was also confirmed in our canine model. We also found significant differences between hemorrhagic (hMI+) and non-hemorrhagic (hMI-) MIs with elevated NOS activity in hemorrhagic tissue, corresponding to relatively impaired resting perfusion in those same regions. Accordingly, our work uncovers new insights into the pathophysiological differences between hemorrhagic and non-hemorrhagic infarctions from the standpoint of perfusion in the infarcted myocardium in the chronic phase of MI. The findings here have the potential to forge new insights into the negative outcomes observed in patients with hemorrhagic MI and lay the groundwork for potential therapeutic targets for hemorrhagic MI patients.

2.3 Methods

2.3.1 Patient Studies

2.3.1.1 Study Population

Studies were approved by the Institutional Review Board of Foothills Medical Center (Calgary, AB, Canada) and all patients gave written informed consent prior to enrollment. Inclusion criteria were successful percutaneous intervention (PCI) achieving a TIMI flow grade 3 within 12 hours of symptom onset. The primary exclusion criteria were previous MI, arrhythmia, renal insufficiency, metallic prosthetic implant, and claustrophobia. Reperfused MI patients (n=14) were recruited following informed consent and were studied with CMR acutely at 3 days and at 6 months post-MI.

2.3.1.2 *Cardiac MRI Studies*

Cardiac MRI scans were acquired in a Siemens 1.5T (MAGNETOM Avanto) MRI system (Siemens Healthcare, Erlangan, Germany). Scouting localizers and shimming were performed prior to acquiring slice-matched short-axis T2*-weighted images, late gadolinium-enhancement (LGE), and first-pass perfusion (FPP) at rest. T2* and LGE protocols covered the whole heart, whereas rest perfusion scans were acquired over 3 mid-to-apical short-axis slices that were matched to T2* and LGE slices. Typical imaging parameters are shown in Table 2.1. T2* maps were constructed from multiple gradient-recalled echo (GRE) acquisitions (8 echoes) in CVI[42] from the T2* module using a nonlinear fitting algorithm. FPP images were acquired during infusion of 0.05 mmol/kg Gd contrast, followed by T1-weighted LGE images that were acquired 10 minutes post-infusion of an additional 0.15 mmol/kg Gd contrast (Magnevist, Bayer AG, Berlin, Germany) using

electrocardiogram (ECG)-gating and phase-sensitive inversion recovery (PSIR) reconstruction with GRE readouts. Slice thickness was 10mm for all sequences.

Table 2.1: CMR Parameters for clinical patient study.

	TR	TE	Flip angle	Readout bandwidth	In-plane resolution
T2* Mapping (6 echoes)	240 ms	2.6-13.7 ms (ΔTE=2.2ms)	10°	355 Hz/pixel	1.6 x 1.6 mm^2
LGE	1 R-R	3.32 ms	25°	235 Hz/pixel	1.6 x 1.6 mm^2
FPP	135 ms	0.99 ms	20°	1628 Hz/pixel	3.4 x 3.4 mm^2

2.3.2 Animal Studies

2.3.2.1 Animal Preparation

Canines (n=23; female, 20-25 kg) were studied according to the protocols approved by the Institutional Animal Care and Use Committee. All animals were subject to reperfused MI by complete occlusion of the left anterior descending artery distal to the first diagonal for 90-180 minutes followed by reperfusion. Animals surviving the MI underwent cardiac MRI within 5-7 days and at 8 weeks post reperfusion. Following the 8-week cardiac MRI, animals were humanely euthanized. Animal hearts were explanted, rinsed of residual blood, and fixed in formalin for histological sectioning and analysis. A subset of heart slices with evidence of hemorrhage were flash frozen immediately after rinsing (i.e., without formalin fixation) to accommodate protein analysis experiments (e.g., western blotting).

2.3.2.2 *Cardiac MRI Studies*

Cardiac MRI was performed in 1.5T (Espree) and 3.0T (Verio) MRI systems (Siemens Healthcare, Erlangen, Germany). Scouting localizers and shimming were performed prior to acquiring slice-matched short-axis T2*-weighted images, late gadolinium-enhancement (LGE), and first-pass perfusion (FPP) at rest. T2* and LGE protocols covered the whole heart, whereas rest perfusion scans were acquired over 3 mid-to-apical short-axis slices that were matched to T2* and LGE slices. Typical imaging parameters for 1.5T and 3.0T sequences are shown in Table 2.2 and Table 2.3, respectively. T2* maps were constructed from multiple gradient-recalled echo (GRE) acquisitions (8-12 echoes) in CVI[42] from the T2* module using a nonlinear fitting algorithm. FPP images were acquired during infusion of 0.05 mmol/kg Gd contrast, followed by T1-weighted LGE images that were acquired 10 minutes post-infusion of 0.15 mmol/kg Gd contrast (Magnevist, Bayer AG, Berlin, Germany) using electrocardiogram (ECG)-gating and phase-sensitive inversion recovery (PSIR) reconstruction. Slice thickness was 8 mm (1.5T) and 6 mm (3.0T). Slice-matched short-axis cines, T2* maps, and LGE images covering the full length of the left ventricle were acquired in that order.

Table 2.2: CMR Imaging Parameters for canine study at 1.5T.

1.5T Canine	**TR**	**TE**	**Flip angle**	**Readout bandwidth**	**In-plane resolution**
T2* Mapping (12 echoes)	211 ms	3.4 – 36.4 ms (ΔTE= 3.15 ms)	12	566 Hz/pixel	1.5 x 1.5 mm^2
LGE	1 R-R	1.83 ms	40	789 Hz/pixel	1.3 x 1.3 mm^2
FPP	194.07 ms	1.07 ms	50	1359 Hz/pixel	1.8 x 1.8 mm^2

Table 2.3: CMR Imaging Parameters for canine study at 3.0T.

3.0T Canine	TR	TE	Flip angle	Readout bandwidth	In-plane resolution
T2* Mapping (8 echoes)	79.66 ms	1.35-9.54 ms (ΔTE=1.17 ms)	12	1184 Hz/pixel	1.6 x 1.6 mm^2
LGE	1 R-R	2 ms	20	287 Hz/pixel	0.7 x 0.7 mm^2
FPP	161 ms	1.01 ms	12	977 Hz/pixel	1.7 x 1.7 mm^2

2.3.3 Histology and Immunohistochemistry

Histological and IHC stains show visual evidence of the targeted parameters in localized regions of interest that can be used to observe differences between hemorrhagic and non-hemorrhagic myocardial tissues. PECAM-1 (endothelial stain) depicts the microvascular network while Prussian Blue highlights ferric iron deposits in hemorrhagic myocardium. Nitric oxide synthase antibodies help elucidate potential NO imbalance discrepancies, while VEGF can identify neovascularization potential.

Apical sections of the canine hearts in the visually identified area of infarction were sliced, embedded in paraffin, then sectioned onto glass slides. Slides were stained with Prussian Blue using an Artisan™ iron stain kit (Agilent, Santa Clara, CA). Contiguous sections including PECAM-1 (CD31), VEGF and eNOS staining were processed according to a standard protocol (BioBank, Cedars Sinai Medical Center) detailed below that includes paraffinizing with EZ solution, antigen retrieval, endogenic peroxidase blocking, primary and secondary antibody incubation, and finally a chromogen 3,3'-Diaminobenzidine. Slides were treated with EZ Prep (Roche Ventana, Cat# 950-100) at 72°C for paraffin removal. Antigen retrieval was performed using a prediluted citrate

solution at pH 6.0 for 64 minutes at 91°C (Roche Ventana, Cat# 950-123). Slides were then blocked with an endogenic peroxidase block for 12 minutes at room temperature using Inhibitor CM (Roche Ventana, Cat# 760-4307). Primary antibody staining commenced with a mouse anti-PECAM-1 (H3) (Santa Cruz Biotechnology, sc-376764) monoclonal diluted 1:200, a mouse anti-eNOS monoclonal antibody (abcam, ab76198) diluted 1:1000 and mouse anti-VEGFA monoclonal antibody (abcam, ab1316) diluted 1:500 using antibody dilution buffer (Roche Ventana, ADB250), incubated for 1 hour at room temp. Antibody detection used DISC anti-mouse HQ RUO (Roche Ventana, Cat# 760-4814) for 12 min at 37°C, followed by DISC anti-HQ HRP RUO (Roche, Cat# 760-4820) for 12 min at room temp. Finally, a chromogen DAB CM (Roche, Cat# 760-4304) was applied for 12 min at room temp.

2.3.4 Stain Digitization

Quantifying the extent of microvascular density and corresponding iron deposition provides a basis on which to judge the interplay between iron burden and local perfusion deficits. Stained slides were digitized at 20x resolution on an Aperio ScanScope AT (Leica Biosystems, IL, USA). Infarct and remote regions were contoured in Aperio ImageScope (Leica Biosystems), and a grid contour pattern was drawn on the infarct zone for regional analysis of select slides. Stain quantification was performed on a subset of PB and CD31 slides using Visiopharm software (Visiopharm, CA, USA) to determine iron and microvascular content. Digital slides were scaled for resolution and registered using a custom software module, in which a gridded contour was scanned across the images to extract regional stain quantification measurements for direct comparison.

2.3.5 Western Blotting

Protein quantification was performed to identify eNOS and VEGF expression in tissues of interest, providing a quantitative validation of the immunohistochemical staining.

From the frozen myocardial tissue, remote, infarcted sections with and without evidence for iron were homogenized in RIPA buffer (Roche, USA) containing protease and phosphatase inhibitors, as previously described (*273, 274*), and then collected and stored at -80°C. Protein quantification was performed using BCA assay (Thermo Scientific) and equal amounts of protein lysates (~30 ug) were separated by SDS-PAGE and transferred onto a nitrocellulose membrane (GE Healthcare). Membranes were blocked with 5% milk or BSA at room temperature for 1 hour and incubated at 4°C overnight with primary antibodies. Primary antibodies for eNOS (32027S) and Phospho-eNOS (9571S) were purchased from Cell Signaling Technology (MA, USA), VEGF (ab1316) and Heme Oxygenase-1 (HO-1) (ab13248) (Abcam, MA, USA) and Heme Carrier Protein-1 (HCP-1) (sc-393460) was purchased from Santa Cruz Biotechnology (TX, USA). GAPDH (5174S) from Cell Signaling was used as a loading control. Immunoblots were then incubated with a secondary antibody conjugated to horse radish peroxidase (HRP) at room temperature for an hour and developed using ECL (Amersham Biosciences). Protein bands were normalized to either GAPDH (HCP-1, HO-1, VEGF) or eNOS (phospho-eNOS) and quantified using NIH-developed ImageJ software.

2.3.6 Image Analysis

Characterizing the state of the heart's viability (LGE) and function (FPP) are important not only to differentiate the subjects between hemorrhagic vs. non-hemorrhagic (T2*-weighted imaging)

groups, but also to provide a reliable index (normalized MPI) on which future comparisons can be made. Standard cardiac imaging sequences (T2*-weighted, FPP, LGE) were obtained for myocardial characterization. All images were analyzed in CVI[42] (Circle Cardiovascular Imaging, Calgary, Alberta, Canada). Myocardium was delineated with epi- and endo-myocardial, blood pool and reference ROI (infarct/remote) contours. Contours were then copied across LGE, T2*-weighted and FPP slices. Care was taken to ensure remote ROI contours avoided artifact-containing regions (e.g., inferior myocardial segments on T2*-weighted slices). Infarct segments matching slice location to rest perfusion slices were retrospectively categorized as hemorrhagic (hMI+) or non-hemorrhagic (hMI-) based on the presence of a hypointense region on T2*-weighted images within the area of infarction. Infarct regions on LGE images and iron-rich hemorrhagic regions on T2*-weighted images were segmented using mean+5SD (*275*) and mean-2SD (*64*) criteria, respectively. Magnetic field strength affects absolute T2* values, so reporting of absolute T2* values include the slices from animals imaged at 3.0T. For each perfusion imaging slice, a *normalized Myocardial Perfusion Index* (*Normalized* MPI)

$$Normalized\ MPI = \frac{Perfusion\ Index_{Infarct}}{Perfusion\ Index_{Remote}} \qquad \text{Equation 2.1}$$

was calculated as a ratio of the upslope of an ROI drawn to cover the extent of infarct (determined from LGE hyperintensity) and the upslope of the remote zone (ROI in an area distant from the infarct region), where the upslope is determined by a best-fit linear approximation of the slope of the signal intensity-time curve during contrast wash-in. Statistical significance was set at $p<0.05$, using a student's t-test to determine differences in perfusion between hMI+ and hMI- territories.

2.3.7 Statistical Analysis

All statistical analyses were performed using IBM SPSS Statistics, V.24 (Chicago, IL, USA). Continuous variables that passed the Shapiro-Wilk normality test are reported as mean ± standard error mean (SEM); otherwise, median and interquartile range (IQR) are used. Categorical variables are reported as values, along with percentages. The differences in baseline characteristics were assessed using Student's *t* test, applying the Welch-Satterthwaite method if the variances violated the homogeneity assumption assessed by Levene's Test. Absolute and relative differences between groups were evaluated using paired Student's *t*-test or independent samples *t*-test. All tests were two-tailed, and a p-value of <0.05 was used to determine statistical significance.

2.4 Results

Cardiac MRI findings (i.e., LVEF, MI size, hemorrhage volume, T2* values) are presented in Table 2.4. In patients, 34 acute and chronic first-pass perfusion slices with matching LGE and T2* were available for analysis, after excluding slices with extensive artifacts, poor signal-to-noise (SNR) ratio or mismatched slice positions. In total, 14 hemorrhagic and 20 non-hemorrhagic slices (set of LGE, T2*-weighted, and FPP) from 14 patients (5 hemorrhagic + 9 non-hemorrhagic) were available for analysis.

Table 2.4: MRI Characteristics for patient and canine data. Values are presented as mean ± SEM. Student's t-test was performed to determine statistical significance with a cutoff of p < 0.05.

	hMI+ [Mean ± SEM]	hMI- [Mean ± SEM]	p-value
Patients			
Acute LGE (%LV)	28.86 ± 3.23	20.86 ± 3.18	0.13
Chronic LGE (%LV)	20.41 ± 2.48	14.30 ± 2.33	0.12
Acute T2*-Based Hemorrhage Volume (%LV)	7.19 ± 1.27	3.49 ± 0.82	0.04
Chronic T2*-Based Hemorrhage Volume (%LV)	10.30 ± 2.62	1.73 ± 0.37	0.01
Acute T2* (ms)	16.13 ± 1.24	24.76 ± 1.76	< 0.01
Chronic T2* (ms)	19.15 ± 1.58	25.75 ± 2.00	0.04
Canines			
Acute LGE (%LV)	32.47 ± 2.64	17.19 ± 4.41	0.01
Chronic LGE (%LV)	13.44 ± 1.27	9.81 ± 2.05	0.18
Acute T2*-Based Hemorrhage Volume (%LV)	7.59 ± 1.25	1.64 ± 0.46	0.03
Chronic T2*-Based Hemorrhage Volume (%LV)	5.91 ± 0.81	1.94 ± 0.55	0.01
Acute T2* (ms) at 3.0T	15.01 ± 1.01	34.34 ± 4.50	< 0.001
Chronic T2* (ms) at 3.0T	17.21 ± 1.92	27.7 ± 1.37	< 0.01

From canine studies, 9 slice-matched LGE, T2*-weighted and FPP images at 1.5T were available, with an additional 56 slice-matched LGE, T2*-weighted and FPP images at 3.0T available for final analyses, after excluding slices with extensive artifacts, poor signal-to-noise (SNR) ratio or mismatched slice positions. In total, 50 hemorrhagic and 14 non-hemorrhagic slices (set of LGE,

T2*-weighted, and FPP) from 23 animals (18 hemorrhagic + 5 non-hemorrhagic). All animals identified to be hemorrhagic showed evidence of iron deposition within the infarction territory on T2*-weighted images, with Prussian Blue staining confirming presence of ferric iron in heart sections that were paraffin embedded. Animal hearts frozen for protein analysis showed visual evidence of hemorrhage. Infarct and LV characteristics are shown in Table 2.4.

2.4.1 Rest perfusion within MI territories in chronic MI patients depends on history of myocardial hemorrhage.

Myocardial perfusion is an important metric of myocardial function and is a key predictor of functional impairment. We investigated alterations in myocardial perfusion in patients with and without history of hemorrhage based on Normalized MPI. At 6-months post-PCI, we observed reduced myocardial perfusion in chronic MI patients with history of hemorrhagic MI compared to their non-hemorrhagic counterparts. This is shown for representative cases in Figure 2.2. Note the significant hypo-enhancement apparent within the MI zones of the hMI+ patient that is not evident in hMI- patient. Similarly, first-pass perfusion frames at peak myocardial enhancement displayed clear perfusion defects (hypo-enhanced zones) in the hMI+ group that were not evident in the hMI- group (Figure 2.2(E, J)). In aggregate, we found that the Normalized MPI in hMI+ patients was significantly lower than in hMI- patients (0.72 ± 0.03 vs. 0.83 ± 0.02; p=0.002) with a difference of 0.11 (95% CI, 0.05 to 0.18), shown in Figure 2.2L. T2* values were mildly correlated with normalized MPI, shown in the regression plot in Figure 2.2M.

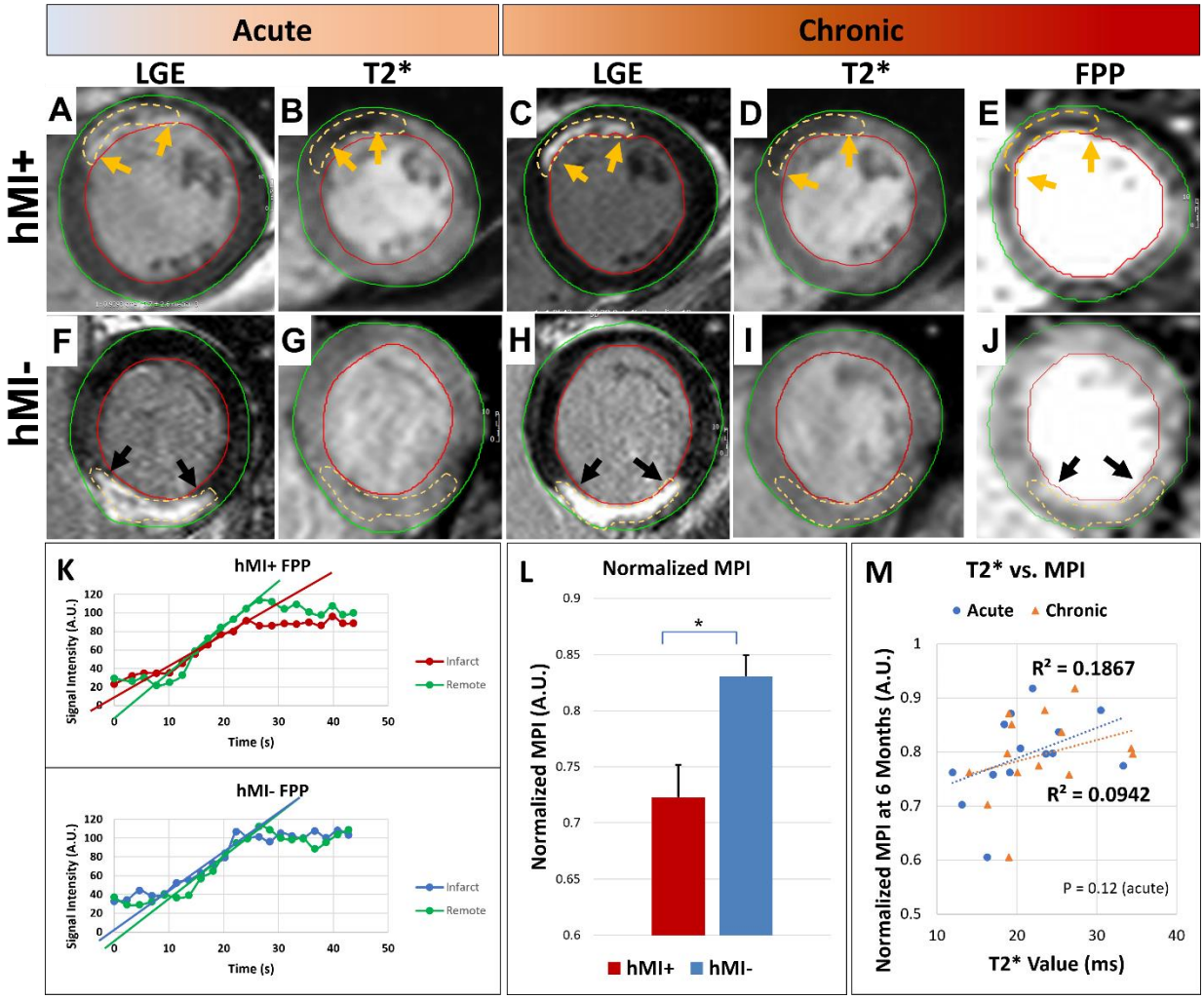

*Figure 2.2: Representative CMR images from hemorrhagic MI patient (hMI+, A-E) and non-hemorrhagic MI patient (hMI-, F-J) in acute (A,B,F,G, 3-days post-MI) and chronic phase (C-E, H-J, 6-months post-MI). **A, C**: LGE slice showing a large anterior-wall MI (arc subtended by orange arrows). **B, D**: Slice-matched T2*-weighted image showing significant hypo-enhancement in MI zone. **E**: First-pass perfusion (FPP) frame showing significant perfusion defect in hMI+ zone at peak myocardial enhancement. **F, H**: LGE slice showing the large inferior-wall infarction (black arrows). **G, I**: Slice-matched T2*-weighted image without hypo-enhancement in the infarct zone (black arrows). **J**: FPP frame without the visible perfusion defect at peak myocardial enhancement seen in hMI+ case (E). **K:** Representative perfusion index curves from hMI+ and hMI- patients. Maximum slope during contrast wash-in is visualized in remote (green), hemorrhagic (red), and non-hemorrhagic (blue) infarcted ROIs. **L:** Normalized Myocardial Perfusion Index at rest in the chronic MI zones of hMI+ and hMI- patients. **M:** Absolute T2* values at 3 days (blue) and 6 months (orange) compared with Normalized MPI.*

2.4.2 Rest perfusion defects in canines with chronic hemorrhagic MIs resembles the findings in patients.

Following the patient data described above, we investigated similar alterations in myocardial perfusion in canines with and without history of hemorrhage. At 8-weeks post-PCI, we observed

reduced myocardial perfusion in chronic MI animals with history of hemorrhagic MI compared to their non-hemorrhagic counterparts. This is shown for representative cases in Figure 2.3. As with the patient data, normalized MPI results were observable by the naked eye – T2*-weighted slices showed stark differences among hMI+ and hMI- groups in the infarct region, with the hMI+ group displaying marked hypo-enhancement (hemorrhagic core) not visualized in the hMI- group, and the FPP frames at peak myocardial enhancement demonstrated perfusion defects in the hMI+ group that were much less pronounced in the hMI- group (Figure 2.3). Consistent with the patient data, normalized MPI in hMI+ canines was significantly lower than in hMI- canines (0.62 ± 0.02 vs. 0.85 ± 0.04, $p < 0.001$), with a difference of 0.23 (95% CI, 0.14 to 0.32), Figure 2.3L. In the animals imaged at 3.0T, T2* values were moderately correlated with normalized MPI, shown in the regression plot in Figure 2.3M.

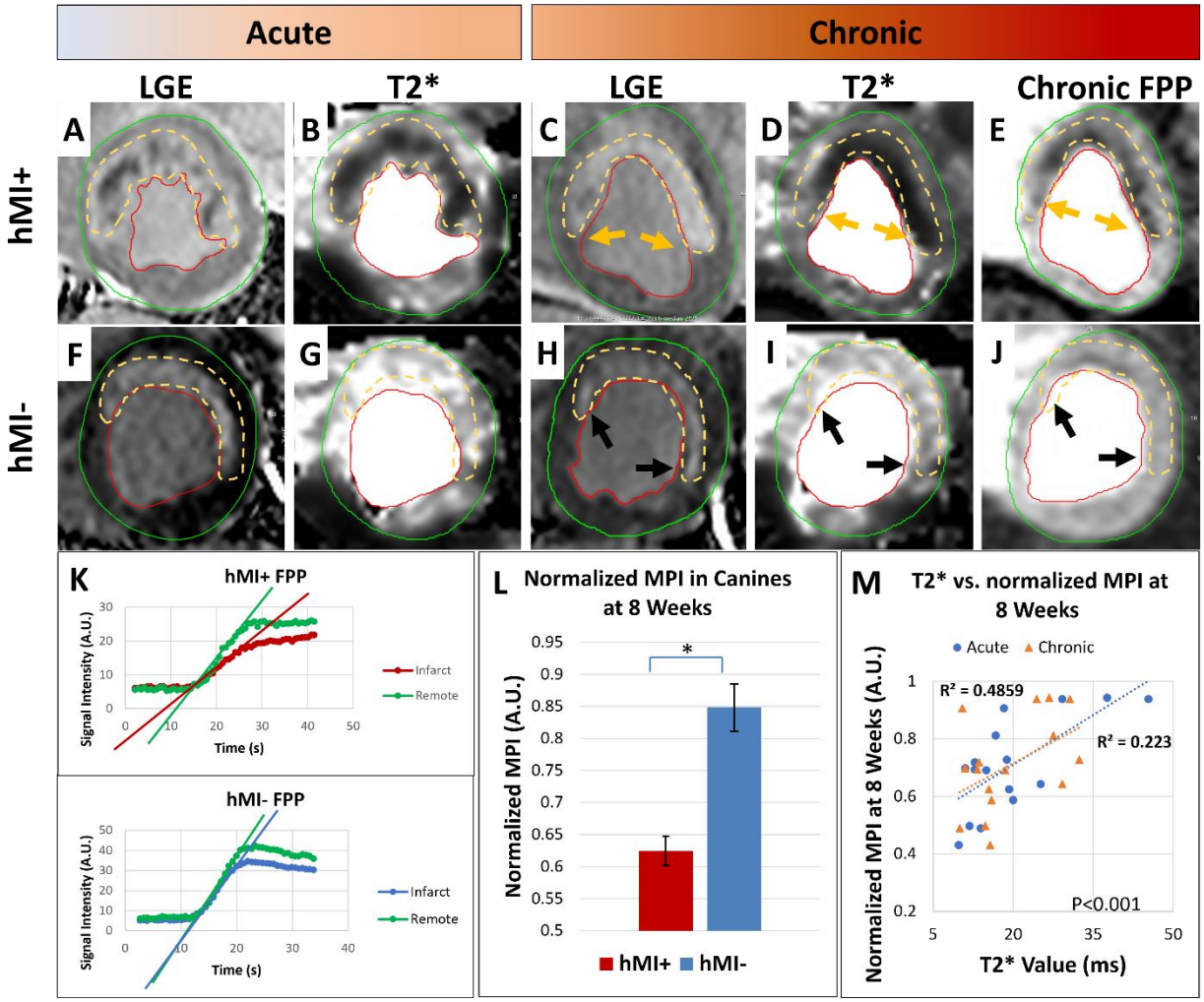

Figure 2.3: Representative CMR images from hemorrhagic MI animals (hMI+, A-E) and non-hemorrhagic MI animals (hMI-, F-J) in acute (A,B,F,G, 3-7 days post-MI) and chronic phase (C-E, H-J, 8-weeks post-MI). ***A, C:*** *LGE slice showing a large anterior-wall MI (arc subtended by yellow arrows).* ***B, D:*** *Slice-matched T2*-weighted image showing significant hypo-enhancement in MI zone.* ***E:*** *First-pass perfusion (FPP) frame showing significant perfusion defect in hMI+ zone at peak myocardial enhancement.* ***F, H:*** *LGE slice showing a large anterior infarction (yellow arrows).* ***G, I:*** *Slice-matched T2*-weighted image with minimal hypo-enhancement in the infarct zone (yellow arrows).* ***J:*** *FPP frame without the visible perfusion defect at peak myocardial enhancement seen in hMI+ case (E).* ***K:*** *Representative perfusion index curves from hMI+ and hMI- animals. Maximum slope during contrast wash-in is visualized in remote (green), hemorrhagic (red), and non-hemorrhagic (blue) infarcted ROIs.* ***L:*** *Normalized MPI in canines (n=22) with hemorrhage (0.62 ± 0.16) and without hemorrhage (0.85 ± 0.14) after 8 weeks post-infarction. Student's t-test resulted in a significant difference between the groups with a p-value < 0.001.* ***M:*** *Absolute T2* values at 3.0T at 3 days (blue) and 8 weeks (orange) compared with Normalized MPI.*

2.4.3 Capillary density within chronic MI territories is correlated with density of iron residues.

Previous studies have shown that hemorrhagic MIs resolve into chronic MI territories with localized iron deposits (*88*). We investigated whether there is any difference in capillary density between chronic MI territories with and without iron using Prussian blue (to stain for ferric iron)

and PECAM-1 (CD31, to stain for capillary density) (*276*). Chronic hemorrhagic infarct regions showed significant presence of Prussian blue stained iron, whereas non-hemorrhagic tissues lacked this iron in the infarct regions. Remote regions were free of Prussian Blue staining in both groups. CD31-stained vessels in the infarct region were positively correlated with density of iron from contiguous Prussian Blue stained slides in corresponding regions (Figure 2.4).

2.4.4 Heme carrier protein 1 expression but not heme oxygenase 1 was elevated within hemorrhagic MIs.

The expression of heme carrier protein 1 (HCP-1) is known to be translationally regulated by iron levels and HCP-1 has been shown to be localized to the cytoplasm in conditions with excess iron (*277*). HCP-1 regulation has also been associated with NO. Therefore, we assessed the expression levels of HCP-1 from non-hemorrhagic and hemorrhagic infarcts. Western blots containing HCP-1 showed significantly elevated expression levels in hemorrhagic infarct regions, as compared with non-hemorrhagic infarct regions (0.54 ± 0.07 vs. 0.16 ± 0.04, respectively; $p = 0.04$), shown in Figure 2.4C. The role of HO-1 in hemorrhagic infarction is not clear, however it would be reasonable to expect a change in HO-1 expression in relation to the iron levels and HCP-1 expression. However, HO-1 western blots did not show significant differences between hemorrhagic and non-hemorrhagic regions (0.47 ± 0.05 vs. 0.64 ± 0.08, respectively; $p > 0.05$).

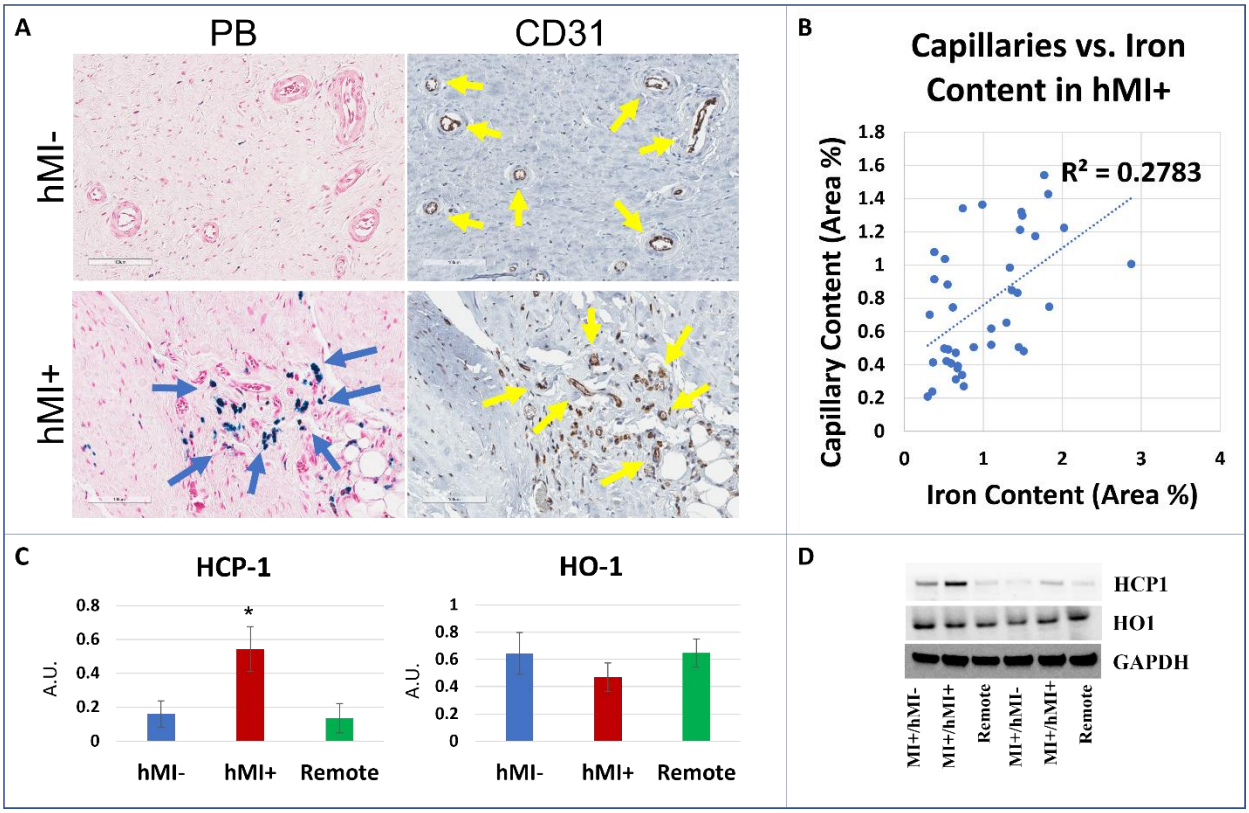

Figure 2.4: Prussian Blue vs. CD31 with HCP-1 and HO-1 IHC and Western Blot Analysis. ***A:*** *Histological staining of Prussian Blue (PB, blue arrows) and endothelial cells (CD31, yellow arrows) in hMI+ and hMI- tissue slices.* ***B:*** *In the hMI+ tissues, quantitative analysis of iron content and capillary content show the correlation between capillaries and iron deposition, indicating that hemorrhagic territories are vascularized, and iron is colocalized with microvasculature.* ***C:*** *HCP-1 and HO-1 protein expression in hemorrhagic, non-hemorrhagic, and remote regions of excised cardiac tissue. HCP-1 showed significant elevation in the hemorrhagic tissue relative to non-hemorrhagic or remote.* ***D:*** *Western Blot from HCP-1 and HO-1 analyses with GAPDH used as a loading control.*

2.4.5 Endothelial nitric oxide synthase activity was elevated in chronic hemorrhagic MI regions.

Nitric oxide bioavailability has been shown to be influenced by imbalances in the iron regulatory state in renal injury (*278*), but this has not been studied in the setting of chronic MI. We therefore investigated the differential behavior of nitric oxide synthase in chronic hMI+ and hMI- tissues as a marker of nitric oxide imbalance. Immunohistochemistry results revealed that vessels in the hMI+ zones had elevated levels of eNOS expression, whereas similar vessels in the hMI- regions did not show significant levels of eNOS expression (Figure 2.5C-D). Phosphorylated eNOS (phospho-eNOS) expression provided further detail on the activation status of these synthases.

Levels of phospho-eNOS expression, normalized to total eNOS (Figure 2.5E), indicated a significant elevation in phospho-eNOS in hemorrhagic myocardial regions relative to non-hemorrhagic infarct regions (1.23 ± 0.11 vs. 0.83 ± 0.08, respectively; p = 0.038). Logically, a perfusion deficit linked to NO imbalance could trigger a reactive increase in NOS expression attempting to rescue the perfusion anomaly. The fact that we detect this increase in NOS, but still have a perfusion defect presents an exciting target for future investigations.

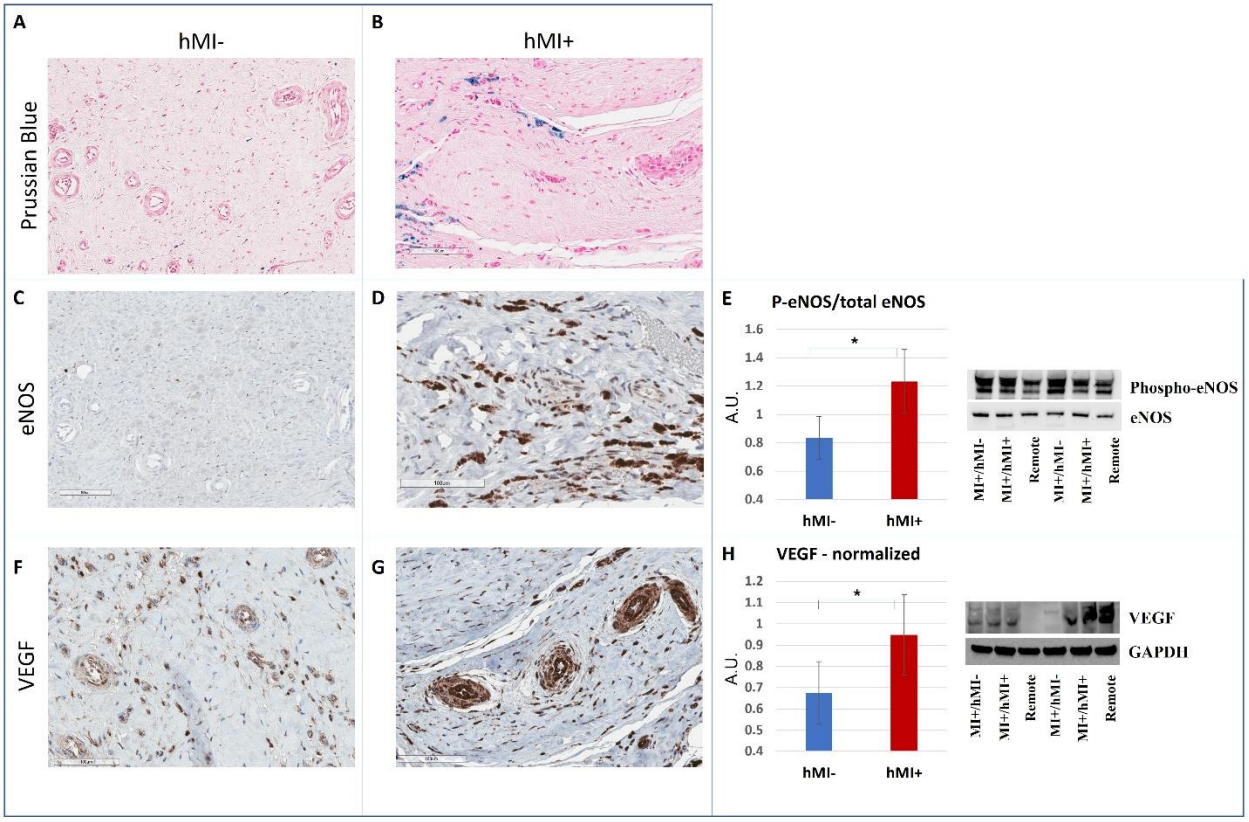

Figure 2.5: Prussian Blue, eNOS, and VEGF staining with Western Blot Analysis. ***A, B:*** *Prussian Blue (PB) stain showing iron content in hMI+ and hMI- tissue regions. PB stains verify that iron is present in hMI+, but not in hMI-.* ***C, D:*** *Endothelial nitric oxide synthase (eNOS) expression in region localized to area of PB images, showing significant presence in hMI+ tissue.* ***E:*** *Phospho-eNOS protein expression, normalized to eNOS, showed significant elevation in hMI+ tissues in western blot validation.* ***F-H:*** *Vascular endothelial growth factor (VEGF) expression in region localized to area of PB images, showing significant elevation in hMI+ tissue, validated by western blot (H).*

2.4.6 VEGF expression within chronic hemorrhagic MI is elevated compared to non-hemorrhagic MI.

Vascular endothelial growth factors are known to have a multitude of functions in the process of MI recovery. We therefore investigated the VEGF expression levels in both hMI+ and hMI- regions. VEGF staining was stronger in the hemorrhagic infarct territories compared with the non-hemorrhagic infarct territories (Figure 2.5F-G). Western blot results confirm this visual evidence, with significantly higher levels of VEGF found in hemorrhagic infarct tissue compared with non-hemorrhagic infarct tissue (0.95 ± 0.09 vs. 0.68 ± 0.07, respectively; $p = 0.009$) (Figure 2.5H). Angiogenesis, promoted by VEGF activity, should boost microvascular expansion to assist local perfusion defects by enhancing blood flow to these areas. The hemorrhagic myocardium seems to be reacting in a compensatory fashion by stimulating angiogenesis via VEGF, yet the perfusion defect is not rescued in these chronic infarction populations.

2.5 Discussion

Recently Borlotti et al. investigated resting perfusion in patient cohort, using T2-weighted MRI as the basis for hemorrhage identification (*92*). In their work, the investigators showed corrected myocardial blood flow (MBF) in the culprit region to best predict LV dysfunction at 6 months. However, T2-weighted MRI for imaging hemorrhage has some confounding factors, such as sensitivity to edema, and T2*-weighted MRI and T2* mapping is considered to be the gold standard (*62, 122, 279*). Similarly, we first set out to confirm our preliminary hypothesis that hemorrhagic infarction territories would have resting perfusion defects in a patient cohort of reperfused ST-elevated MI, which was indexed on the basis of Normalized MPI. We additionally

showed the effect translated well in a canine model of reperfused myocardial infarction, which will allow for future development of therapeutics to lessen the severity and impact on this subset of MI patients. Additionally, future studies may investigate baseline signal intensity variations caused by surface coil inhomogeneities in a hemorrhagic MI population, and the resulting impact of baseline correction methods on normalized resting perfusion indices.

Having confirmed our initial hypothesis across both a patient cohort and animal model, we then investigated the tissue level changes occurring during hemorrhagic MIs, to better understand the pathophysiology and elucidate any potential mechanistic differences. To accomplish this, we performed a series of histological, immunohistochemical, and western blot experiments designed to evaluate the local, tissue-level environment. Having previously reported that iron is preferentially deposited in chronic hemorrhagic infarctions (*88*), we first evaluated our T2*-weighted MRI findings by staining for iron with Prussian Blue, as well as with a PECAM-1 stain to highlight regional vasculature, which showed significant iron (Fe^{3+}) deposits in territories of hemorrhagic infarction. From Western Blotting analysis, we investigated the protein expression of two constituents involved in iron metabolism, HCP-1 and HO-1, to provide insight into the hemorrhagic infarction molecular mechanisms surrounding heme-iron and its breakdown products (biliverdin, CO, and free iron). HCP-1 is a known heme-iron transporter that can be induced in hypoxic conditions. Additionally, Gnana-Prakasam et al. showed in a study of hemochromatosis leading to iron overload in the retina of mice that HCP-1 became upregulated (*280*), an indication that HCP-1 may play a role in the iron overload induced by hemorrhagic myocardial infarction. Nitric oxide, a constituent which we have shown plays a role in hemorrhagic MI, has also been shown to be involved in the regulation of HCP-1 expression via

the stabilization of HIF-1α. Our observed elevation in HCP-1 protein expression in the hemorrhagic infarct territories confirmed the presence of persistent heme-iron in these tissues, but may have a more complex role in the introduction of heme-iron compounds to the fragile infarct territory, as heme itself is also pro-inflammatory and cytotoxic, driving endothelial cell injury and heme-induced inflammatory pathologies (*281*). HO-1 expression has been studied in the context of ischemia reperfusion injury in heart transplant patients, with suggestions that the CO produced by its activity is protective (*282*). However, other studies have indicated that the oxidation end-products of HO-1 contribute to vasospasm in the cerebral vessels of the visual cortex (*272*). HO-1 inhibition has also been investigated as a potential therapeutic target for limiting iron deposits by blocking the liberation of iron from the heme compound (*186*). In our study, the protein expression of HO-1 did not show a significant difference between hemorrhagic and non-hemorrhagic MI tissues. Although the cardioprotective effect of HO-1 has been well studied in the context of myocardial infarction generally, investigation of a role for HO-1 specifically in hemorrhagic infarction is limited. Therefore, based on our data from this study, we assume that the inability of a supplemental increase in HO-1 levels in a post-hemorrhagic MI setting could be mediating, at least in part, some of the chronic adverse cardiac effects observed in hMI. Nonetheless, further investigation is needed in this direction to unravel the underlying mechanisms of HO-1 signaling in hemorrhagic MI. In addition, the overall heme pathway in the setting of hemorrhagic infarction would require further targeted study to investigate its involvement in persistence of iron deposits and myocardial perfusion in hemorrhagic MI.

We further hypothesized that a nitric oxide imbalance may be implicated in the observed perfusion deficit effects in hemorrhagic infarctions, given NO's interaction with iron

(*283*) and ROS (*54*) in this setting. Briefly, previous studies have captured the capability of cell-free hemoglobin and heme-containing compounds to scavenge NO (*284, 285*), leading to a reduced state of bioavailability in these iron-overload conditions (e.g., Thalassemia, Hemochromatosis, Sickle Cell). Furthermore, iron deposits can then mediate reactive oxygen species generation via the Fenton reaction. A study by Drexler et al. investigated the effects of a NO inhibitor on the blood flow of infarcted rats and found that L-NMMA (basal NO inhibitor) had a blunted coronary vasoconstrictor effect in the chronic phase following larger MIs, which suggests a defect in the NO homeostasis (*286*). Glean et al. showed that non-reperfused CHF rats had reduced NO bioavailability and skeletal muscle vascular control was improved upon the introduction of nitrite (an NO precursor) (*287*). Given that that study involved non-reperfused animals, which therefore would contain non-hemorrhagic infarcts, it would be logical to conclude that the iron deposits in chronic hemorrhagic infarctions could further exacerbate this impaired vascular control. Vinchi et al. showed that hemopexin (a heme scavenger) could rescue the nitric oxide bioavailability in a heme overloaded mouse model (*288*), showing the potential for the modulation of NO homeostasis via heme levels, which may then have the potential to impact local perfusion defects. Finally, a study in a rat model of iron-overloaded renal injury showed that not only was NO bioavailability reduced, but there was a compensatory increase in both eNOS and iNOS expression (*278*). Indeed, we found that endothelial NOS was being preferentially activated in hMI+ tissues, likely an effect of the rapid consumption of nitric oxide by local iron deposits and reactive oxygen species, and potentially acting in a compensatory fashion. Together, this would have an effect that significantly contributes to the dearth in bioavailability of the NO constituents. Combined, these upregulated responses indicate a hemorrhagic infarction-specific

dysfunction in the nitric oxide pathway, motivated by a complex interaction between chronic local iron deposits, reactive oxygen species, nitric oxide constituents and a damaged microvascular network.

Vascular endothelial growth factors (VEGF) consist of a family of proteins with a wide range of effects, and their therapeutic potential as injectable agents in chronic coronary artery disease has been extensively investigated in both animals and clinical trials (*289*). In the ischemic myocardium, VEGF is involved early in the recovery process after acute myocardial infarctions in a capacity thought to enhance the delivery of inflammatory cells to the ischemic territory via loosening of the endothelial cell barriers (*203*), as well as its commonly understood role of promoting angiogenesis. While animal studies have shown promising improvements in cardiac function, randomized clinical trials of angiogenic growth factors have had mixed results (*203*). However, there have not been targeted trials of patients with acute MI or even more specifically, hemorrhagic MI. The chronic elevation in VEGF protein expression in hemorrhagic infarction territories that we identified exemplifies an environment that appears persistently pro-angiogenic, likely compensatory to the perfusion deficits in these regions, yet the perfusion remains depressed despite this elevation in VEGF. Confoundingly, this elevated VEGF expression in chronic hemorrhagic MIs may potentially be acting as a trigger for loosened endothelial barriers in the chronic phase, contributing to further endothelial dysfunction.

Given our hypothesis of iron-driven vascular dysfunction in chronic hemorrhagic MIs, as described in detail above, we studied a subset of dogs with hemorrhagic MI that received DFP in order to modulate the iron content in chronic hemorrhagic MI. Removal of the iron trigger could then beneficially impact the downstream effects on nitric oxide balance and vasodilatory

impairment. DFP has been shown to be highly efficacious in the removal of cardiac iron in numerous clinical studies (*290-294*). A study by Behrouzi et al. examined the effects of DFP on a porcine model of hemorrhagic MI (*205*), resulting in early resolution of hemorrhage and edema as well as reduced ventricular enlargement and hypertrophy in animals in the DFP group. In the present study, we have shown the potential of DFP to rescue resting perfusion defects in a hemorrhagic MI canine model. At 8 weeks, the normalized MPI of animals that received DFP was significantly elevated compared with hMI+ animals that did not. However, the normalized MPI values did not reach those of hMI- animals, which could be due to a separate mechanism impacting the perfusion defect independent of the iron-driven pathway described here. A study by Duffy et al. looked at the potential of another iron chelator, Deferoxamine (DFO), to improve endothelial function of forearm resistance vessels in patients with coronary artery disease (CAD), showing the dichotomy between endothelium-dependent and endothelium-independent effects of the iron chelation (*295*).

2.6 Conclusion

Major adverse cardiac events (MACE) present a significant hurdle in the prognosis of hemorrhagic myocardial infarctions. Elucidating the pathological relationships alongside noninvasive imaging biomarkers in hemorrhagic myocardial infarctions can help promote understanding and drive therapeutic developments in these severe types of infarctions. This study is the first, to our knowledge, to investigate the impact of iron-driven damages in hemorrhagic myocardial infarctions on the nitric oxide microenvironment and related physiological markers of heme metabolism and neovascularization in relation to resting myocardial perfusion defects. As such,

the results described herein constitute a significant step in linking hMI to the observed adverse outcomes in this patient population. Accordingly, we lay the groundwork for further investigations into the pathophysiological effects surrounding hemorrhagic infarctions, as well as novel therapeutics targeting these pathways.

Chapter 3: Deferiprone Iron Chelation Therapy for Chronic Hemorrhagic Myocardial Infarctions

3.1 Abstract

Background: Iron chelators have been shown to be effective in a variety of iron-overload disorders. Chronic iron deposition in hemorrhagic myocardial infarction (MI) subjects is associated with defects in resting perfusion. This study aimed to assess the impact of iron chelation via Deferiprone (DFP) on a canine model of chronic hemorrhagic MI.

Methods and Results: 22 canines underwent ischemia reperfusion surgery with 180 minutes of LAD occlusion to produce hemorrhagic infarctions. The treatment group received DFP (30-40 mg/kg, BID) beginning after surgery and continuing for 8 weeks. Animals were followed with MRI scans at 7 days and 8 weeks, with 8 of the animals continuing with an additional chronic study at 6 months. Resting perfusion at 8 weeks was significantly elevated in DFP-treated animals compared to controls (0.75 ± 0.03 vs. 0.59 ± 0.02, respectively; $p < 0.01$), whereas resting perfusion at 6 months was not significantly different between groups (0.59 ± 0.09 vs. 0.52 ± 0.06, $p = 0.55$). LV volume analysis showed potential benefits for improved LV remodeling in the DFP group at 6 months, with end-diastolic LV mass significantly reduced relative to controls (71.77 ± 3.27 vs. 94.05 ± 6.08, respectively; p = 0.02).

Conclusion: This is the first study to show the potential for iron chelation via DFP in hemorrhagic MI to mitigate resting perfusion defects in chronically infarcted animals. This has important

implications toward uncovering the causal relationship between hemorrhagic MIs and major adverse cardiovascular events (MACE).

3.2 Introduction

As discussed in Chapter 1, iron plays a crucial role in numerous biological functions and its balance is therefore tightly controlled. Both iron deprivation and overload cause dysregulation of the normal function of organ systems throughout the body. In the case of iron overload in thalassemia patients, several studies have investigated the potential of treatment with iron chelation to limit iron-induced complications (*291, 294, 296, 297*). Improvement in the availability of chelators and assessment of iron overload via MRI (particularly in the heart and liver) has been attributed to improved disease management, allowing for near-normalization of life expectancies in this population (*296*). Additionally, iron overload has been implicated in the incidence of CAD and cancer, as well as cardiac complications stemming from both cardiac and non-cardiac morbidities (*88, 182-184, 197, 199-202, 206*).

During incidences of IMH, RBCs extravasate into the myocardial interstitium, eventually externalizing heme and iron. Studies by Kali et al. and Bulluck et al. have shown the progression of acute IMH into chronic iron deposition leading to prolonged inflammation and adverse remodeling of the LV (*88, 197*). Several iron chelators exist clinically, including Deferoxamine (DFO), Deferasirox (DFX), and Deferiprone (DFP), which each have distinct characteristics. Namely, DFP is available as an oral tablet and is the smallest molecule chelator of the three, allowing improved membrane permeability and myocardial efficacy, compared with the larger, short-acting, subcutaneous administration of DFO (*298-301*). DFX is the most recently developed

chelator, with a longer half-life than DFP, although its efficacy in iron removal following IMH has not been validated (*302*). Pepe et al. studied DFP, DFO, and DFX in the treatment of thalassemia major patients, showing DFP to have the highest efficacy in removing cardiac iron, while DFX showed promising results in controlling liver iron (*294*). Recently, Behrouzi et al. investigated the action of iron chelation with DFP in a porcine model of I/R injury, showing that while infarct size was not changed, hemorrhage resolution and adverse remodeling were improved in the chelated animals (*205*). However, the study failed to show functional improvement at 1-month post-MI. A retrospective study by Pennell et al. of iron-chelated thalassemia patients showed a reduced risk of HF in concordance with their improvement in LVEF (*301*), which may be correlated to improved mitochondrial function by limiting the impact of free iron (*296*).

In Chapter 2, we have shown that iron-laden myocardial infarctions in the chronic phase succumb to defects in resting perfusion even though compensatory response pathways are preferentially activated, which we theorize would restore normal rest perfusion in the absence of iron. The continued presence and deposition of iron in chronic MI confounded by IMH is hypothesized to be a key driver of adverse remodeling via perfusion deficits at rest, furthering adverse remodeling and cardiac rhythm anomalies. Therefore, in this canine model study of chronic hemorrhagic MI, we propose that iron chelation via DFP will abrogate the resting perfusion defects in animals with chronic iron deposition, providing an impetus for improved functional and anatomical recovery of the LV. To study this, we followed 22 canines through an 8-week course of DFP treatment with CMR scans in the acute (5-7 days) and chronic (8 weeks) phase post-MI. Given the consensus that the iron chelator must be consistently present in the body to optimally limit iron-induced damage (*296, 303*), we followed a subset of animals (n=8) for 6 months to further investigate the dynamic

evolution of resting perfusion beyond the end of the iron chelation therapy. The 6-month study further isolates the driving factors behind the defects in rest perfusion in these subjects.

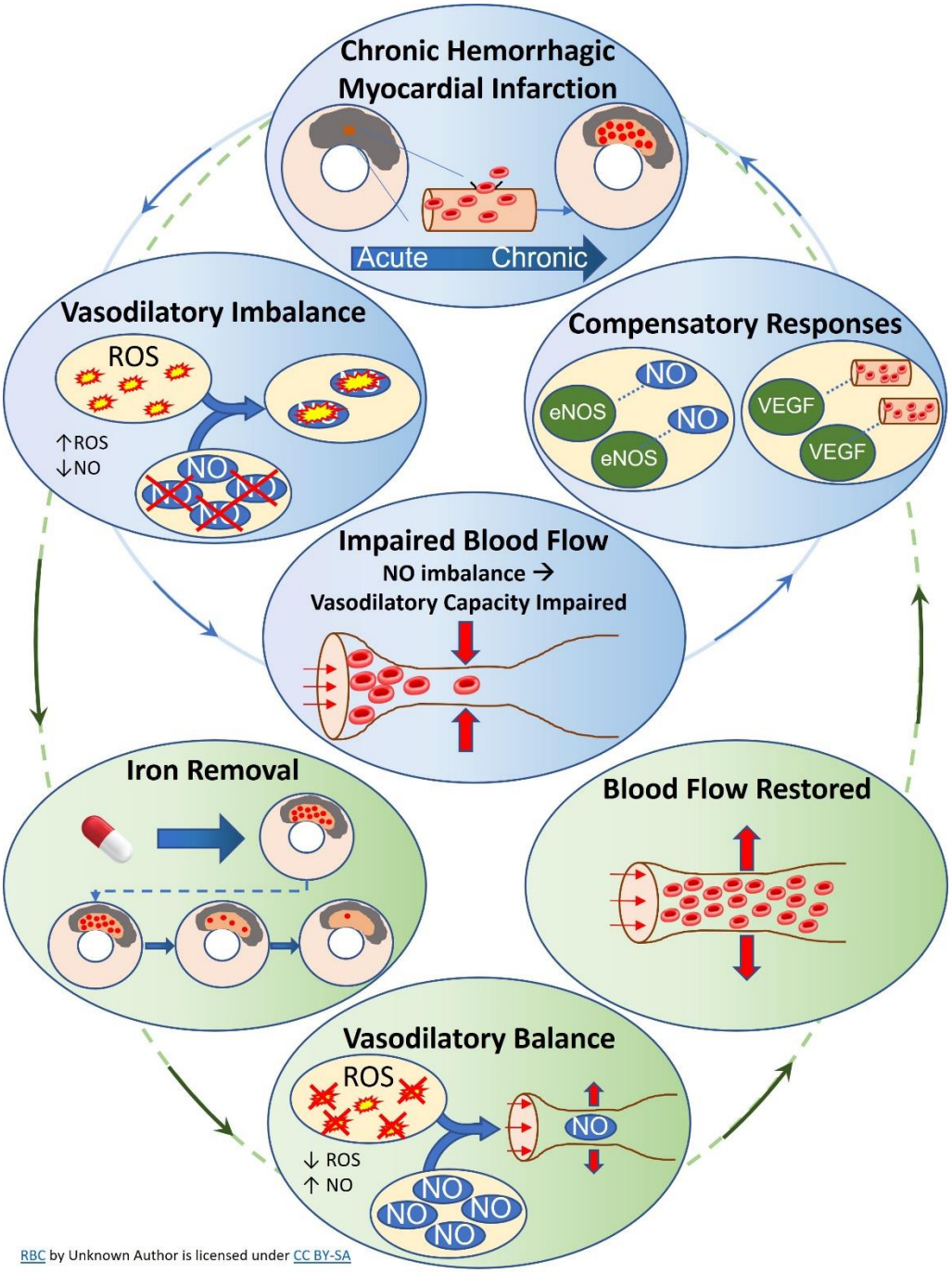

Figure 3.1: Proposed Mechanism for the Impact of Iron Chelation on Rest Perfusion. The figure shows how iron removal via DFP modulates the myocardial microvasculature, leading to improved resting perfusion. Pill Image is licensed under CC BY-NC. RBC Image is licensed under CC BY-SA

3.3 Methods

3.3.1 Animal Studies

3.3.1.1 Animal Preparation

Canines (n=22; female, 20-25 kg) were studied according to the protocols approved by the Institutional Animal Care and Use Committee. All animals were subject to reperfused MI via complete occlusion of the left anterior descending artery distal to the first diagonal for 180 minutes followed by artery reopening, as described previously (*88*). Briefly, the heart was exposed via lateral thoracotomy and a suture ligated the LAD. Infarction was confirmed visually and via ST-segment elevation on the ECG. Animals underwent cardiac MRI within 5-7 days and at 8 weeks post reperfusion, while 8 animals were additionally followed for extended chronic studies at 6 months post-MI. Following the final cardiac MRI, animals were humanely euthanized. Animal hearts were explanted, rinsed of residual blood, and fixed in formalin for histological sectioning and analysis.

3.3.1.2 Cardiac MRI Studies

Cardiac MRI was performed in 1.5T (Espree) and 3.0T (Verio, Biograph) MRI systems (Siemens Healthcare, Erlangen, Germany). Scouting localizers and shimming were performed prior to acquiring slice-matched cine, short-axis T2*-weighted, late gadolinium-enhancement (LGE), and first-pass perfusion (FPP) images at rest. Cine, T2*-weighted and LGE protocols covered the whole heart, whereas rest perfusion scans were acquired over 3 mid-to-apical short-axis slices

that were matched to T2*-weighted and LGE slices. Typical imaging parameters for 1.5T and 3.0T sequences are shown in Table 3.1 and Table 3.2, respectively. T2* maps were constructed from multiple gradient-recalled echo (GRE) acquisitions (8-12 echoes). FPP images were acquired during infusion of 0.05 mmol/kg Gd contrast, followed by T1-weighted LGE images that were acquired 10 minutes post-infusion of 0.15 mmol/kg Gd contrast (Magnevist, Bayer AG, Berlin, Germany) using electrocardiogram (ECG)-gating and phase-sensitive inversion recovery (PSIR) reconstruction. Slice thickness was 8 mm (1.5T) and 6 mm (3.0T).

Table 3.1: CMR Imaging Parameters for the canine study at 1.5T.

1.5T Canine	TR	TE	Flip angle	Readout bandwidth	In-plane resolution
Cine (23 phases)	21.84 ms	1.3 ms	67	930 Hz/pixel	0.6 x 0.6 mm^2
T2* Mapping (12 echoes)	211 ms	3.4 – 36.4 ms (ΔTE= 3.15 ms)	12	566 Hz/pixel	1.5 x 1.5 mm^2
LGE	1 R-R	1.83 ms	40	789 Hz/pixel	1.3 x 1.3 mm^2
FPP	194.07 ms	1.07 ms	50	1359 Hz/pixel	1.8 x 1.8 mm^2

Table 3.2: CMR Imaging Parameters for the canine study at 3.0T.

3.0T Canine	TR	TE	Flip angle	Readout bandwidth	In-plane resolution
Cine (25 phases)	2.66 ms	1.33 ms	50	1265 Hz/pixel	1.3 x 1.3 mm^2
T2* Mapping (8 echoes)	79.66 ms	1.35-9.54 ms (ΔTE=1.17 ms)	12	1184 Hz/pixel	1.6 x 1.6 mm^2
LGE	1 R-R	2 ms	20	287 Hz/pixel	0.7 x 0.7 mm^2
FPP	161 ms	1.01 ms	12	977 Hz/pixel	1.7 x 1.7 mm^2

Slice-matched short-axis cines, T2* maps, and LGE images covering the full length of the left ventricle were acquired in that order.

3.3.1.3 Iron Chelation

Following the surgical procedure, animals were administered an iron chelator, Deferiprone (DFP, $C_7H_9NO_2$, molecular weight 139 g/mol), to chelate both intra- and extracellular iron (Apopharma Inc., Toronto, ON, Canada) in the myocardium. Drug administration began on the day of surgery at a dose of 30-40 mg/kg (BID, PO) given twice per day at 8-hour intervals and continued for a duration of 8 weeks. This dose was selected based on the FDA-approved range for DFP used in clinical trials (i.e., 75-99 mg/kg/day). Animals were monitored for adverse reactions and side effects and dosage was adjusted if required. All animals included in the DFP group received the full dose for 8 weeks and did not experience significant reactions to the chelator (minor reactions in the acute stages included blood in the urinary output).

3.3.2 Image Analysis

Standard CMR imaging sequences (cine, T2*-weighted, FPP, LGE) were obtained at each MRI follow-up and imported into CVI[42] (Circle Cardiovascular Imaging, Calgary, Alberta, Canada) software for contouring, segmentation, and analysis. Cine image stacks were configured with endocardial and epicardial contours across phases and slices covering the entire LV. Phases corresponding to end-systole and end-diastole were automatically detected by the software and visually verified for accuracy. LV volumes (LVEDV, LVESV) and function (EF) were calculated based on the prescribed phases. For LGE, T2*-weighted, and FPP images, the myocardium was delineated with epi- and endo-myocardial, blood pool and reference ROI (infarct/remote)

contours. Contours were then copied across LGE, T2*-weighted, and FPP slices and adjusted as needed for trigger delay or artifact discrepancies. Care was taken to ensure ROI contours avoided artifact-containing regions (e.g., inferior myocardial segments on T2*-weighted slices). Infarct regions and iron-rich regions were identified using the criteria described previously. For each perfusion imaging slice, a *normalized Myocardial Perfusion Index* (*Normalized* MPI, Equation 1.1) was calculated as described in Chapter 2.

3.3.3 Statistical Analysis

Statistical tests were organized and executed in the IBM SPSS Statistics software, V.24 (Chicago, IL, USA). Data was checked for normal distribution using the Shapiro-Wilk normality test, applying the Welch-Satterthwaite method if the variances violated Levene's test for homogeneity of variance. The differences in unpaired group characteristics were assessed using Student's *t*-test, while change in FPP over time (i.e., change between 8 weeks and 6 months) was analyzed via a paired samples t-test. Data are reported as mean ± standard error mean (SEM), and all tests were two-tailed, using a p-value of <0.05 to determine statistical significance.

3.4 Results

3.4.1 Deferiprone partially abrogates rest perfusion defects in canines with hemorrhagic infarction at 8 weeks.

The iron chelator Deferiprone (DFP, ApoPharma) is known to bind both intra- and extracellular iron. Given the prevalence of iron deposition in chronic hemorrhagic infarctions, combined with its adverse vasodilatory effects described in Chapters 1 and 2, we investigated the potential of

iron removal via DFP to rectify chronic impairments in rest perfusion observed in hemorrhagic animals. Animals given DFP (PO, BID, 30-40 mg/kg) had significantly elevated (i.e., improved)

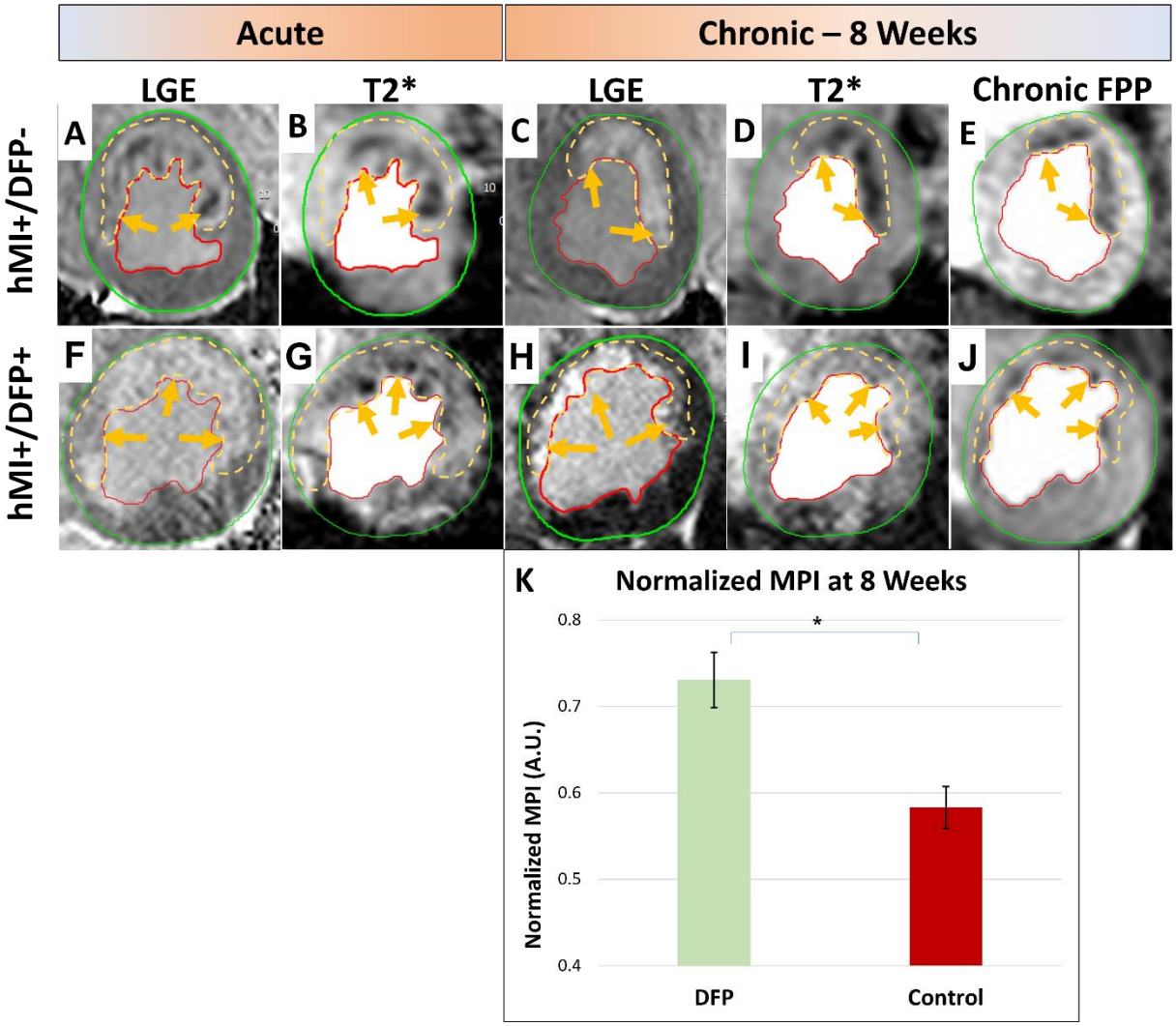

Figure 3.2: Iron Chelation Impact on Rest Perfusion.

Representative CMR images from non-chelated hMI+ animals (A-E) and chelated (DFP) hMI+ animals (F-J) in acute (A, B, F, G, 3-7 days post-MI) and chronic phase (C-E, H-J, 8-weeks post-MI). ***A, C:*** *LGE slice showing a large anterior-wall MI (arc subtended by yellow arrows).* ***B, D:*** *Slice-matched T2*-weighted image showing significant hypo-enhancement in MI zone.* ***E:*** *First-pass perfusion (FPP) frame showing significant perfusion defect in hMI+ zone at peak myocardial enhancement.* ***F, H:*** *LGE slice showing a large anterior infarction (yellow arrows).* ***G, I:*** *Slice-matched T2*-weighted image with lessening hypo-enhancement in the infarct zone (yellow arrows) as the infarct progresses from acute (G) to chronic (I).* ***J:*** *FPP frame with reduced perfusion defect at peak myocardial enhancement compared to the non-chelated animal (E).* ***K:*** *Normalized MPI in hMI+ canines with (n=8, 0.75) and without (n=12, 0.59) DFP chelation, 8 weeks post-infarction. Student's t-test resulted in a significant difference between the groups with a p-value < 0.01.*

normalized MPI compared with hemorrhagic animals that did not receive DFP (0.75 ± 0.03 vs. 0.59 ± 0.02, respectively; $p < 0.01$, Figure 3.2). While this level did not reach that of non-hemorrhagic animals (i.e., 0.85 ± 0.04, Chapter 2), it may yet provide significant benefits in alleviating adverse outcomes associated with perfusion defects in patients suffering hemorrhagic myocardial infarctions.

3.4.2 Rest Perfusion Defects Revert to non-chelated levels in the absence of DFP.

Scientific consensus is that consistent chelator presence is required to limit the adverse effects of excess iron (*296*). Following completion of the 8-week course of DFP, we investigated the extended chronic impacts of hemorrhagic MI on rest perfusion at 6 months. Specifically, whether improvements in rest perfusion at 8 weeks would persist at 6 months in the absence of continued iron chelation. There were 9 short-axis perfusion slices available for analysis in the non-DFP group, while 13 slices were available in the DFP group. Animals that received DFP for 8 weeks did not maintain significantly different normalized MPI at 6 months compared with animals that did not receive a course of DFP (0.59 ± 0.09 vs. 0.52 ± 0.06, respectively; $p = 0.55$, Figure 3.3).

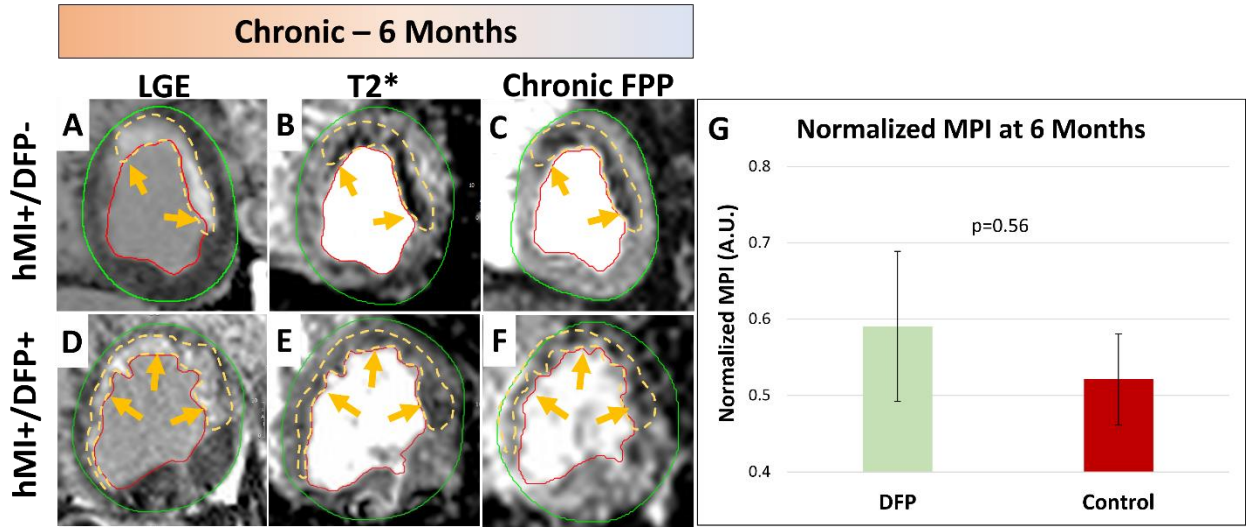

Figure 3.3. Iron Chelation – Extended Chronic Effects. DFP treatment was terminated at 8 weeks. There was no difference in normalized MPI between DFP and control groups at 6 months (0.59 ± 0.09 vs. 0.52 ± 0.06, respectively; p = 0.55).

Additionally, animals in the DFP group had significant decreases in normalized MPI between 8-weeks (0.73 ± 0.03) and 6-months (0.59 ± 0.09, p = 0.03), whereas the rest perfusion of animals in the control group did not change (0.58 ± 0.02 vs. 0.52 ± 0.06, p = 0.18).

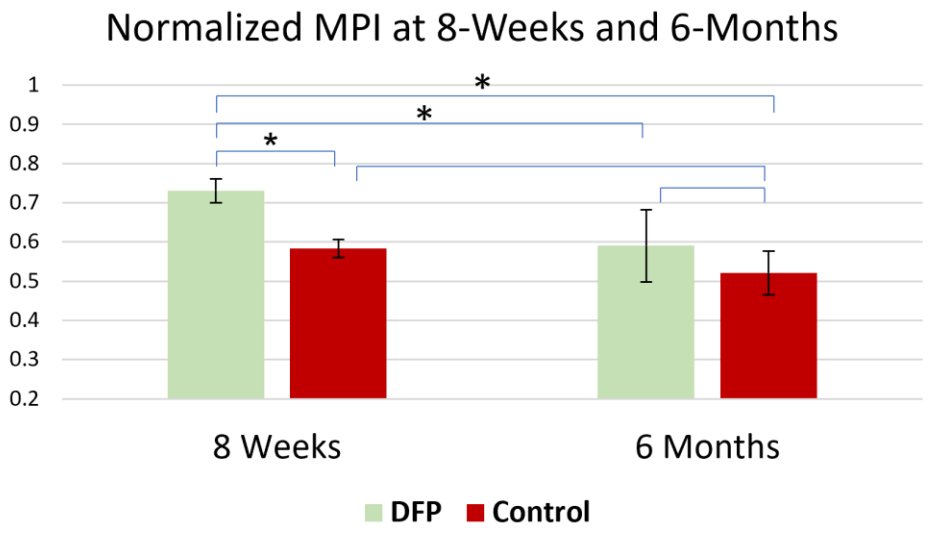

Figure 3.4: Normalized MPI Change From 8 Weeks to 6 Months. DFP-treated animals showed a significant change from 8 weeks to 6 months (p=0.03), whereas control animals did not show a significant change over time (p=0.18).

3.4.3 LV Remodeling Shows Differences at 6 Months

Analysis of LV volume parameters showed no difference between groups at 8 weeks or 6 months. Interestingly, LV mass analysis showed the DFP-treated group had significantly decreased end-diastolic mass at 6 months compared to animals that did not receive DFP ($p = 0.02$). Other parameters did not show statistical significance, although end-systolic mass also showed a strong trend toward a decrease in the DFP group at 6 months compared to controls ($p = 0.051$). Results are shown in

Table 3.3.

Table 3.3: LV remodeling parameters in DFP-treated vs untreated canines at day 7, week 8, and month 6 post-MI.

	DFP+ [Mean ± SEM]	DFP- [Mean ± SEM]	p-value
Day 7			
End-diastolic Volume (mL)	46.28 ± 1.38	53.64 ± 4.78	0.18
End-systolic Volume (mL)	27.22 ± 1.05	31.98 ± 3.48	0.23
End-diastolic Mass (g)	79.52 ± 1.65	94.84 ± 6.72	0.06
End-systolic Mass (g)	82.74 ± 1.71	97.09 ± 6.62	0.07
8 Weeks			
End-diastolic Volume (mL)	59.46 ± 5.09	52.29 ± 2.38	0.14
End-systolic Volume (mL)	36.08 ± 4.39	27.49 ± 2.20	0.08
End-diastolic Mass (g)	67.79 ± 4.28	77.87 ± 5.13	0.25
End-systolic Mass (g)	70.93 ± 4.37	81.66 ± 5.33	0.23
6 Months			
End-diastolic Volume (mL)	61.41 ± 4.06	69.48 ± 6.74	0.39
End-systolic Volume (mL)	40.52 ± 3.11	39.55 ± 5.06	0.89
End-diastolic Mass (g)	71.77 ± 3.27	94.05 ± 6.08	*0.02*
End-systolic Mass (g)	76.81 ± 3.32	97.14 ± 7.22	0.05

3.5 Discussion

While iron chelation therapy has become a cornerstone treatment for many iron-overload conditions, its use in the post-MI setting is still in its nascent stages. Given the extensive evidence of organ and vascular dysfunction resulting from iron imbalance, and the presence of elevated iron deposition in chronic MI, iron chelation becomes a promising target for treatment of

hemorrhagic MI patients. In this chronic study of iron chelation in a canine model of I/R injury and post-infarction remodeling, we have shown that removal of myocardial iron through chelation with DFP leads to significant normalization of resting myocardial perfusion in hemorrhagic MI animals. While our data did not show significant differences in functional parameters such as LVEF, the implications of improved resting perfusion are nonetheless significant, and may lead to decreased cardiac abnormalities and adverse events in a larger long-term study given the combined impact of chronic iron deposition and resting perfusion defects on cardiac dysfunction and adverse events. In their 4-week study of DFP in a porcine model of I/R injury, Behrouzi et al. showed a decrease in myocardial hypertrophy in the chelated group, indicating that LV remodeling may be influenced by iron chelation, while similarly finding no difference in LVEF.

Additionally, our data suggest that iron chelation may need to be maintained to elicit persistent benefits in myocardial perfusion, as termination of the DFP treatment at 8 weeks caused rest perfusion defects that had recovered at 8 weeks to resurface at 6 months, although end-diastolic mass was significantly elevated in the control animals indicating the potential for conserved LV remodeling in the DFP-treated group beyond the iron chelation regimen period. While the former finding may not be surprising given the scientific consensus regarding chelation therapy in systemic iron overload, both are important developments as the persistent effects of iron chelation in chronic hemorrhagic MI has not been previously reported.

3.6 Conclusion

As an independent predictor of adverse events, hemorrhagic MI has been shown to result in adverse LV remodeling, cardiac arrythmias, and deficits in resting perfusion and LV function. IMH is a common consequence of myocardial reperfusion therapy, which stands as the standard of treatment for acute MI patients. Therefore, alleviating the negative effects of IMH in chronic MI patients is of critical significance in reducing the adverse events in this population. Currently, there are no adjunctive therapies targeting I/R injury and the downstream deposition of iron in the chronic myocardial infarct territory. The results of this study identify iron chelation therapy via DFP as an important differential treatment option in the IMH patient subpopulation to limit cytotoxic iron and the negative sequelae observed in chronic IMH subjects. In this context, early identification of myocardial hemorrhage becomes increasingly important to provide iron chelation therapy for these patients. Further studies are warranted to determine the optimal window of efficacy for iron chelation in patients with IMH. Additionally, future investigations should identify the effect of various therapy regimens on chronic iron deposition and adverse events.

Chapter 4: Therapeutic Hypothermia for Hemorrhagic MI in Swine

4.1 Abstract

Background: Therapeutic hypothermia (TH) has shown promising results in animal studies and some retrospective subgroup analyses of clinical trials, though prospective randomized clinical trial results have been largely unsuccessful. The impact of TH on hemorrhagic MI and chronic iron deposition has not previously been investigated. Therefore, the aim of this study was to evaluate the potential of TH to alter chronic iron deposition in a pig model of hemorrhagic MI.

Methods and Results: 25 female farm pigs were enrolled into the study. 90 minutes of LAD occlusion was conducted, followed by 30 minutes of reperfusion prior to induction of TH. Hypothermia was performed via a 60-minute pericardial saline infusion of either pre-chilled (4-8°C) or warm (35-37°C) sterile saline. MRI studies were performed at day 3-7, 1 month, and 2 months post-MI. TH had no effect on infarct size at any time point, nor was microvascular obstruction (MVO) different between groups during the acute MRI. Iron deposition was significantly decreased in the TH group compared to controls at 2 months, characterized both by T2*-derived hemorrhage volume (0.62% ± 0.18 vs. 2.25% ± 0.61, respectively; $p = 0.02$) and absolute T2* values (28.25 ms ± 1.37 vs. 22.03 ms ± 1.70, respectively; $p = 0.02$). Additionally, left ventricular ejection fraction (LVEF) was significantly increased at 2 months in the TH group compared to controls (42.78% ± 1.86 vs. 36.31% ± 1.48, respectively; $p = 0.04$).

Conclusion: Treatment of hemorrhagic swine with post-reperfusion therapeutic hypothermia resulted in reduced chronic iron deposition and improved LVEF at 2 months post-MI. The

cardioprotective benefits identified in this study may play a key role in limiting the burden of hemorrhagic MI and lay the groundwork for future investigations into iron modulation in hemorrhagic MI via therapeutic hypothermia.

4.2 Introduction

Myocardial infarction (MI) remains a major burden in global healthcare as a leading cause of heart failure and death (*268*). Upon primary percutaneous intervention (PCI), coronary reperfusion frequently leads to a significant adverse consequence – myocardial hemorrhage, encompassing breakdown of the vascular integrity, leakage of fluid and red blood cells (RBCs), and chronic build-up of iron in the myocardium (*22-24*). There is increasing evidence that patients experiencing hemorrhagic myocardial infarctions have significantly worse prognoses than those experiencing non-hemorrhagic infarctions (*169*). Numerous studies have investigated the potential of adjunctive therapies to alleviate ischemia/reperfusion (I/R) injury and improve patient outcomes (*304-317*), including several animal and clinical trials investigating myocardial temperature modulation (*231-235, 237, 238, 242, 318, 319*). One promising intervention, therapeutic hypothermia, has shown significant beneficial effects in swine models of MI (*318*), while results from clinical trials remain mixed. Many plausible explanations for these inconclusive outcomes have been proposed (*217, 320*), however a key element of these infarctions has consistently been overlooked – intramyocardial hemorrhage (IMH).

The cardioprotective effects of therapeutic hypothermia are more nuanced than a simple reduction in metabolic demand. The proposed pathways involve mitochondrial permeability stabilization, nitric oxide production, reactive oxygen species (ROS) neutralization, and

rebalancing calcium channel dysregulation (*169, 172, 248*). Additionally, heat-shock proteins and survival kinases have been implicated in the hypothermia-mediated preservation of reperfusion-induced cell destruction (*247*). Further, the modulation of the cell death pathways autophagy and mitophagy through hypothermic intervention may play an additional role in the preservation of myocardial function (*230*). Therapeutic hypothermia appears to have a bimodal effect on coronary blood flow – with hypothermia-induced increases in healthy subjects and blood flow decreases in CAD patients subjected to mild hypothermia (*321, 322*). Reductions in coronary and cerebral blood flow is one of the hypothesized mechanisms by which therapeutic hypothermia acts (*220*). In this way, therapeutic hypothermia may act as an analogous treatment to ischemic conditioning by limiting coronary reperfusion post-PCI. Taken together, these mechanisms serve to enhance the ability of the myocardium to mitigate ischemia/reperfusion (I/R) injury and improve consequent healing and recovery.

A significant component of I/R injury, myocardial hemorrhage, has not been investigated in a comprehensive manner in animal and clinical studies of therapeutic hypothermia, leading to a potential overlooking of a plausible cornerstone benefit of this promising therapeutic intervention. Having shown that increased iron build-up in chronic hemorrhagic MIs is associated with poor functional characteristics (*88, 197, 204*), and that sequestration of iron stores via an oral iron chelator (Deferiprone) abrogates these deficits (*205*), it is logical to hypothesize that beneficial modulation of intramyocardial iron is an important outcome measure for any adjunctive therapeutic study. Yet, no study to date has investigated the impact of therapeutic hypothermia on myocardial hemorrhage or chronic iron deposition in either animal models or

clinical studies. We aim to cover this critical aspect of hypothermic intervention in this study using a swine model of I/R injury with localized mild hypothermia via pericardial saline perfusion (*256*).

Studies have shown the negative influence that hemorrhagic MI has on the remodeling of the LV in the chronic phase (*88, 197, 204*). Hemorrhagic MI and subsequent increased iron deposition are associated with increased LV wall thickening and diastolic dilatation, leading to LV dysfunction and increased incidence of arrythmias and HF (*23*). While the link between hemorrhagic MI and adverse remodeling remains under investigation (*89, 323, 324*), studies have shown that iron removal via chelation therapy leads to improved LV remodeling (*205*), indicating that iron may play a critical role in this process. Iron removal, as discussed in Chapter 3 in a canine model of I/R injury, leads to an improvement in rest perfusion defects in iron-chelated animals. However, the iron chelation must be continuously administered to maintain the beneficial effects. A therapy targeting I/R injury that confers prolonged and persistent iron reduction effects would be of extensive value in alleviating the negative outcomes associated with hemorrhagic MI. While therapeutic hypothermia has not been implicated in the process of iron deposition in chronic hemorrhagic MI, Prasad et al. showed in a rat model of deep hypothermia that reperfused hearts had decreased free iron and oxygen radical generation when subjected to hypothermic conditions (*241*), laying the groundwork for the potential down-regulation of iron deposition in hemorrhagic MIs via therapeutic hypothermia. Gambert et al. also showed the potential for deep hypothermia to decrease free radical generation in a rat model of I/R injury (*240*). Additionally, Marek-Iannucci et al. have shown the potential for post-reperfusion therapeutic hypothermia in a swine model to increase autophagic flux and enhance mitophagy, while simultaneously increasing mitochondrial biogenesis (*230*). This combination of improved

cell cycling may serve as an additional positive driver of iron clearance by removing dysfunctional cells and allowing the recovery process to progress unencumbered by the toxic effects of myocardial iron. In fact, the investigators showed that therapeutic hypothermia initiated 30 minutes after reperfusion led to improved functional recovery via LVEF measured with ultrasound.

While the optimal initiation time for therapeutic hypothermia has yet to be established, many studies investigating hypothermia use a pre-reperfusion hypothermia model based on the idea that I/R injury occurs in the super-acute phase (i.e., within minutes following reperfusion). While these studies have shown positive results in animals, the difficulty of implementation in an emergency clinical setting provides a significant obstacle. Further, deriving therapeutic benefit from post-reperfusion hypothermia would be of significant interest for simplified integration into clinical workflows, as well as providing a treatment option when pre- or intra-PCI hypothermia is impractical. While Shi et al. has concluded that post-reperfusion hypothermia does not confer positive benefits in a rat model (*266*), other studies have found beneficial results in both rat and swine models (*229, 230*).

Previous studies investigating therapeutic hypothermia have primarily focused on infarct size as a primary outcome measure, which has frequently failed to show a positive effect in clinical trials. However, hemorrhage stands as an independent predictor of MACE, and as such serves as an important target for adjunctive therapies. Namely, beneficial effects on LV remodeling through hemorrhage mitigation, in the absence of infarct size modulation has the potential to significantly improve outcomes and limit adverse events. Given that therapeutic hypothermia has been shown to be effective in the brain, with clinical trial sub-analyses and animal studies in an MI

setting having shown positive results, we hypothesized that regional therapeutic hypothermia in the heart can reduce the effects of hemorrhage and improve left ventricular functional recovery in the setting of I/R injury in chronic MI animals. We tested this in a swine model of hemorrhagic MI by imposing local myocardial hypothermia and evaluating the tissue specific and functional changes using serial CMR with appropriate controls.

4.3 Methods

4.3.1 Animal Model

All animal studies followed protocols approved by the Institutional Animal Care and Use Committee (IACUC) of Cedars Sinai Medical Center. Female farm pigs (30-35 kg) were acquired and allowed a quarantine period prior to initiation of any studies. Following quarantine, pigs were assigned to either treatment or control group, and prepared for surgery via sedation, anesthesia, and intubation. Anesthesia was maintained via inhaled isoflurane at 1-3%. LAD occlusion and pericardial saline procedures followed a swine model of ischemia/reperfusion MI that has been described previously (*256*). An 8-Fr balloon catheter was introduced via the carotid artery and advanced to the LAD under fluoroscopic guidance. Upon confirmation of positioning distal to the first diagonal branch of the LAD, the balloon was inflated to sufficient pressure to produce total occlusion of the artery distal to the balloon. LAD occlusion was confirmed via angiogram and continued for 90 minutes. Amiodarone was given pre-occlusion, and along with Lidocaine throughout the procedure as an anti-arrhythmic. Additionally, heparin bolus was infused pre-intervention and during reperfusion to prevent blood clotting. Phenylephrine was given as a bolus in case of blood pressure drops. Blood pressure, expired CO_2, oxygen saturation, and ECG

were monitored continuously. In case of ventricular fibrillation, defibrillation was attempted via adhesive chest pads, followed by standard defibrillator pads until cardiac rhythm was restored. At the conclusion of the 90-minute occlusion period, the balloon was deflated, and myocardial perfusion allowed to resume. Myocardial reperfusion was confirmed via angiogram and latent vascular spasm, if present, was treated with nitroglycerin infusion. Following 10-15 minutes of reperfusion, placement of the pericardial catheter was initiated. A 12-Fr dual-lumen dialysis catheter (Mahurkar-Elite, Medtronic, Dublin, Ireland) was introduced via sub-xiphoidal puncture and advanced intro the pericardial space under fluoroscopic guidance. Premature ventricular contractions (PVCs) confirmed entry into the pericardium, and proper positioning was confirmed via dye injection. At 30-minutes post-reperfusion, pericardial saline infusion was initiated by infusing sterile saline into one lumen, with the second lumen opened allowing fluid to flow into an outflow sump. For hypothermia group animals, saline was pre-chilled to 4-8°C, while control animals received pre-warmed saline at 36-38°C. Saline was infused at a rate of 1250 mL/hr, with an insulated infusion bag (packed with ice packs for the hypothermia group) to maintain saline temperature throughout the hour-long infusion. For the initial minutes of pericardial infusion, saline flow rate was ramped up slowly to mitigate vital parameter fluctuations and cardiac tamponade, while ensuring blood was not entering the outflow tract which could indicate LV perforation. At the conclusion of the 60-minute pericardial saline infusion, the LV temperature was recorded invasively via trans-thoracic measurement with a thermocouple needle (ThermoWorks, American Fork, UT, United States). Catheter aspiration was applied prior to removal to limit fluid buildup in the pericardium. Following the terminal MRI study, animals were humanely euthanized according to IACUC protocol and hearts were

explanted and preserved for further analysis. An apical cap was sliced and frozen at -80°C, with the remainder of the heart fixed in 10% formalin.

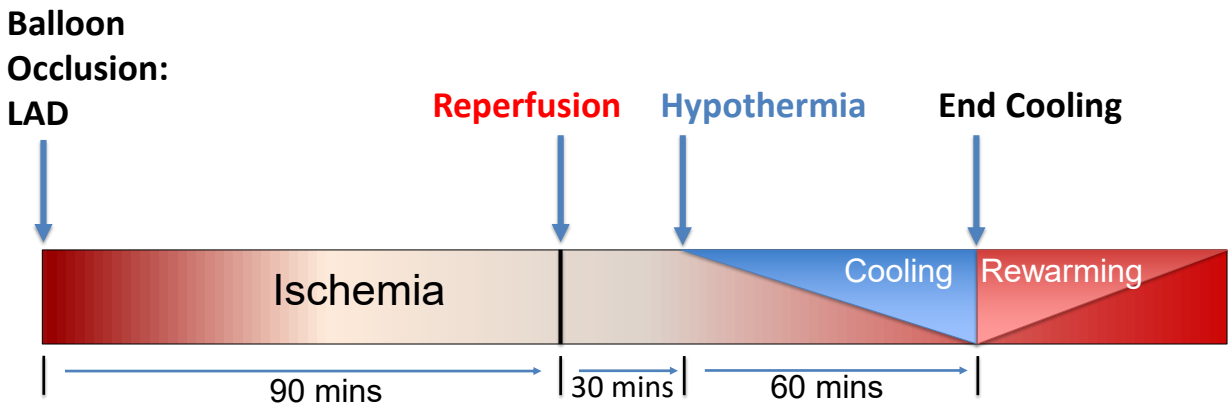

Figure 4.1: Pericardial saline surgical model. After anesthetizing and intubating the animals, a catheter was introduced via carotid artery and advanced to the LAD under fluoroscopic control. Upon positioning the balloon distal to the 1st diagonal branch, the balloon was inflated to completely occlude distal blood flow and confirmed with contrast injection cine. After 90 minutes of LAD occlusion, the balloon was deflated, and reperfusion confirmed. Following reperfusion, a pericardial catheter was introduced via sub-xyphoid puncture, and placement confirmed under fluoroscopic guidance. 30 minutes post-reperfusion, pericardial saline infusion was initiated and continued for 60 minutes, after which aspiration of the catheter was performed to ensure saline did not remain in the pericardial space. For the hypothermia group, saline infusate was cooled to 4-8 °C, whereas body temperature saline (36-38 °C) was infused in the control group.

4.3.2 Imaging Studies

Serial cardiac MRI was performed on 3.0T MRI systems (Biograph, Siemens Healthcare, Erlangen, Germany) at day 3, 1 month, and 2 months post-MI. Imaging localizers were scanned to initiate subject orientation prior to beginning the imaging studies. Long axis and whole-heart stacks of slice-matched cine, T2*-weighted, and late gadolinium enhancement (LGE) were acquired with a slice thickness of 6 mm and 0 mm gap. Imaging parameters are shown in Table 4.1. All images were acquired via breath-held sequences, with ECG-gating used to trigger T2*-weighted and LGE sequences. T2*-weighted gradient-recalled echo (GRE) acquisitions with 8 echoes were used to construct T2* maps for hemorrhage and iron deposition analysis. T1-weighted LGE images were acquired 10-15 minutes after infusion of 0.2 mmol/kg Gadolinium (Gd) contrast via phase-

sensitive inversion recovery (PSIR) reconstruction. An inversion-time (TI) scout was run prior to acquiring LGE images to optimize initial TI. TI was increased incrementally on subsequent slices to maintain contrast.

Table 4.1: MRI Parameters

	TR	TE	Flip angle	Readout bandwidth	In-plane resolution
Cine (35 phases)	3.22 ms	1.61 ms	38°	1370 Hz/pixel	1.4 x 1.4 mm^2
T2* Mapping (8 echoes)	83.51 ms	1.41-10.02 ms (ΔTE=1.23 ms)	12°	1185 Hz/pixel	1.6 x 1.6 mm^2
LGE	1 R-R	1.48 ms	20°	585 Hz/pixel	1.3 x 1.3 mm^2

4.3.3 Data Analysis

Cardiac MRI images obtained from serial studies were imported and analyzed in CVI[42] (Circle Cardiovascular Imaging, Calgary, Alberta, Canada). Long axis cine series had LV extent contours drawn from the mitral valve to the apex. The full cine stack was then contoured with epicardial and endocardial contours, applying papillary muscle contours as required. Software-derived systolic and diastolic phases were visually confirmed for accuracy and then used for calculation of LV volumes and ejection fraction (EF). The 4-chamber long-axis cine at end-diastole was used to measure long axis and short axis lengths for sphericity index calculation. Sphericity index was defined as the ratio of the short axis to long axis length. LGE and T2*-weighted images were contoured by matching the sequence trigger delay time from cine phases and copying endothelial and epithelial contours over to the corresponding LGE and T2*-weighted images, checked for

accuracy, and adjusted as needed. Remote contours were then placed in the non-infarcted region of the myocardium and used as the basis for thresholding measurements of infarct volume (LGE) and hemorrhage/iron volume (T2*-weighted). Mean + 5 SD (*275*) and mean - 2 SD (*64*) thresholds were used to segment infarct and hemorrhagic regions, respectively, as previously described. Care was taken to exclude artifact-containing regions, particularly inferior myocardium on T2*-weighted images that suffer from magnetic susceptibility artifacts at the heart-lung interface. Hyper-enhanced regions on LGE that contain a hypo-enhanced core were contoured for microvascular obstruction (MVO) measurement. Infarct volume is reported as the total hyper-enhanced volume (including MVO volume) divided by the total myocardial volume. Similarly, T2*-derived hemorrhage volume is reported as the total hypo-enhanced volume divided by total myocardial volume. Hypo-enhanced region contours on T2*-weighted images were copied to T2* maps for absolute T2* relaxation constant measurement. T2* values (ms) were derived as weighted averages across three slices.

4.3.4 Statistical Analysis

All statistical analysis was performed in SPSS version 24 (IBM, Chicago, IL, USA). Data are reported as mean ± mean standard error (SEM) unless otherwise noted. Assumption of normality was assessed using a Shapiro-Wilk test. For datasets that did not satisfy the assumption of normality, a logarithmic transformation was applied, and normality reassessed. Variance homogeneity was confirmed by performing single factor ANOVA on data residuals. Comparisons between 2 means used a two-tailed student's t-test. Analysis of change in parameters over time (e.g., change in infarct size between day 3, 1 month, and 2 months) was performed via repeated measures ANOVA. The assumption of sphericity was confirmed, and where violated a Greenhouse-Geisser

correction was applied. For data that showed statistically significant differences over time, a pairwise comparison was performed via *post hoc* analysis with Bonferroni adjustment to observe specific differences between time points. Statistical significance was set to $p < 0.05$ for all results.

Results

In total 25 pigs were enrolled in the study, 6 animals deceased due to surgical complications and 3 additional animals were euthanized prior to the study endpoint. Finally, 16 farm pigs completed the 2-month follow-up studies, 10 of which are included in the therapeutic hypothermia group and 6 in the control group. However, 3 animals were excluded from final analysis due to disruptions during the pericardial saline procedure – 2 animals had temperature recording malfunctions, and 1 animal had pre-existing myocarditis preventing insertion of the pericardial catheter. Therefore, the final group sizes for analysis were 8 animals in the hypothermia group and 5 animals in the control group.

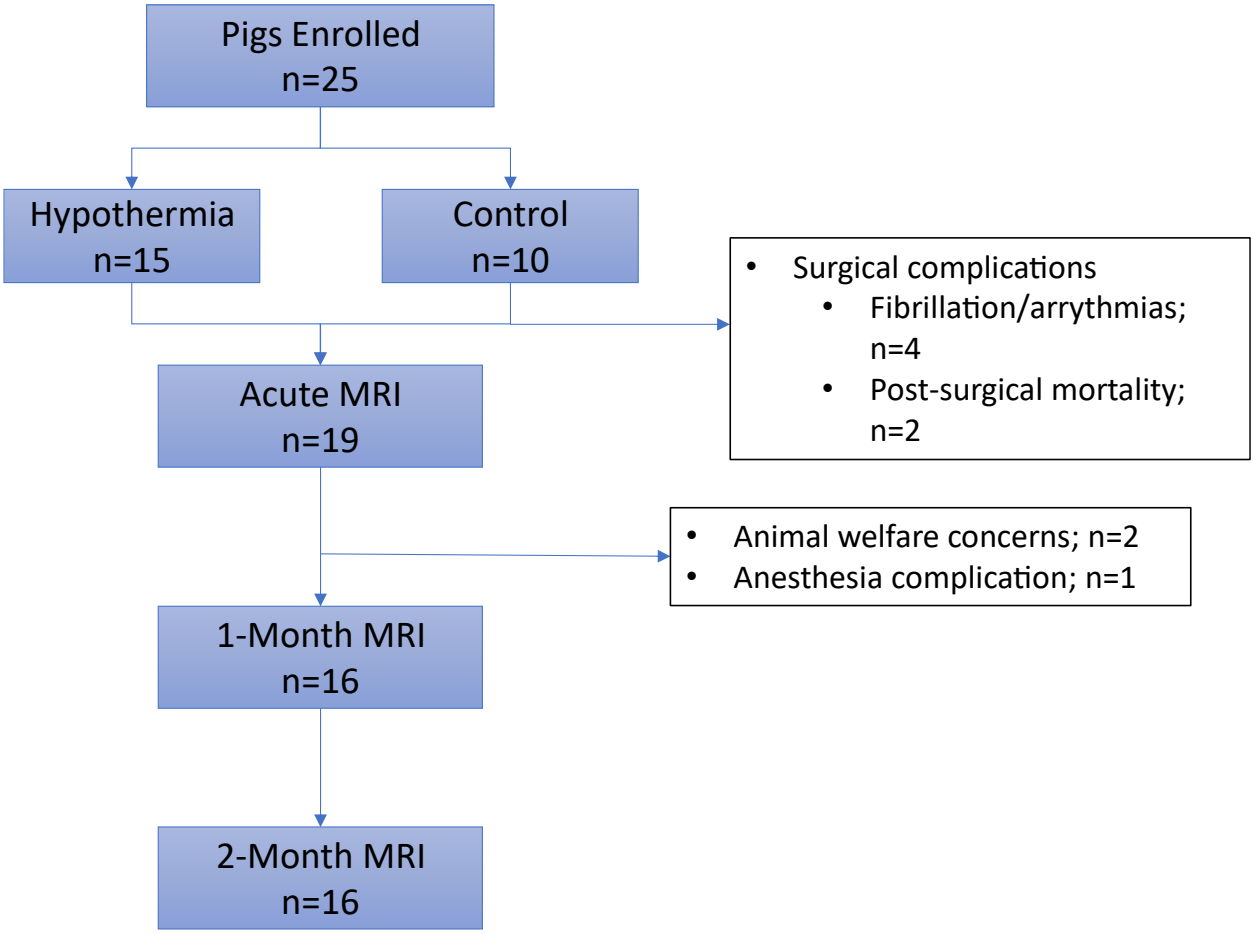

Figure 4.2: Study enrollment flow chart. 25 pigs were approved by IACUC and enrolled in the study, with 15 allocated to the treatment (hypothermia) group and 10 in the control (normothermia) group. 6 animals deceased either during the surgical procedure or shortly thereafter, with an additional 3 animals euthanized prior to the 1-month MRI due to abnormal or worrisome condition/behavior. Finally, 16 female farm pigs completed the 2-month study and were available for analysis.

4.3.5 Therapeutic Hypothermia Does Not Affect Infarct Size

Infarct size was not different between hypothermia and control groups at any time point ($p>0.05$). Infarct sizes within groups significantly decreased over time from day 3 to 1 month for both hypothermia ($p<0.01$) and controls ($p=0.02$), day 3 to 2 months ($p<0.01$), and 1 month to 2 months ($p<0.02$). Representative cases from each time point for both groups are shown in Figure 4.4.

4.3.6 Therapeutic Hypothermia Has No Impact on Acute MVO

An acute microvascular damage consequence of I/R injury, MVO has been shown to be an independent predictor of MACE and is used as a measure of treatment benefit but dissipates by the chronic phase of MI. Therapeutic hypothermia did not have an effect on MVO on day 3 LGE MRI, as both groups had statistically equivalent MVO volume (hypothermia: 3.21% ± 0.79 vs. control: 2.97% ± 0.37, p=0.84). MVO was not observed in the 1-month or 2-month LGE images in either group, as shown in Figure 4.3.

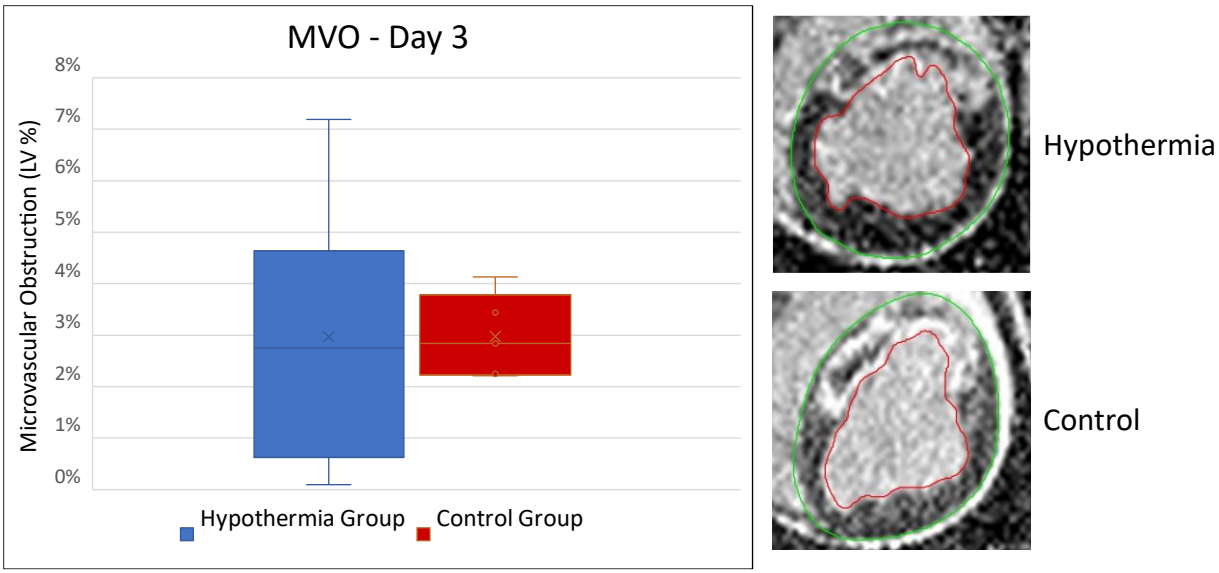

Figure 4.3: Microvascular obstruction (MVO) was not different between groups at day 3. MVO, observed as a hypointense core within the infarct region, measured at day 3 MRI did not show significant differences between hypothermia group and controls. Representative LGE images are shown.

4.3.7 Chronic Iron Deposition is Decreased in Hypothermia-Treated Animals

T2*-derived hemorrhage volume at day 3 was no different in the hypothermia group compared with controls (4.61 ± 1.69 vs. 4.88 ± 1.67, p=0.91). At 1 month, the hypothermia group had significantly decreased hemorrhage volume compared to controls (1.02 ± 0.24 vs. 2.62 ± 0.48,

p=0.01). Similarly, the 2-month results show significantly decreased hemorrhage volume in hypothermia group compared to controls (0.62 ± 0.18 vs. 2.25 ± 0.61, p=0.02). Repeated measures ANOVA show that at 1 month, both hypothermia and control groups had significantly decreased hemorrhage volume compared with day 3 (p=0.04, p=0.01, respectively). However, while the hemorrhage volume at 2 months was significantly lower than day 3 in both groups (p=0.02), 2-month hemorrhage volume was not different from 1-month in either group (p>0.05). Results shown in Figure 4.6.

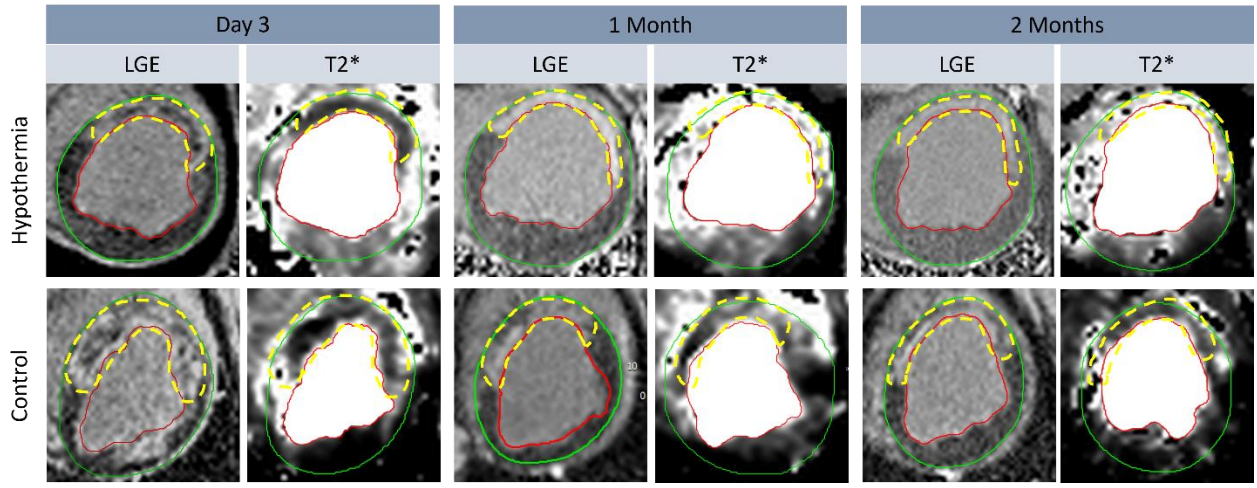

Figure 4.4: LGE and T2 map MRI at day 3, 1-month, and 2-months for representative cases in hypothermia and control groups. At day 3, both groups had similar infarct sizes with microvascular obstruction present in the infarct core, with similar levels of intramyocardial hemorrhage visible on T2* maps (hypointense regions in the infarct zone). At 1 month, both groups had similar levels of infarct shrinkage, with hemorrhage volume reduction present to a significantly greater degree in the hypothermia group. At 2 months, infarct sizes remained equivalent, and the hypothermia group maintained a significantly reduced level of hemorrhage volume compared with controls. The hypothermia group had significantly reduced myocardial temperatures compared with controls (35.75 ± 0.25 °C vs. 38.04 ± 0.34 °C, p<0.001) at the end of pericardial saline infusion.*

Analysis of the change in hemorrhage volume between groups from day 3 to 1 month showed a trend towards greater decreases in the hypothermia group (-66.57% ± 10.38) compared to controls (-46.62% ± 4.74) but was not statistically significant (p=0.25). The change from day 3 to 2 months showed significantly greater decreases in the hypothermia group (-82.90% ± 6.35)

compared to controls (-54.49% ± 8.38, p=0.046). Hemorrhage volume changes between day 3 and 1 month and day 3 and 2 months are shown in Figure 4.5.

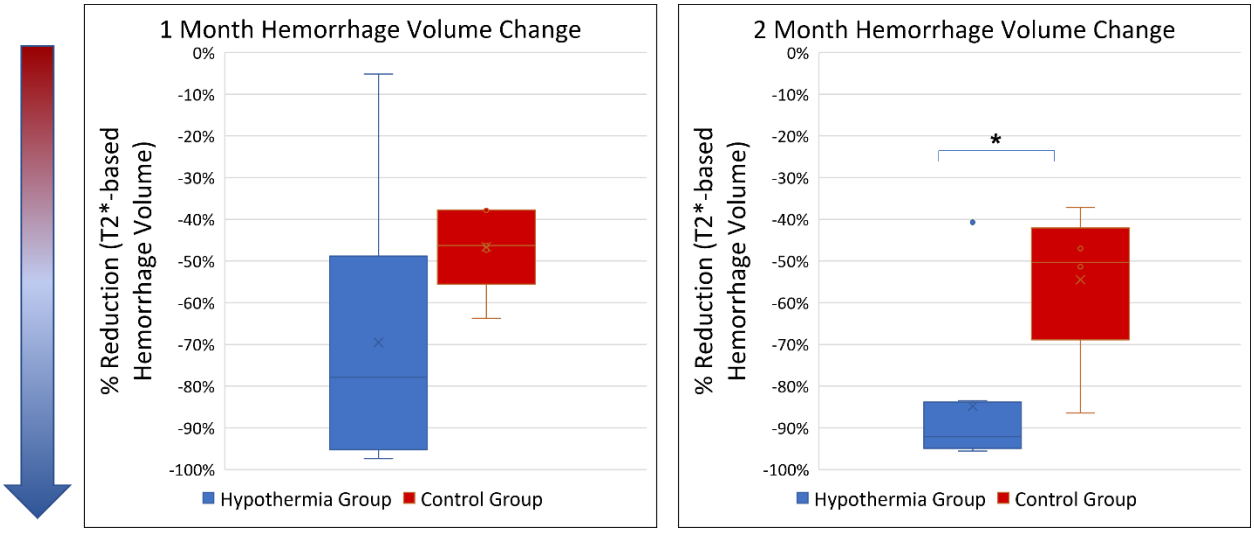

Figure 4.5: Hypothermia-mediated resolution of iron deposition at 2 months post-MI. At 1-month post-MI, the reduction in hemorrhage volume trended toward a greater decrease in the hypothermia group (-66.57 ± 10.38%) vs. controls (-46.62 ± 4.74%) but did not reach significance. (p=0.25), largely due to an animal in the treatment group with small hemorrhage at day 3 that remained similar at 1 month. Change in hemorrhage volume between day 3 and 2 months showed a significant reduction in the hypothermia group (-82.90 ± 6.35%) compared to the control group (-54.49 ± 8.38, p=0.046).

Hemorrhage volume normalized by infarct size (IS) similarly showed no difference between groups at day 3 (p=0.68). At 1 month, animals in the hypothermia group had significantly decreased IS-normalized hemorrhage volume (7.72% ± 16.2) compared to controls (19.62% ± 2.79, p<0.01). Similarly, at 2 months, hypothermia-treated animals had significantly decreased IS-normalized hemorrhage volume (7.20% ± 1.86) compared to controls (29.41% ± 6.14, p<0.01). Results shown in Figure 4.6.

Absolute T2* values from T2* maps followed a similar trajectory, with no difference between groups at day 3 (p=0.30) or 1 month (p=0.18). At 2 months, the hypothermia group had significantly increased T2* values (i.e., decreased iron content) compared to controls (28.25 ms ± 1.37 vs. 22.03 ms ± 1.70, p=0.02). Repeated measures ANOVA showed no change in T2* values

over time in the control group (p>0.05), whereas the hypothermia group had significantly different T2* values at 2 months compared to both day 3 (p<0.01) and 1 month (p=0.02). Results shown in Figure 4.6.

4.3.8 Ejection Fraction is Increased in Hypothermia-Treated Animals at 2 Months

Left ventricular ejection fraction (LVEF) at 3 days post-MI in the hypothermia group (31.84% ± 3.75) was not different from controls (35.56% ± 5.63, p=0.58). This statistical equivalence

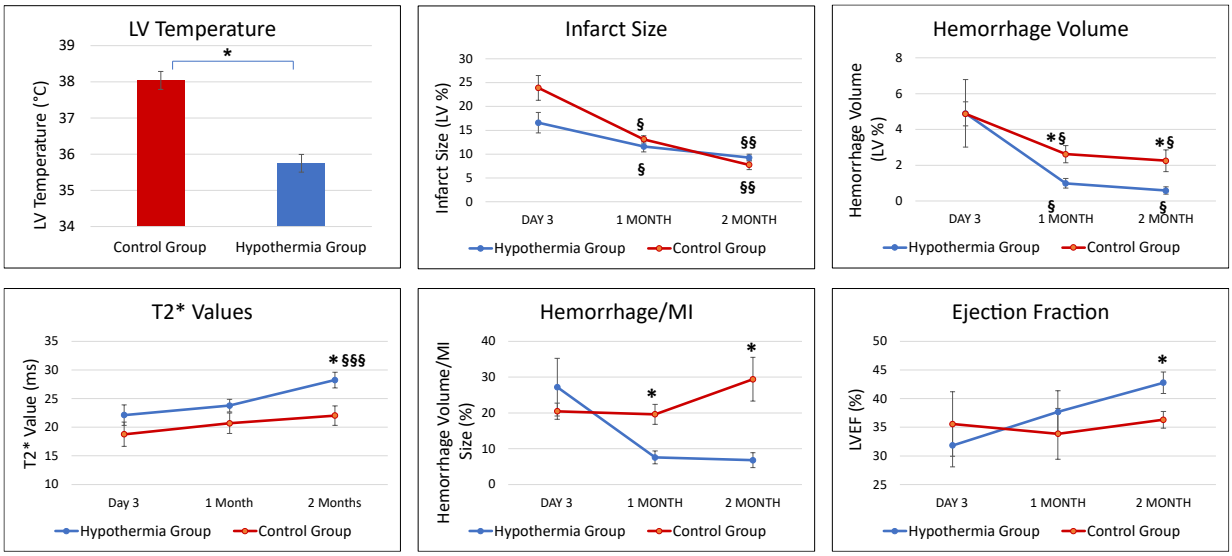

Figure 4.6: MRI Results Over Time in Hypothermia vs. Control Animals.

***A)** Invasively measured myocardial temperature at the conclusion of pericardial saline infusion showed significantly reduced temperature in the hypothermia group compared to controls. **B)** Infarct size was not different between hypothermia group and controls at each time point. Repeated measures ANOVA showed a significant difference across time in both groups. **C)** Hemorrhage volume was not different between groups at day 3 MRI but was significantly decreased in the hypothermia group at both 1-month and 2-month time points. Repeated measures ANOVA showed the 1-month hemorrhage volume to be different from day 3, while only the hypothermia group continued decreasing from 1-month to 2-months. **D)** Absolute T2* values measured from T2* maps showed no difference between groups at day 3 or 1 month but was significantly increased (lower iron content) in the hypothermia group at 2 months. Repeated measures ANOVA showed no change over time in the control group, whereas the hypothermia group had significantly increased T2* values at 2 months relative to day 3 and 1 month, though there was no difference between day 3 and 1 month. **E)** Hemorrhage volume normalized by infarct size showed no difference at day 3 but was significantly decreased in the hypothermia group at both 1-month and 2-month time points, compared with controls. Repeated measures ANOVA showed no significant differences across time for either group. **F)** Ejection fraction was not different between groups at day 3 or 1 month, but at 2 months was significantly increased in the hypothermia group compared with controls. Repeated measures ANOVA showed no significant changes across time in either group.*
** Between groups p<0.05*
§ Within groups change from acute p<0.05
§§ Within groups change from acute and between 1-2 months p<0.05
§§§ Within groups change between 1-3 and 2-3 months p<0.05

continued at the 1-month MRI (37.67% ± 3.71 vs. 33.85% ± 4.45, respectively; p = 0.52). However, at 2 months, animals in the hypothermia group had significantly increased LVEF (42.78% ± 1.86) compared to controls (36.31% ± 1.48, p=0.04). Repeated measures ANOVA showed no difference in LVEF over time within groups (p>0.05). Results shown in Figure 4.6.

4.3.9 Therapeutic Hypothermia Improves Left Ventricular Remodeling

Sphericity index is a measure of the LV anatomical shape as a ratio of short axis to long axis length, which tends to increase as the LV remodels in the post-MI setting. Analysis of the myocardial sphericity showed a significantly lower sphericity index (i.e., improved remodeling) in the hypothermia group (0.55 ± 0.01) compared to controls (0.59 ± 0.01, p=0.04), shown in Figure 4.7.

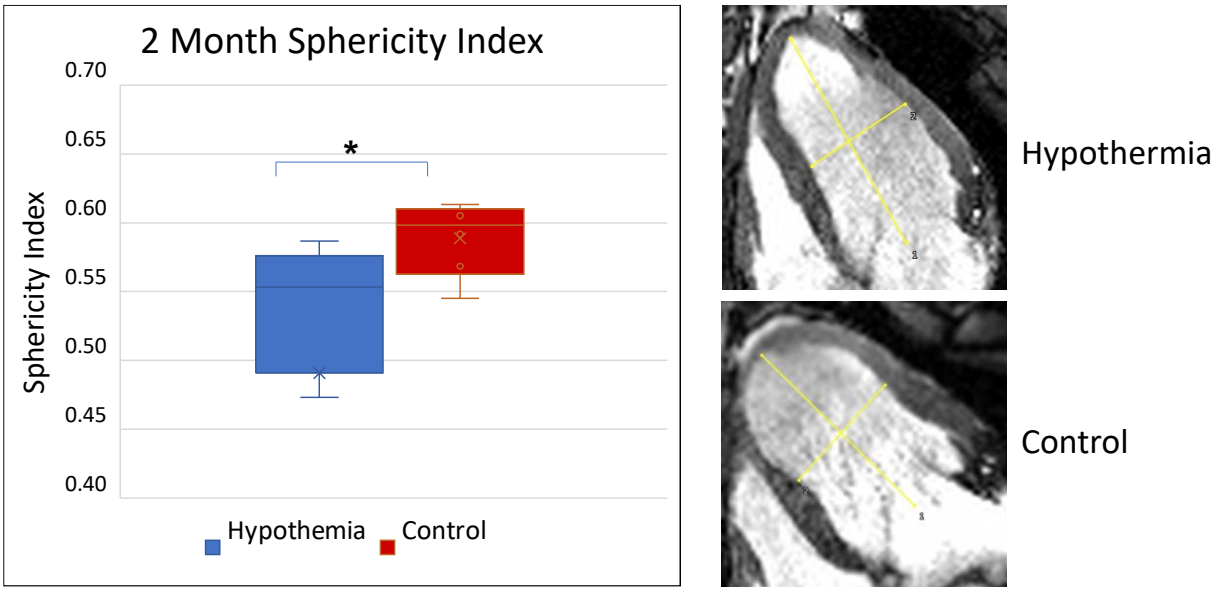

Figure 4.7: Hypothermia mitigates diastolic LV dilatation. Sphericity index at 2 months, measured as the ratio of short axis to long axis length at end-diastole, was significantly decreased in the hypothermia group compared with controls (0.55 ± 0.01 vs. 0.59 ± 0.01, p = 0.037). Representative images from 4-chamber cine MRI at end-diastole are shown.

4.4 Discussion

Previous investigations of therapeutic hypothermia have had mixed results, with animal studies showing significant protective effects of moderate hypothermia (*170, 230, 318, 319*) while randomized clinical trials have been largely unsuccessful at reproducing positive results. However, retrospective re-analysis correcting for delayed hypothermia induction in the COOL-MI and ICE-IT trials, and pooled analysis of the RAPID-MI ICE and CHILL-MI trials segregating patients with large myocardium-at-risk (MaR) have yielded positive findings showing that hypothermia results in reduced acute infarct size (*225, 325*). These results should be interpreted with caution, especially given that MaR has been shown to have confounding factors when assessed via T2-weighted MRI in the presence of concurrent IMH. This particular aspect of MI (i.e., IMH) has been consistently overlooked in therapeutic hypothermia studies. Despite having been shown to be a strong independent predictor of adverse events, prior studies failed to differentiate subjects based on presence of IMH, instead focusing on infarct size as the primary outcome measure along with the controversial use of MaR. While this may be understandable given that therapeutic hypothermia in swine models and specific post-hoc analyses of clinical trials have elicited positive benefits in terms of infarct size reduction, future investigations would benefit from broadening their cardioprotective outcome scope to include effects on IMH. A recent review by El Farissi et al. explored the current state of therapeutic hypothermia, providing a significantly positive outlook for therapeutic hypothermia as an adjunctive treatment while falling short of considering the potential benefits of hypothermia in terms of IMH (*320*). Therefore, this is the first study, to our knowledge, to investigate the impact of therapeutic hypothermia on IMH in an animal model of I/R injury.

The significant cytotoxic effects of chronic iron deposition in multiple disease states have driven the introduction of iron chelation therapies, which now serve as a mainline treatment option for many patients. Reasonably, careful control of iron deposition is an important aspect to consider in morbidities suffering from iron imbalance. Previous studies have shown the propensity for chronic iron deposition in cases of hemorrhagic myocardial infarction, as well as the detrimental effects on LV remodeling occurring in these subjects (*88, 197, 323*). Therefore, segregating patients by presence of IMH would be an important step towards elucidating preferential benefits conferred by therapeutic hypothermia. Towards that end, we investigated the specific modulation of hemorrhage and subsequent chronic iron deposition by therapeutic hypothermia and the resulting structural and functional changes in the left ventricle. Despite showing no difference in infarct size throughout the 2-month study between groups, we showed specific cardioprotective benefits in the hypothermia group including reduced chronic iron deposition, lessened adverse structural remodeling, and improved ejection fraction. Of particular interest relating to the varied clinical trial results, we showed significant differences in iron deposition (T2*-weighted MRI), LV remodeling (sphericity index), and LV function (LVEF) at 2 months post-MI, while there were no statistically significant differences in T2* value or LVEF at 1-month post-MI. These results indicate that the cardioprotective benefits conferred by therapeutic hypothermia may not emerge in the acute or early chronic phase of MI recovery. This is an important finding given that many of the randomized clinical trial outcomes reported findings at 30-45 days post-MI (*227, 232-235, 237*), and as such may prematurely conclude a lack of benefit. Additionally, the progression of MI into the chronic phase in patients follows a longer timeframe, typically 6 months post-MI (*326, 327*), than that in a pig model which often uses 2 months post-

MI as the chronic endpoint (*328, 329*) , indicating that future trials in MI patients would benefit from lengthened endpoints in order to properly capture therapeutic benefits in the chronic phase. One limitation of this study was the inability to characterize the chronic effects of TH on resting myocardial perfusion, given that the significant reductions in iron observed in the hypothermia-treated animals may have a positive impact on chronic perfusion. The infarcted myocardium in the pigs studied experienced severe thinning, and as such we were unable to reliably extract rest perfusion MRI data from these regions. This limitation could be overcome by use of an alternative animal model that does not experience such severe infarct thinning, or by direct investigation in a clinical study.

Our findings are particularly interesting in the context of optimal hypothermia initiation timing within the window of I/R injury. Post-reperfusion hypothermia has had conflicting results in previous studies. In a rat model, Shi et al. did not find therapeutic benefit of post-reperfusion hypothermia. However, the pig model used in this study has been shown to produce beneficial effects on autophagy and mitophagy pathways, as well as LVEF improvement assessed using ultrasound. Animal model differences may play a factor in these discrepancies, though the positive results from the pig model are more likely to translate clinically than small animal models. Additionally, post-reperfusion hypothermia would be of significant interest in the case of acute segmentation of MI type into hemorrhagic vs. non-hemorrhagic, providing a differential treatment option in more severe MI cases when peri-surgical adjunctive therapy is not viable or unavailable. While identification of IMH still requires MRI analysis, it is conceivable that a future rapid screening test may be able to differentiate hemorrhagic MI in the super-acute phase. In the

absence of such a test, post-reperfusion hypothermia remains beneficial, particularly due to the ease of clinical workflow implementation.

4.5 Conclusion

Therapeutic hypothermia initiated in the post-reperfusion window of myocardial I/R injury confers cardioprotective effects that manifest in the chronic phase of MI. Our findings that infarct size is not affected by post-reperfusion hypothermia agree with previous studies showing a lack of benefit on acute infarct size when hypothermia is initiated after reperfusion. Despite this seemingly negative outcome, we show beneficial effects of reduced iron deposition and improved LV remodeling and function in the chronic stage through T2*-weighted and cine MRI. The impact of therapeutic hypothermia on hemorrhage-derived chronic iron deposition has not previously been investigated. Our study is the first to show the significantly impactful effects of iron reduction though localized myocardial hypothermia, laying the groundwork for future investigations developing the relationship between hypothermia, hemorrhage, LV function, and adverse outcomes. Additionally, future clinical trials may be well-served by incorporating expanded outcome measures such as iron deposition, as well as extending the longitudinal timeframe to account for the potential delayed emergence of these hypothermia-mediated effects.

Chapter 5: Summary and Future Directions

5.1 Summary

Myocardial infarction plays a significant role in the global burden of cardiovascular disease, which has remained the primary cause of death despite advancements in scientific understanding and treatment strategies over the last few decades. Microvascular dysfunction has become a leading target for the next generation of therapies aiming to alleviate the negative outcomes associated with ischemia reperfusion injury. Patients suffering from intramyocardial hemorrhage have the worst outcomes in this patient population, and IMH has been identified as an independent predictor of these outcomes. A key feature found in MI burdened with IMH that persists through the chronic phase of MI is the deposition of intramyocardial iron. Given the potential toxicity of iron and the precise control the human body naturally asserts over iron balance, this excess deposition of iron is a critical target when considering treatment of MI patients. There are no existing clinical therapies for the treatment of IMH, with only 1 FDA-approved adjunctive therapy indicated for ischemia reperfusion injury, signifying the need for additional development of therapies in this area.

This dissertation investigated the impact of IMH on the physiological characteristics and function of the left ventricle during chronic MI, while applying 2 different therapeutic strategies for mitigating the excess deposition of intramyocardial iron. To accomplish this, a study encompassing the full range of molecular, animal, and clinical data was designed to investigate the microvascular environment in chronic MI laden with iron deposits in relation to defects in resting perfusion and iron content. Cardiac MRI serial studies enabled the overarching analysis

of MI parameters and guidance of therapeutic efficacy. The major contributions from this work laid out in Chapter 2 are that T2*-weighted MRI can detect chronic rest perfusion defects in hemorrhagic MI and that microvascular dysfunction associated with hemorrhagic MI involves upregulation of nitric oxide synthases and angiogenic growth factors (i.e., eNOS, VEGF). Further, 2 large animal studies were undertaken to investigate the effects of two therapies for chronic iron in the myocardium and the resulting impact on LV function. First, a canine model of I/R injury in which the animals were treated with the iron chelator, DFP, was used to determine the effect of chronic iron on myocardial perfusion and function, which was described in Chapter 3. The major contributions of Chapter 3 are that chronic rest perfusion defects in animals with hemorrhagic MI can be recovered when treated with DFP, and termination of DFP leads to reappearance of perfusion defects. Second, a swine model of I/R injury in which the animals received therapeutic hypothermia via pericardial perfusion was used to investigate the chronic impacts of TH on hemorrhagic MI. The major contributions of this study, described in Chapter 4, are that post-reperfusion hypothermia has a significantly beneficial effect on chronic iron deposition assessed via T2*-weighted MRI, and hypothermia-treated animals had significantly improved LV function that emerged in the chronic phase.

5.2 Effect of Iron Chelation Therapy on the Impact of Iron Deposition on Chronic Resting Myocardial Perfusion in Hemorrhagic Myocardial Infarction

This comprehensive study characterized the differences in chronic resting perfusion between hemorrhagic and non-hemorrhagic infarcts in both patients and canines, adding protein expression analysis to further develop understanding of the vascular microenvironment in

chronic MI. A mechanistic pathway was developed from the protein expression insights gained from western blotting, histology, and immunohistochemistry experiments. This laid out a potential vehicle through which iron negatively affects perfusion in the coronary microvessels in chronic hemorrhagic MI.

Secondly, a large animal study was conducted to examine the effects of Deferiprone (DFP), an iron chelator that has shown high efficacy in removing intramyocardial iron, on LV remodeling and function in a canine model of chronic MI. The highly insightful findings of this study showed that regional resting myocardial perfusion may be recovered in hemorrhagic subjects treated with DFP, alleviating the differential chronic perfusion defects observed in hemorrhagic subjects with chronic iron deposition. Additionally, the study showed that termination of the DFP therapy at 8 weeks post-MI resulted in re-emergence of the resting perfusion defects in hemorrhagic animals at 6 months. Finally, while no difference in LVEF was present, the study identified a potential benefit in LV remodeling in DFP-treated animals, showing a significantly decreased end-diastolic mass at 6 months. This finding should be interpreted with caution, however, as the acute MRI studies also showed a strong trend toward reduced end-diastolic mass in the DFP group. This could either indicate a positive benefit from the DFP therapy or could simply be a result of inherent anatomical differences between animals in the groups. Further studies would be required to strengthen these conclusions in terms of the impact of DFP therapy on LV remodeling.

The results of these studies have identified potential targets for therapies to limit the adverse effects of IMH and provided strong evidence for the efficacy of iron chelation using DFP. Extensions of this work could identify additional therapeutic options, for example a combination therapy targeting both iron and nitric oxide to ensure vasodilatory balance is restored in the

microvasculature. Further, additionally studies are warranted to investigate the iron chelation regimen itself, optimizing the dosage, timeframe, and adding additional iron chelators as has been studied in iron balance disorders such as thalassemia. Lastly, translation of DFP therapy for hemorrhagic MI patients into clinical trials will be an important step in bringing this transformative therapy into clinical practice.

5.3 Localized Therapeutic Hypothermia as Adjunctive Therapy for Mitigating Chronic Iron Deposition and Improved Chronic LV Function in Hemorrhagic Myocardial Infarction

The therapeutic hypothermia (TH) study in a swine model of MI is the first to show the potential for TH to positively effect chronic iron deposition in animals with hemorrhagic MIs. Though previous randomized clinical trials have had mixed results, significant potential remains for this promising therapy in the treatment of MI and I/R injury. Using a recently developed method of localized TH via post-reperfusion pericardial saline infusion, the study identified a significant reduction in chronic iron deposition at 2 months in hypothermia-treated animals, while showing no differences in infarct size at any time point and no differences in T2* values (iron content) at either day 3 or 1 month. The implications of these results are extensive. First, this is the first study to show the efficacy of TH to reduce iron deposition in chronic MI. Second, the dynamic development of both iron deposition and LV function (LVEF) over the 2-month study exemplifies the importance of serially following patients in TH studies into the chronic phase to fully capture the beneficial impact. Lastly, the study identifies beneficial effects of TH in the absence of infarct size reductions using a post-reperfusion model of hypothermia, allowing existing clinical workflows that aim to minimize door-to-balloon time to remain unchanged.

The future directions for TH as an adjunctive therapy in MI patients include further optimizing the hypothermia protocol and the potential to combine this treatment with other promising therapies. It is clear from the randomized clinical trials that a uniform therapeutic strategy in TH has not yet been established, with varying target temperatures, durations of hypothermia, and methods of application. Additionally, the primary endpoints in these studies differ and frequently are set at 30 days post-MI, which may not allow full maturation of the LV remodeling process. There is a need for comparative investigations that evaluate these optimization parameters to begin working toward a more uniform, optimized TH protocol. Further studies are also warranted that investigate the impact of TH, induced prior to or at the time of reperfusion, on IMH and chronic iron deposition and LV remodeling. Early initiation of hypothermia has been associated with improved outcomes in terms of infarct size and adverse events in certain studies and subgroup analyses, but it remains to be seen how this will impact the progression of chronic iron deposition in hemorrhagic infarcts.

Several of the clinical studies discussed in this dissertation evaluated efficacy based on a measurement of area-at-risk (AAR) using T2-weighted MRI, which has been shown to be confounded by the presence of hemorrhage and may not accurately depict the true AAR. Therefore, future studies of TH would be well-served by including a T2*-weighted and T2* mapping MRI sequence during follow-up imaging to identify and track the progression of iron deposition.

Another potentially interesting extension of this work would be the combination of TH with other promising therapeutic options, such as iron chelation or a nitric oxide-targeted therapy. Therapeutic hypothermia already embodies a multi-faceted approach given its distinct effects on

the vasculature, but a combination therapy may serve as the future gold standard in MI treatment due to the complex cascade of events that induce reperfusion injury.

The hypothermia induction method used in this study required a complex surgical procedure involving sub-xiphoid puncture and fluoroscopically guided insertion of a catheter into the pericardial space. This procedure did not require specialized equipment and therefore made it easier to implement, however, the passive method used to induce hypothermia may not be appropriate for the clinical setting. Given the existence of FDA-approved intravascular hypothermia devices such as the InnerCool RTX (Zoll Medical, MA, USA), it is likely that future TH studies will continue to use existing machines, which can also provide dynamic and precise control over myocardial temperature. Similarly, surface cooling devices such as the InnerCool STX (Zoll Medical, MA, USA) may prove to be a lower barrier of entry method that can be applied on a wider scale, although without the same ability to isolate the hypothermic effect to the myocardium.

Additionally, based on the results of this study, it seems logical to hypothesize that TH may have a preferential benefit in MI patients with IMH. If this turns out to be the case, then TH may find efficacious use as a hemorrhage-specific treatment option. The main obstacle for this use-case would be the early identification of hemorrhage, which currently requires an MRI exam. However, having proven to be a safe therapeutic option, another potential scenario for future studies would be the application of TH to all MI patients as is currently done, followed by segregating the patient population into those with hemorrhage and those without with the intention to isolate beneficial effects in the hemorrhagic subpopulation.

References

1. A. D. Widgerow, Ischemia-reperfusion injury: influencing the microcirculatory and cellular environment. *Ann Plast Surg* **72**, 253-260 (2014).
2. R. K. Kharbanda, Cardiac conditioning: a review of evolving strategies to reduce ischaemia–reperfusion injury. *Heart* **96**, 1179-1186 (2010).
3. G. K. Hansson, Inflammation, Atherosclerosis, and Coronary Artery Disease. *New England Journal of Medicine* **352**, 1685-1695 (2005).
4. U. Baber *et al.*, Prevalence, Impact, and Predictive Value of Detecting Subclinical Coronary and Carotid Atherosclerosis in Asymptomatic Adults: The BioImage Study. *Journal of the American College of Cardiology* **65**, 1065-1074 (2015).
5. E. M. Tuzcu *et al.*, High Prevalence of Coronary Atherosclerosis in Asymptomatic Teenagers and Young Adults. *Circulation* **103**, 2705-2710 (2001).
6. J. P. Strong *et al.*, Prevalence and Extent of Atherosclerosis in Adolescents and Young AdultsImplications for Prevention From the Pathobiological Determinants of Atherosclerosis in Youth Study. *JAMA* **281**, 727-735 (1999).
7. J. D. Berry *et al.*, Prevalence and Progression of Subclinical Atherosclerosis in Younger Adults With Low Short-Term but High Lifetime Estimated Risk For Cardiovascular Disease. *Circulation* **119**, 382-389 (2009).
8. K. A. Reimer, R. B. Jennings, The "wavefront phenomenon" of myocardial ischemic cell death. II. Transmural progression of necrosis within the framework of ischemic bed size (myocardium at risk) and collateral flow. *Laboratory investigation; a journal of technical methods and pathology* **40**, 633-644 (1979).
9. M. J. Davies, Stability and instability: two faces of coronary atherosclerosis: the Paul Dudley White Lecture 1995. *Circulation* **94**, 2013-2020 (1996).
10. Y. Sandoval, K. Thygesen. (2017).
11. E. Braunwald, Evolution of the management of acute myocardial infarction: a 20th century saga. *The Lancet* **352**, 1771-1774 (1998).
12. R. Teixeira, L. Gonçalves, B. Gersh, Acute myocardial infarction — Historical notes. *International Journal of Cardiology* **167**, 1825-1834 (2013).
13. A. Maroo, E. Topol, The early history and development of thrombolysis in acute myocardial infarction. *Journal of Thrombosis and Haemostasis* **2**, 1867-1870 (2004).
14. D. C. Rijken, D. Collen, Purification and characterization of the plasminogen activator secreted by human melanoma cells in culture. *Journal of Biological Chemistry* **256**, 7035-7041 (1981).

15. Effectiveness of intravenous thrombolytic treatment in acute myocardial infarction. Gruppo Italiano per lo Studio della Streptochinasi nell'Infarto Miocardico (GISSI). *Lancet* **1**, 397-402 (1986).

16. S. S. Virani *et al.*, Heart Disease and Stroke Statistics- 2021 Update. *Circulation* **143**, e254-e743 (2021).

17. P. A. Heidenreich *et al.*, Forecasting the impact of heart failure in the United States: a policy statement from the American Heart Association. *Circulation. Heart failure* **6**, 606-619 (2013).

18. K. Reddy, A. Khaliq, R. J. Henning, Recent advances in the diagnosis and treatment of acute myocardial infarction. *World journal of cardiology* **7**, 243-276 (2015).

19. S. Johansson, A. Rosengren, K. Young, E. Jennings, Mortality and morbidity trends after the first year in survivors of acute myocardial infarction: a systematic review. *BMC cardiovascular disorders* **17**, 53-53 (2017).

20. D. Doukas *et al.*, Clinical characteristics and outcomes of patients with severe left ventricular dysfunction undergoing cardiac MRI viability assessment prior to revascularization. *The International Journal of Cardiovascular Imaging* **37**, 675-684 (2021).

21. A. M. Beek, R. Nijveldt, A. C. van Rossum, Intramyocardial hemorrhage and microvascular obstruction after primary percutaneous coronary intervention. *The international journal of cardiovascular imaging* **26**, 49-55 (2010).

22. O. Husser *et al.*, Cardiovascular magnetic resonance-derived intramyocardial hemorrhage after STEMI: influence on long-term prognosis, adverse left ventricular remodeling and relationship with microvascular obstruction. *International journal of cardiology* **167**, 2047-2054 (2013).

23. N. Amabile *et al.*, Incidence, predictors, and prognostic value of intramyocardial hemorrhage lesions in ST elevation myocardial infarction. *Catheterization and Cardiovascular Interventions* **79**, 1101-1108 (2012).

24. J. Ganame *et al.*, Impact of myocardial haemorrhage on left ventricular function and remodelling in patients with reperfused acute myocardial infarction. *European heart journal* **30**, 1440-1449 (2009).

25. E. Larose *et al.*, Predicting late myocardial recovery and outcomes in the early hours of ST-segment elevation myocardial infarction: traditional measures compared with microvascular obstruction, salvaged myocardium, and necrosis characteristics by cardiovascular magnetic resonance. *Journal of the American College of Cardiology* **55**, 2459-2469 (2010).

26. R. J. Burns *et al.*, The relationships of left ventricular ejection fraction, end-systolic volume index and infarct size to six-month mortality after hospital discharge following myocardial infarction treated by thrombolysis. *Journal of the American College of Cardiology* **39**, 30-36 (2002).

27. G. Heusch *et al.*, Cardiovascular remodelling in coronary artery disease and heart failure. *The Lancet* **383**, 1933-1943 (2014).

28. W. B. Wince, R. J. Kim, T2-weighted CMR of the area at risk—a risky business? *Nature Reviews Cardiology* **7**, 547-549 (2010).

29. H. W. Kim *et al.*, Relationship of T2-Weighted MRI Myocardial Hyperintensity and the Ischemic Area-At-Risk. *Circulation research* **117**, 254-265 (2015).

30. D. P. O'Regan *et al.*, Reperfusion Hemorrhage Following Acute Myocardial Infarction: Assessment with T2* Mapping and Effect on Measuring the Area at Risk. *Radiology* **250**, 916-922 (2009).

31. H. Bulluck *et al.*, T1 mapping and T2 mapping at 3T for quantifying the area-at-risk in reperfused STEMI patients. *Journal of Cardiovascular Magnetic Resonance* **17**, 73 (2015).

32. D. Liu *et al.*, CMR native T1 mapping allows differentiation of reversible versus irreversible myocardial damage in ST-segment–elevation myocardial infarction: an OxAMI study (Oxford Acute Myocardial Infarction). *Circulation: Cardiovascular Imaging* **10**, e005986 (2017).

33. A. Kali *et al.*, Native T1 mapping by 3-T CMR imaging for characterization of chronic myocardial infarctions. *JACC: Cardiovascular Imaging* **8**, 1019-1030 (2015).

34. A. G. Almeida *et al.*, Multimodality imaging of myocardial viability: an expert consensus document from the European Association of Cardiovascular Imaging (EACVI). *European Heart Journal - Cardiovascular Imaging* **22**, e97-e125 (2021).

35. E. J. Velazquez *et al.*, Coronary-artery bypass surgery in patients with left ventricular dysfunction. *New England Journal of Medicine* **364**, 1607-1616 (2011).

36. E. J. Velazquez *et al.*, Coronary-artery bypass surgery in patients with ischemic cardiomyopathy. *New England Journal of Medicine* **374**, 1511-1520 (2016).

37. R. Senior *et al.*, Clinical practice of contrast echocardiography: recommendation by the European Association of Cardiovascular Imaging (EACVI) 2017. *Eur Heart J Cardiovasc Imaging* **18**, 1205-1205af (2017).

38. P. Nihoyannopoulos, J. L. Vanoverschelde, Myocardial ischaemia and viability: the pivotal role of echocardiography. *Eur Heart J* **32**, 810-819 (2011).

39. R. Sicari *et al.*, Stress Echocardiography Expert Consensus Statement--Executive Summary: European Association of Echocardiography (EAE) (a registered branch of the ESC). *Eur Heart J* **30**, 278-289 (2009).

40. A. Giorgetti *et al.*, Baseline/postnitrate tetrofosmin SPECT for myocardial viability assessment in patients with postischemic severe left ventricular dysfunction: new evidence from MRI. *J Nucl Med* **46**, 1285-1293 (2005).

41. R. Senior, S. Kaul, U. Raval, A. Lahiri, Impact of revascularization and myocardial viability determined by nitrate-enhanced Tc-99m sestamibi and Tl-201 imaging on mortality and functional outcome in ischemic cardiomyopathy. *J Nucl Cardiol* **9**, 454-462 (2002).

42. V. A. Roelants, J. L. Vanoverschelde, T. M. Vander Borght, J. A. Melin, Reverse redistribution on exercise-redistribution (201)Tl SPECT in chronic ischemic dysfunction: predictive of functional outcome after revascularization? *J Nucl Med* **43**, 621-627 (2002).

43. V. Dilsizian, T. P. Rocco, N. M. Freedman, M. B. Leon, R. O. Bonow, Enhanced detection of ischemic but viable myocardium by the reinjection of thallium after stress-redistribution imaging. *N Engl J Med* **323**, 141-146 (1990).

44. C. Anagnostopoulos, A. Georgakopoulos, N. Pianou, S. G. Nekolla, Assessment of myocardial perfusion and viability by positron emission tomography. *Int J Cardiol* **167**, 1737-1749 (2013).

45. N. Ghosh, O. E. Rimoldi, R. S. Beanlands, P. G. Camici, Assessment of myocardial ischaemia and viability: role of positron emission tomography. *Eur Heart J* **31**, 2984-2995 (2010).

46. M. F. Di Carli *et al.*, Value of metabolic imaging with positron emission tomography for evaluating prognosis in patients with coronary artery disease and left ventricular dysfunction. *Am J Cardiol* **73**, 527-533 (1994).

47. A. J. Reimann *et al.*, Late enhancement using multidetector row computer tomography: a feasibility study with low dose 80 kV protocol. *Eur J Radiol* **66**, 127-133 (2008).

48. T. Matsuda *et al.*, Diagnostic accuracy of late iodine enhancement on cardiac computed tomography with a denoise filter for the evaluation of myocardial infarction. *The international journal of cardiovascular imaging* **31**, 177-185 (2015).

49. D. F. Adams, S. J. Hessel, P. F. Judy, J. A. Stein, H. L. Abrams, Computed tomography of the normal and infarcted myocardium. *AJR Am J Roentgenol* **126**, 786-791 (1976).

50. J. Schulz-Menger *et al.*, Standardized image interpretation and post-processing in cardiovascular magnetic resonance - 2020 update : Society for Cardiovascular Magnetic Resonance (SCMR): Board of Trustees Task Force on Standardized Post-Processing. *J Cardiovasc Magn Reson* **22**, 19 (2020).

51. L. C. Amado *et al.*, Accurate and objective infarct sizing by contrast-enhanced magnetic resonance imaging in a canine myocardial infarction model. *J Am Coll Cardiol* **44**, 2383-2389 (2004).

52. R. J. Kim *et al.*, Relationship of MRI delayed contrast enhancement to irreversible injury, infarct age, and contractile function. *Circulation* **100**, 1992-2002 (1999).

53. A. Lerman, D. R. Holmes, J. Herrmann, B. J. Gersh, Microcirculatory dysfunction in ST-elevation myocardial infarction: cause, consequence, or both? *European heart journal* **28**, 788-797 (2007).

54. D. N. Granger, P. R. Kvietys, Reperfusion injury and reactive oxygen species: The evolution of a concept. *Redox Biol* **6**, 524-551 (2015).

55. N. Galea *et al.*, Microvascular obstruction extent predicts major adverse cardiovascular events in patients with acute myocardial infarction and preserved ejection fraction. *European radiology* **29**, 2369-2377 (2019).

56. S. de Waha *et al.*, Relationship between microvascular obstruction and adverse events following primary percutaneous coronary intervention for ST-segment elevation myocardial infarction: an individual patient data pooled analysis from seven randomized trials. *European heart journal* **38**, 3502-3510 (2017).

57. I. Eitel *et al.*, Comprehensive prognosis assessment by CMR imaging after ST-segment elevation myocardial infarction. *Journal of the American College of Cardiology* **64**, 1217-1226 (2014).

58. G. Ambrosio, K. Savino, CMR Assessment of Microvascular Obstruction in STEMI. *Journal of the American College of Cardiology* **64**, 1227-1230 (2014).

59. K. C. Wu *et al.*, Quantification and time course of microvascular obstruction by contrast-enhanced echocardiography and magnetic resonance imaging following acute myocardial infarction and reperfusion. *J Am Coll Cardiol* **32**, 1756-1764 (1998).

60. M. B. Britten, A. M. Zeiher, V. Schächinger, Microvascular dysfunction in angiographically normal or mildly diseased coronary arteries predicts adverse cardiovascular long-term outcome. *Coronary artery disease* **15**, 259-264 (2004).

61. K. C. Wu, CMR of microvascular obstruction and hemorrhage in myocardial infarction. *Journal of Cardiovascular Magnetic Resonance* **14**, 1-16 (2012).

62. D. Carrick *et al.*, Myocardial Hemorrhage After Acute Reperfused ST-Segment-Elevation Myocardial Infarction: Relation to Microvascular Obstruction and Prognostic Significance. *Circ Cardiovasc Imaging* **9**, e004148 (2016).

63. C. S. Lotan, S. K. Miller, G. B. Cranney, G. M. Pohost, G. A. Elgavish, The effect of postinfarction intramyocardial hemorrhage on transverse relaxation time. *Magnetic resonance in medicine* **23**, 346-355 (1992).

64. D. P. O'Regan *et al.*, Assessment of severe reperfusion injury with T2* cardiac MRI in patients with acute myocardial infarction. *Heart* **96**, 1885-1891 (2010).

65. S. D. Gertz *et al.*, Cardiac morphologic findings in patients with acute myocardial infarction treated with recombinant tissue plasminogen activator. *The American journal of cardiology* **65**, 953-961 (1990).

66. H. Fujiwara *et al.*, A clinicopathologic study of patients with hemorrhagic myocardial infarction treated with selective coronary thrombolysis with urokinase. *Circulation* **73**, 749-757 (1986).

67. D. Mathey, J. Schofer, K. Kuck, U. Beil, G. Klöppel, Transmural, haemorrhagic myocardial infarction after intracoronary streptokinase. Clinical, angiographic, and necropsy findings. *British heart journal* **48**, 546 (1982).

68. B. F. Waller *et al.*, Status of the myocardium and infarct-related coronary artery in 19 necropsy patients with acute recanalization using pharmacologic (streptokinase, r-tissue plasminogen activator), mechanical (percutaneous transluminal coronary angioplasty) or combined types of reperfusion therapy. *Journal of the American College of Cardiology* **9**, 785-801 (1987).

69. R. J. Capone, A. S. Most, Myocardial hemorrhage after coronary reperfusion in pigs. *The American Journal of Cardiology* **41**, 259-266 (1978).

70. L. Higginson *et al.*, Determinants of myocardial hemorrhage after coronary reperfusion in the anesthetized dog. *Circulation* **65**, 62-69 (1982).

71. A. G. Goodwill, G. M. Dick, A. M. Kiel, J. D. Tune, Regulation of Coronary Blood Flow. *Comprehensive Physiology* **7**, 321-382 (2017).

72. H. R. Schelbert, Anatomy and physiology of coronary blood flow. *Journal of Nuclear Cardiology* **17**, 545-554 (2010).

73. R. A. Kloner, C. E. Ganote, R. B. Jennings, The "no-reflow" phenomenon after temporary coronary occlusion in the dog. *The Journal of clinical investigation* **54**, 1496-1508 (1974).

74. R. M. Judd *et al.*, Physiological basis of myocardial contrast enhancement in fast magnetic resonance images of 2-day-old reperfused canine infarcts. *Circulation* **92**, 1902-1910 (1995).

75. R. P. Betgem *et al.*, Intramyocardial haemorrhage after acute myocardial infarction. *Nat Rev Cardiol* **12**, 156-167 (2015).

76. R. P. Amier *et al.*, Predictors of intramyocardial hemorrhage after reperfused ST-segment elevation myocardial infarction. *Journal of the American Heart Association*, (2017).

77. E. Braunwald, R. A. Kloner, Myocardial reperfusion: a double-edged sword? *The Journal of clinical investigation* **76**, 1713-1719 (1985).

78. A. N. Mather, T. A. Fairbairn, S. G. Ball, J. P. Greenwood, S. Plein, Reperfusion haemorrhage as determined by cardiovascular MRI is a predictor of adverse left ventricular remodelling and markers of late arrhythmic risk. *Heart* **97**, 453-459 (2011).

79. J. Czernin *et al.*, Effect of Acute and Long-term Smoking on Myocardial Blood Flow and Flow Reserve. *Circulation* **91**, 2891-2897 (1995).

80. D. W. Erkelens, Insulin resistance syndrome and type 2 diabetes mellitus. *Am J Cardiol* **88**, 38j-42j (2001).

81. E. Casiglia *et al.*, Cardiovascular mortality in non-insulin-dependent diabetes mellitus. A controlled study among 683 diabetics and 683 age- and sex-matched normal subjects. *Eur J Epidemiol* **16**, 677-684 (2000).

82. S. M. Haffner, S. Lehto, T. Rönnemaa, K. Pyörälä, M. Laakso, Mortality from coronary heart disease in subjects with type 2 diabetes and in nondiabetic subjects with and without prior myocardial infarction. *N Engl J Med* **339**, 229-234 (1998).

83. I. Iltis *et al.*, Defective Myocardial Blood Flow and Altered Function of the Left Ventricle in Type 2 Diabetic Rats: A Noninvasive In Vivo Study Using Perfusion and Cine Magnetic Resonance Imaging. *Investigative Radiology* **40**, 19-26 (2005).

84. I. Iltis, F. Kober, C. Dalmasso, P. J. Cozzone, M. Bernard, Noninvasive Characterization of Myocardial Blood Flow in Diabetic, Hypertensive, and Diabetic–Hypertensive Rats Using Spin-Labeling MRI. *Microcirculation* **12**, 607-614 (2005).

85. R. Pop-Busui *et al.*, Sympathetic dysfunction in type 1 diabetes. *Journal of the American College of Cardiology* **44**, 2368-2374 (2004).

86. Y.-D. Tang *et al.*, Low Thyroid Function Leads to Cardiac Atrophy With Chamber Dilatation, Impaired Myocardial Blood Flow, Loss of Arterioles, and Severe Systolic Dysfunction. *Circulation* **112**, 3122-3130 (2005).

87. M. J. Kruse *et al.*, Myocardial Blood Flow and Inflammatory Cardiac Sarcoidosis. *JACC: Cardiovascular Imaging* **10**, 157-167 (2017).

88. A. Kali *et al.*, Chronic manifestation of postreperfusion intramyocardial hemorrhage as regional iron deposition: a cardiovascular magnetic resonance study with ex vivo validation. *Circulation. Cardiovascular imaging* **6**, 218-228 (2013).

89. T. Bochaton *et al.*, Association of myocardial hemorrhage and persistent microvascular obstruction with circulating inflammatory biomarkers in STEMI patients. *PLOS ONE* **16**, e0245684 (2021).

90. A. Kapetanopoulos *et al.*, Acute resting myocardial perfusion imaging in patients with diabetes mellitus: results from the emergency room assessment of sestamibi for evaluation of chest pain (ERASE Chest Pain) trial. *Journal of Nuclear Cardiology* **11**, 570-577 (2004).

91. L. J. Shaw *et al.*, Prognostic estimation of coronary artery disease risk with resting perfusion abnormalities and stress ischemia on myocardial perfusion SPECT. *Journal of Nuclear Cardiology* **15**, 762-773 (2008).

92. A. Borlotti *et al.*, Acute Microvascular Impairment Post-Reperfused STEMI Is Reversible and Has Additional Clinical Predictive Value: A CMR OxAMI Study. *JACC Cardiovasc Imaging* **12**, 1783-1793 (2019).

93. I. Morishima *et al.*, Risk stratification of patients with prior myocardial infarction and advanced left ventricular dysfunction by gated myocardial perfusion SPECT imaging. *Journal of Nuclear Cardiology* **15**, 631-637 (2008).

94. K. Nishisato *et al.*, Impaired cardiac sympathetic innervation and myocardial perfusion are related to lethal arrhythmia: quantification of cardiac tracers in patients with ICDs. *Journal of Nuclear Medicine* **51**, 1241-1249 (2010).

95. B. J. Chow *et al.*, Treadmill exercise produces larger perfusion defects than dipyridamole stress N-13 ammonia positron emission tomography. *Journal of the American College of Cardiology* **47**, 411-416 (2006).

96. L. Shaw, A. Iskandrian, Prognostic value of stress gated SPECT in patients with known or suspected coronary artery disease. *J Nucl Cardiol* **11**, 171-185 (2004).

97. R. Hachamovitch *et al.*, Incremental prognostic value of myocardial perfusion single photon emission computed tomography for the prediction of cardiac death: differential stratification for risk of cardiac death and myocardial infarction. *Circulation* **97**, 535-543 (1998).

98. N. P. Johnson *et al.*, Prognostic value of fractional flow reserve: linking physiologic severity to clinical outcomes. *Journal of the American College of Cardiology* **64**, 1641-1654 (2014).

99. P. A. Tonino *et al.*, Fractional flow reserve versus angiography for guiding percutaneous coronary intervention. *New England Journal of Medicine* **360**, 213-224 (2009).

100. J. K. Min *et al.*, Diagnostic Accuracy of Fractional Flow Reserve From Anatomic CT Angiography. *JAMA* **308**, 1237-1245 (2012).

101. C. Tesche *et al.*, Coronary CT Angiography–derived Fractional Flow Reserve. *Radiology* **285**, 17-33 (2017).

102. V. R. Taqueti *et al.*, Coronary microvascular dysfunction and future risk of heart failure with preserved ejection fraction. *European heart journal* **39**, 840-849 (2018).

103. S. E. Bingham, R. Hachamovitch, Incremental Prognostic Significance of Combined Cardiac Magnetic Resonance Imaging, Adenosine Stress Perfusion, Delayed Enhancement, and Left Ventricular Function Over Preimaging Information for the Prediction of Adverse Events. *Circulation* **123**, 1509-1518 (2011).

104. R. J. Gibbons, U. S. Valeti, P. A. Araoz, A. S. Jaffe, The quantification of infarct size. *Journal of the American College of Cardiology* **44**, 1533-1542 (2004).

105. O. P. Simonetti *et al.*, An Improved MR Imaging Technique for the Visualization of Myocardial Infarction. *Radiology* **218**, 215-223 (2001).

106. D. S. Fieno *et al.*, Contrast-enhanced magnetic resonance imaging of myocardium at risk. *Journal of the American College of Cardiology* **36**, 1985-1991 (2000).

107. N. Murata *et al.*, Macrocyclic and other non–group 1 gadolinium contrast agents deposit low levels of gadolinium in brain and bone tissue: preliminary results from 9 patients with normal renal function. *Investigative radiology* **51**, 447-453 (2016).

108. T. Kanda *et al.*, Gadolinium-based contrast agent accumulates in the brain even in subjects without severe renal dysfunction: evaluation of autopsy brain specimens with inductively coupled plasma mass spectroscopy. *Radiology* **276**, 228-232 (2015).

109. M. Ramalho, J. Ramalho, L. M. Burke, R. C. Semelka, Gadolinium Retention and Toxicity—An Update. *Advances in Chronic Kidney Disease* **24**, 138-146 (2017).

110. J. W. Choi, W.-J. Moon, Gadolinium Deposition in the Brain: Current Updates. *kjr* **20**, 134-147 (2018).

111. B. J. Guo, Z. L. Yang, L. J. Zhang, Gadolinium Deposition in Brain: Current Scientific Evidence and Future Perspectives. *Frontiers in Molecular Neuroscience* **11**, (2018).

112. R. J. Kim, E.-L. Chen, J. o. A. Lima, R. M. Judd, Myocardial Gd-DTPA kinetics determine MRI contrast enhancement and reflect the extent and severity of myocardial injury after acute reperfused infarction. *Circulation* **94**, 3318-3326 (1996).

113. W. G. Rehwald, D. S. Fieno, E.-L. Chen, R. J. Kim, R. M. Judd, Myocardial magnetic resonance imaging contrast agent concentrations after reversible and irreversible ischemic injury. *Circulation* **105**, 224-229 (2002).

114. M.-F. Bellin, A. J. Van Der Molen, Extracellular gadolinium-based contrast media: an overview. *European journal of radiology* **66**, 160-167 (2008).

115. G. B. Chavhan, P. S. Babyn, B. Thomas, M. M. Shroff, E. M. Haacke, Principles, techniques, and applications of T2*-based MR imaging and its special applications. *Radiographics* **29**, 1433-1449 (2009).

116. L. J. Anderson *et al.*, Cardiovascular T2-star (T2*) magnetic resonance for the early diagnosis of myocardial iron overload. *European Heart Journal* **22**, 2171-2179 (2001).

117. G. Liu, G. Sobering, A. W. Olson, P. Van Gelderen, C. T. Moonen, Fast echo-shifted gradient-recalled MRI: combining a short repetition time with variable T2* weighting. *Magnetic resonance in medicine* **30**, 68-75 (1993).

118. P. Triadyaksa, M. Oudkerk, P. E. Sijens, Cardiac T2* mapping: Techniques and clinical applications. *Journal of Magnetic Resonance Imaging* **52**, 1340-1351 (2020).

119. S. B. Reeder, A. Z. Faranesh, J. L. Boxerman, E. R. McVeigh, In vivo measurement of T* 2 and field inhomogeneity maps in the human heart at 1.5 T. *Magnetic resonance in medicine* **39**, 988-998 (1998).

120. C. M. Sandino, P. Kellman, A. E. Arai, M. S. Hansen, H. Xue, Myocardial T2* mapping: influence of noise on accuracy and precision. *Journal of Cardiovascular Magnetic Resonance* **17**, 7 (2015).

121. L. Anderson *et al.*, Cardiovascular T2-star (T2*) magnetic resonance for the early diagnosis of myocardial iron overload. *European heart journal* **22**, 2171-2179 (2001).

122. A. Kumar *et al.*, Detection and Quantification of Myocardial Reperfusion Hemorrhage Using T2*-Weighted CMR. *JACC: Cardiovascular Imaging* **4**, 1274-1283 (2011).

123. T. F. Christian *et al.*, Absolute myocardial perfusion in canines measured by using dual-bolus first-pass MR imaging. *Radiology* **232**, 677-684 (2004).

124. F. Kober, T. Jao, T. Troalen, K. S. Nayak, Myocardial arterial spin labeling. *Journal of Cardiovascular Magnetic Resonance* **18**, 22 (2016).

125. M. J. Fair *et al.*, Initial investigation of free-breathing 3D whole-heart stress myocardial perfusion MRI. *Glob Cardiol Sci Pract* **2020**, e202038-e202038 (2020).

126. Y. Tian *et al.*, Whole-heart, ungated, free-breathing, cardiac-phase-resolved myocardial perfusion MRI by using Continuous Radial Interleaved simultaneous Multi-slice acquisitions at sPoiled steady-state (CRIMP). *Magnetic Resonance in Medicine* **84**, 3071-3087 (2020).

127. A. Schuster *et al.*, Quantitative assessment of magnetic resonance derived myocardial perfusion measurements using advanced techniques: microsphere validation in an explanted pig heart system. *Journal of Cardiovascular Magnetic Resonance* **16**, 82 (2014).

128. A. G. Pohlman, The course of the blood through the heart of the fetal mammal, with a note on the reptilian and amphibian circulations. *The Anatomical Record* **3**, 75-109 (1909).

129. M. Prinzmetal, E. M. Ornitz Jr, B. Simkin, H. Bergman, Arterio-venous anastomoses in liver, spleen, and lungs. *American Journal of Physiology-Legacy Content* **152**, 48-52 (1947).

130. J. I. Hoffman, The history of the microsphere method for measuring blood flows with special reference to myocardial blood flow: a personal memoir. *Am J Physiol Heart Circ Physiol* **312**, H705-h710 (2017).

131. R. Glenny, S. Bernard, M. Brinkley, Validation of fluorescent-labeled microspheres for measurement of regional organ perfusion. *Journal of Applied Physiology* **74**, 2585-2597 (1993).

132. P. Kowallik *et al.*, Measurement of regional myocardial blood flow with multiple colored microspheres. *Circulation* **83**, 974-982 (1991).

133. B. De Bruyne, J. Sarma, Fractional flow reserve: a review. *Heart* **94**, 949 (2008).

134. R. S. Driessen *et al.*, Impact of Revascularization on Absolute Myocardial Blood Flow as Assessed by Serial [15O]H2O Positron Emission Tomography Imaging. *Circulation: Cardiovascular Imaging* **11**, e007417 (2018).

135. R. C. Hendel *et al.*, Multicenter clinical trial to evaluate the efficacy of correction for photon attenuation and scatter in SPECT myocardial perfusion imaging. *Circulation* **99**, 2742-2749 (1999).

136. D. S. Berman *et al.*, Underestimation of extent of ischemia by gated SPECT myocardial perfusion imaging in patients with left main coronary artery disease. *Journal of nuclear cardiology* **14**, 521-528 (2007).

137. R. Nakazato, D. S. Berman, E. Alexanderson, P. Slomka, Myocardial perfusion imaging with PET. *Imaging in medicine* **5**, 35 (2013).

138. P. J. Slomka, R. J. H. Miller, L.-H. Hu, G. Germano, D. S. Berman, Solid-State Detector SPECT Myocardial Perfusion Imaging. *Journal of Nuclear Medicine* **60**, 1194-1204 (2019).

139. B. F. Hutton *et al.*, Development of clinical simultaneous SPECT/MRI. *The British Journal of Radiology* **91**, 20160690 (2018).

140. S. Bergmann *et al.*, Quantification of regional myocardial blood flow in vivo with H215O. *Circulation* **70**, 724-733 (1984).

141. J. O. Prior *et al.*, Quantification of myocardial blood flow with 82Rb positron emission tomography: clinical validation with 15O-water. *European Journal of Nuclear Medicine and Molecular Imaging* **39**, 1037-1047 (2012).

142. O. Muzik *et al.*, Validation of Nitrogen-13-Ammonia Tracer Kinetic Model for Quantification of Myocardial Blood Flow Using PET. *Journal of Nuclear Medicine* **34**, 83-91 (1993).

143. C. Byrne, P. Hasbak, A. Kjaer, J. J. Thune, L. Køber, Impaired myocardial perfusion is associated with increasing end-systolic- and end-diastolic volumes in patients with non-ischemic systolic heart failure: a cross-sectional study using Rubidium-82 PET/CT. *BMC Cardiovasc Disord* **19**, 68 (2019).

144. S. Seitun *et al.*, CT Myocardial Perfusion Imaging: A New Frontier in Cardiac Imaging. *BioMed Research International* **2018**, 7295460 (2018).

145. L. Yang *et al.*, Meta-analysis: diagnostic accuracy of coronary CT angiography with prospective ECG gating based on step-and-shoot, Flash and volume modes for detection of coronary artery disease. *European radiology* **24**, 2345-2352 (2014).

146. D. H. Yang, Y.-H. Kim, CT myocardial perfusion imaging: current status and future perspectives. *The International Journal of Cardiovascular Imaging* **33**, 1009-1020 (2017).

147. K. Nieman, S. Balla, Dynamic CT myocardial perfusion imaging. *Journal of Cardiovascular Computed Tomography* **14**, 303-306 (2020).

148. K. Wei *et al.*, Quantification of Myocardial Blood Flow With Ultrasound-Induced Destruction of Microbubbles Administered as a Constant Venous Infusion. *Circulation* **97**, 473-483 (1998).

149. A. Feher, A. J. Sinusas, Quantitative Assessment of Coronary Microvascular Function. *Circulation: Cardiovascular Imaging* **10**, e006427 (2017).

150. J. P. Greenwood *et al.*, Cardiovascular magnetic resonance and single-photon emission computed tomography for diagnosis of coronary heart disease (CE-MARC): a prospective trial. *The Lancet* **379**, 453-460 (2012).

151. J. Schwitter *et al.*, MR-IMPACT II: Magnetic Resonance Imaging for Myocardial Perfusion Assessment in Coronary artery disease Trial: perfusion-cardiac magnetic resonance vs. single-photon emission computed tomography for the detection of coronary artery disease: a comparative multicentre, multivendor trial. *European heart journal* **34**, 775-781 (2013).

152. J. Schwitter *et al.*, Superior diagnostic performance of perfusion-cardiovascular magnetic resonance versus SPECT to detect coronary artery disease: The secondary endpoints of the multicenter multivendor MR-IMPACT II (Magnetic Resonance Imaging for Myocardial Perfusion Assessment in Coronary Artery Disease Trial). *Journal of Cardiovascular Magnetic Resonance* **14**, 1-10 (2012).

153. H. Engblom *et al.*, Fully quantitative cardiovascular magnetic resonance myocardial perfusion ready for clinical use: a comparison between cardiovascular magnetic resonance imaging and positron emission tomography. *Journal of Cardiovascular Magnetic Resonance* **19**, 78 (2017).

154. J. Schwitter *et al.*, Assessment of Myocardial Perfusion in Coronary Artery Disease by Magnetic Resonance. *Circulation* **103**, 2230-2235 (2001).

155. A. A. Qayyum *et al.*, Quantification of myocardial perfusion using cardiac magnetic resonance imaging correlates significantly to rubidium-82 positron emission tomography in patients with severe coronary artery disease: A preliminary study. *European Journal of Radiology* **83**, 1120-1128 (2014).

156. T. F. Christian, A. H. Aletras, A. E. Arai, Estimation of absolute myocardial blood flow during first-pass MR perfusion imaging using a dual-bolus injection technique:

Comparison to single-bolus injection method. *Journal of Magnetic Resonance Imaging* **27**, 1271-1277 (2008).

157. P. D. Gatehouse *et al.*, Accurate assessment of the arterial input function during high-dose myocardial perfusion cardiovascular magnetic resonance. *Journal of Magnetic Resonance Imaging: An Official Journal of the International Society for Magnetic Resonance in Medicine* **20**, 39-45 (2004).

158. K. D. Knott *et al.*, Quantitative myocardial perfusion in coronary artery disease: A perfusion mapping study. *Journal of Magnetic Resonance Imaging* **50**, 756-762 (2019).

159. F. E. Mordini *et al.*, Diagnostic accuracy of stress perfusion CMR in comparison with quantitative coronary angiography: fully quantitative, semiquantitative, and qualitative assessment. *JACC. Cardiovascular imaging* **7**, 14-22 (2014).

160. M. C. Ziadi, R. S. B. Beanlands, The clinical utility of assessing myocardial blood flow using positron emission tomography. *Journal of Nuclear Cardiology* **17**, 571-581 (2010).

161. A. M. Larghat *et al.*, Reproducibility of first-pass cardiovascular magnetic resonance myocardial perfusion. *Journal of Magnetic Resonance Imaging* **37**, 865-874 (2013).

162. A. Seitz *et al.*, Impact of baseline calibration on semiquantitative assessment of myocardial perfusion reserve by adenosine stress MRI. *The International Journal of Cardiovascular Imaging* **36**, 521-532 (2020).

163. P. Kellman *et al.*, Myocardial perfusion cardiovascular magnetic resonance: optimized dual sequence and reconstruction for quantification. *J Cardiovasc Magn Reson* **19**, 43 (2017).

164. C. M. Scannell *et al.*, Deep-Learning-Based Preprocessing for Quantitative Myocardial Perfusion MRI. *Journal of Magnetic Resonance Imaging* **51**, 1689-1696 (2020).

165. K. D. Knott *et al.*, The Prognostic Significance of Quantitative Myocardial Perfusion. *Circulation* **141**, 1282-1291 (2020).

166. R. Jaffe, A. Dick, B. H. Strauss, Prevention and treatment of microvascular obstruction-related myocardial injury and coronary no-reflow following percutaneous coronary intervention: a systematic approach. *JACC Cardiovasc Interv* **3**, 695-704 (2010).

167. R. Jaffe, T. Charron, G. Puley, A. Dick, B. H. Strauss, Microvascular Obstruction and the No-Reflow Phenomenon After Percutaneous Coronary Intervention. *Circulation* **117**, 3152-3156 (2008).

168. S. Verma *et al.*, Fundamentals of Reperfusion Injury for the Clinical Cardiologist. *Circulation* **105**, 2332-2336 (2002).

169. D. L. Carden, D. N. Granger, Pathophysiology of ischaemia–reperfusion injury. *The Journal of Pathology* **190**, 255-266 (2000).

170. C.-H. Huang *et al.*, Hypothermia treatment preserves mitochondrial integrity and viability of cardiomyocytes after ischaemic reperfusion injury. *Injury* **46**, 233-239 (2015).

171. D. N. Granger, Ischemia-reperfusion: mechanisms of microvascular dysfunction and the influence of risk factors for cardiovascular disease. *Microcirculation* **6**, 167-178 (1999).

172. M. Ruiz-Meana, D. García-Dorado, Pathophysiology of Ischemia-Reperfusion Injury: New Therapeutic Options for Acute Myocardial Infarction. *Revista Española de Cardiología (English Edition)* **62**, 199-209 (2009).

173. D. N. Granger, P. R. Kvietys, Reperfusion therapy-What's with the obstructed, leaky and broken capillaries? *Pathophysiology : the official journal of the International Society for Pathophysiology* **24**, 213-228 (2017).

174. Ł. A. Małek *et al.*, Platelet Reactivity and Intramyocardial Hemorrhage in Patients With ST-Segment Elevation Myocardial Infarction. *Clinical and Applied Thrombosis/Hemostasis* **20**, 553-558 (2014).

175. N. Abbaspour, R. Hurrell, R. Kelishadi, Review on iron and its importance for human health. *J Res Med Sci* **19**, 164-174 (2014).

176. J. Hirst, Mitochondrial complex I. *Annu Rev Biochem* **82**, 551-575 (2013).

177. T. Ravingerová *et al.*, The Molecular Mechanisms of Iron Metabolism and Its Role in Cardiac Dysfunction and Cardioprotection. *Int J Mol Sci* **21**, (2020).

178. R. Yip, P. Dallman, Iron: Present knowledge in nutrition. *Edited by: Bowman BA and Russell RM*, 311-328 (1996).

179. P. T. Lieu, M. Heiskala, P. A. Peterson, Y. Yang, The roles of iron in health and disease. *Mol Aspects Med* **22**, 1-87 (2001).

180. J. L. Beard, J. R. Connor, Iron status and neural functioning. *Annu Rev Nutr* **23**, 41-58 (2003).

181. M. L. Failla, Trace elements and host defense: recent advances and continuing challenges. *J Nutr* **133**, 1443s-1447s (2003).

182. M. F. Hoes *et al.*, Iron deficiency impairs contractility of human cardiomyocytes through decreased mitochondrial function. *European journal of heart failure* **20**, 910-919 (2018).

183. S. D. De, S. Krishna, A. Jethwa, Iron status and its association with coronary heart disease: systematic review and meta-analysis of prospective studies. *Atherosclerosis* **238**, 296-303 (2015).

184. C. P. Wen *et al.*, High serum iron is associated with increased cancer risk. *Cancer Res* **74**, 6589-6597 (2014).

185. S. Milic *et al.*, The Role of Iron and Iron Overload in Chronic Liver Disease. *Med Sci Monit* **22**, 2144-2151 (2016).

186. Q.-M. Wang *et al.*, Inhibiting heme oxygenase-1 attenuates rat liver fibrosis by removing iron accumulation. *World journal of gastroenterology* **19**, 2921-2934 (2013).

187. S. Nomura *et al.*, Changes in renal microcirculation induced by infusion of (Fe3+)-and (Fe2+)-myoglobin during hemorrhagic hypotension in the anesthetized rat: influence of L-NAME and 8-Br-cyclic GMP. *Nephron* **73**, 243-250 (1996).

188. J. O. Defraigne *et al.*, Preservation of cortical microcirculation after kidney ischemia-reperfusion: value of an iron chelator. *Annals of vascular surgery* **8**, 457-467 (1994).

189. P. Yatmark *et al.*, Effects of Iron Chelators on Pulmonary Iron Overload and Oxidative Stress in beta-Thalassemic Mice. *Pharmacology* **96**, 192-199 (2015).

190. J. Neves *et al.*, Disruption of the Hepcidin/Ferroportin Regulatory System Causes Pulmonary Iron Overload and Restrictive Lung Disease. *EBioMedicine* **20**, 230-239 (2017).

191. F. Guidotti *et al.*, Pulmonary dysfunction in thalassaemia major: is there any relationship with body iron stores? *British journal of haematology* **176**, 309-314 (2017).

192. E. Cotroneo *et al.*, Iron homeostasis and pulmonary hypertension: iron deficiency leads to pulmonary vascular remodeling in the rat. *Circulation research* **116**, 1680-1690 (2015).

193. S. R. Bertoli *et al.*, Chronic iron overload induces vascular dysfunction in resistance pulmonary arteries associated with right ventricular remodeling in rats. *Toxicology letters* **295**, 296-306 (2018).

194. L. Zecca, M. B. H. Youdim, P. Riederer, J. R. Connor, R. R. Crichton, Iron, brain ageing and neurodegenerative disorders. *Nature Reviews Neuroscience* **5**, 863-873 (2004).

195. M. Kobayashi *et al.*, Pathological Roles of Iron in Cardiovascular Disease. *Curr Drug Targets* **19**, 1068-1076 (2018).

196. K. Wijarnpreecha, S. Kumfu, S. C. Chattipakorn, N. Chattipakorn, Cardiomyopathy associated with iron overload: how does iron enter myocytes and what are the implications for pharmacological therapy? *Hemoglobin* **39**, 9-17 (2015).

197. H. Bulluck *et al.*, Residual Myocardial Iron Following Intramyocardial Hemorrhage During the Convalescent Phase of Reperfused ST-Segment-Elevation Myocardial Infarction and Adverse Left Ventricular Remodeling. *Circulation: Cardiovascular Imaging* **9**, e004940 (2016).

198. K. V. Kowdley, K. E. Brown, J. Ahn, V. Sundaram, ACG Clinical Guideline: Hereditary Hemochromatosis. *Am J Gastroenterol* **114**, 1202-1218 (2019).

199. J. Jian *et al.*, Effects of iron deficiency and iron overload on angiogenesis and oxidative stress—a potential dual role for iron in breast cancer. *Free Radical Biology and Medicine* **50**, 841-847 (2011).

200. J. Eckard *et al.*, Effects of cellular iron deficiency on the formation of vascular endothelial growth factor and angiogenesis. *Cancer Cell International* **10**, 28 (2010).

201. X. Huang, Does iron have a role in breast cancer? *The Lancet Oncology* **9**, 803-807 (2008).

202. A. A. Alkhateeb, B. Han, J. R. Connor, Ferritin stimulates breast cancer cells through an iron-independent mechanism and is localized within tumor-associated macrophages. *Breast Cancer Research and Treatment* **137**, 733-744 (2013).

203. X. Wu, M. R. Reboll, M. Korf-Klingebiel, K. C. Wollert, Angiogenesis After Acute Myocardial Infarction. *Cardiovasc Res*, (2020).

204. I. Cokic *et al.*, Iron deposition following chronic myocardial infarction as a substrate for cardiac electrical anomalies: initial findings in a canine model. *PloS one* **8**, e73193-e73193 (2013).

205. B. Behrouzi *et al.*, Action of iron chelator on intramyocardial hemorrhage and cardiac remodeling following acute myocardial infarction. *Basic Research in Cardiology* **115**, 24 (2020).

206. L. L. Cooper *et al.*, Microvascular Function Contributes to the Relation Between Aortic Stiffness and Cardiovascular Events. *Circulation: Cardiovascular Imaging* **9**, e004979 (2016).

207. A. M. Komarov, I. T. Mak, W. B. Weglicki, Iron potentiates nitric oxide scavenging by dithiocarbamates in tissue of septic shock mice. *Biochimica et biophysica acta* **1361**, 229-234 (1997).

208. A. Kali *et al.*, Persistent Microvascular Obstruction After Myocardial Infarction Culminates in the Confluence of Ferric Iron Oxide Crystals, Proinflammatory Burden, and Adverse Remodeling. *Circulation. Cardiovascular imaging* **9**, (2016).

209. D. A. Siwik, D. L. Chang, W. S. Colucci, Interleukin-1beta and tumor necrosis factor-alpha decrease collagen synthesis and increase matrix metalloproteinase activity in cardiac fibroblasts in vitro. *Circulation research* **86**, 1259-1265 (2000).

210. N. B. Spath, N. L. Mills, N. L. Cruden, Novel cardioprotective and regenerative therapies in acute myocardial infarction: a review of recent and ongoing clinical trials. *Future Cardiology* **12**, 655-672 (2016).

211. J. Loscalzo, Is oxygen therapy beneficial in acute myocardial infarction? Simple question, complicated mechanism, simple answer. *N Engl J Med* **377**, 1286-1287 (2017).

212. J. R. Spears *et al.*, Aqueous oxygen hyperbaric reperfusion in a porcine model of myocardial infarction. *Journal of Invasive Cardiology* **14**, 160-166 (2002).

213. J. R. Spears *et al.*, Aqueous oxygen attenuation of reperfusion microvascular ischemia in a canine model of myocardial infarction. *Asaio Journal* **49**, 716-720 (2003).

214. G. W. Stone *et al.*, Effect of supersaturated oxygen delivery on infarct size after percutaneous coronary intervention in acute myocardial infarction. *Circulation: Cardiovascular Interventions* **2**, 366-375 (2009).

215. S. W. David *et al.*, Evaluation of intracoronary hyperoxemic oxygen therapy in acute anterior myocardial infarction: The IC-HOT study. *Catheterization and Cardiovascular Interventions* **93**, 882-890 (2019).

216. R. A. Kloner *et al.*, Update on Cardioprotective Strategies for STEMI: Focus on Supersaturated Oxygen Delivery. *JACC: Basic to Translational Science*, (2021).

217. L. O. Chavez, M. Leon, S. Einav, J. Varon, Editor's Choice- Inside the cold heart: A review of therapeutic hypothermia cardioprotection. *European heart journal. Acute cardiovascular care* **6**, 130-141 (2017).

218. N. E. Shumway, F. J. Lewis, Induced ventricular fibrillation for experimental intracardiac surgery under hypothermia. *Ann Surg* **143**, 230 (1956).

219. H. Swan, I. Zeavin, Cessation of circulation in general hypothermia. III. Technics of intracardiac surgery under direct vision. *Ann Surg* **139**, 385-396 (1954).

220. S. Azmoon *et al.*, Neurologic and cardiac benefits of therapeutic hypothermia. *Cardiology in review* **19**, 108-114 (2011).

221. J. L. Pool, L. A. Kessler, Mechanism and Control of Centrally Induced Cardiac Irregularities During Hypothermia: Part I. Clinical Observations. *Journal of neurosurgery* **15**, 52-64 (1958).

222. F. Rincon, S. A. Mayer, in *Seminars in neurology*. (Copyright© 2006 by Thieme Medical Publishers, Inc., 333 Seventh Avenue, New …, 2006), vol. 26, pp. 387-395.

223. M. M. Zviman *et al.*, A new method for inducing hypothermia during cardiac arrest. *Critical care medicine* **32**, S369-S373 (2004).

224. S. A. Bernard *et al.*, Treatment of comatose survivors of out-of-hospital cardiac arrest with induced hypothermia. *New England Journal of Medicine* **346**, 557-563 (2002).

225. D. Erlinge *et al.*, A pooled analysis of the effect of endovascular cooling on infarct size in patients with ST-elevation myocardial infarction. *EuroIntervention: journal of EuroPCR in collaboration with the Working Group on Interventional Cardiology of the European Society of Cardiology* **8**, 1435-1440 (2013).

226. C. Grines, I.-I. Investigators, Intravascular cooling adjunctive to percutaneous coronary intervention for acute myocardial infarction. *Transcatheter cardiovascular therapeutics*, (2004).

227. W. O'Neill, A prospective randomized trial of mild systemic hypothermia during PCI treatment of ST elevation MI; the COOL MI trial. *15th Annual Transcatheter Cardiovascular Therapeutics* **16**, (2003).

228. L. C. Otterspoor *et al.*, Safety and feasibility of local myocardial hypothermia. *Catheterization and Cardiovascular Interventions* **87**, 877-883 (2016).

229. T. Mochizuki, S. Yu, T. Katoh, K. Aoki, S. Sato, Cardioprotective effect of therapeutic hypothermia at 34°C against ischaemia/reperfusion injury mediated by PI3K and nitric oxide in a rat isolated heart model. *Resuscitation* **83**, 238-242 (2012).

230. S. Marek-Iannucci *et al.*, Myocardial hypothermia increases autophagic flux, mitochondrial mass and myocardial function after ischemia-reperfusion injury. *Scientific reports* **9**, 10001-10001 (2019).

231. L. C. Otterspoor, L. X. van Nunen, M. van 't Veer, N. P. Johnson, N. H. J. Pijls, Intracoronary Hypothermia Before Reperfusion to Reduce Reperfusion Injury in Acute Myocardial

Infarction: A Novel Hypothesis and Technique. *Ther Hypothermia Temp Manag* **7**, 199-205 (2017).

232. D. Erlinge *et al.*, Rapid Endovascular Catheter Core Cooling Combined With Cold Saline as an Adjunct to Percutaneous Coronary Intervention for the Treatment of Acute Myocardial Infarction: The CHILL-MI Trial: A Randomized Controlled Study of the Use of Central Venous Catheter Core Cooling Combined With Cold Saline as an Adjunct to Percutaneous Coronary Intervention for the Treatment of Acute Myocardial Infarction. *Journal of the American College of Cardiology* **63**, 1857-1865 (2014).

233. S. R. Dixon *et al.*, Induction of mild systemic hypothermia with endovascular cooling during primary percutaneous coronary intervention for acute myocardial infarction. *Journal of the American College of Cardiology* **40**, 1928-1934 (2002).

234. M. Noc *et al.*, COOL AMI EU pilot trial: a multicentre, prospective, randomised controlled trial to assess cooling as an adjunctive therapy to percutaneous intervention in patients with acute myocardial infarction. *EuroIntervention : journal of EuroPCR in collaboration with the Working Group on Interventional Cardiology of the European Society of Cardiology* **13**, e531-e539 (2017).

235. G. Nichol *et al.*, Prospective, multicenter, randomized, controlled pilot trial of peritoneal hypothermia in patients with ST-segment- elevation myocardial infarction. *Circulation. Cardiovascular interventions* **8**, e001965-e001965 (2015).

236. K. Inoue, S. Ando, F. Gyuan, T. Takaba, A study of the myocardial protective effect of rapid cooling based on intracellular Ca, intracellular pH, and HSP70. *Annals of thoracic and cardiovascular surgery : official journal of the Association of Thoracic and Cardiovascular Surgeons of Asia* **9**, 301-306 (2003).

237. M. Gotberg *et al.*, A pilot study of rapid cooling by cold saline and endovascular cooling before reperfusion in patients with ST-elevation myocardial infarction. *Circulation. Cardiovascular interventions* **3**, 400-407 (2010).

238. C. Testori *et al.*, Out-of-hospital initiation of hypothermia in ST-segment elevation myocardial infarction: a randomised trial. *Heart (British Cardiac Society)* **105**, 531-537 (2019).

239. J. Bobi *et al.*, Moderate Hypothermia Modifies Coronary Hemodynamics and Endothelium-Dependent Vasodilation in a Porcine Model of Temperature Management. *J Am Heart Assoc* **9**, e014035 (2020).

240. S. Gambert *et al.*, Deep hypothermia during ischemia improves functional recovery and reduces free-radical generation in isolated reperfused rat heart. *The Journal of Heart and Lung Transplantation* **23**, 487-491 (2004).

241. M. Renuka Prasad *et al.*, Reduced free radical generation during reperfusion of hypothermically arrested hearts. *Molecular and Cellular Biochemistry* **111**, 97-102 (1992).

242. G. Fuernau *et al.*, Mild Hypothermia in Cardiogenic Shock Complicating Myocardial Infarction. *Circulation* **139**, 448-457 (2019).

243. J. W. Cho *et al.*, Moderate and deep hypothermia produces hyporesposiveness to phenylephrine in isolated rat aorta. *Korean J Thorac Cardiovasc Surg* **46**, 402-412 (2013).

244. J. Li *et al.*, Targeted Temperature Management Suppresses Hypoxia-Inducible Factor-1α and Vascular Endothelial Growth Factor Expression in a Pig Model of Cardiac Arrest. *Neurocrit Care*, 1-10 (2021).

245. P. R. Evora *et al.*, Nitric oxide and prostacyclin-dependent pathways involvement on in vitro induced hypothermia. *Cryobiology* **54**, 106-113 (2007).

246. S. H. Lee *et al.*, Nitric oxide-mediated inhibition of phenylephrine-induced contraction in response to hypothermia is partially modulated by endothelial Rho-kinase. *Int J Med Sci* **17**, 21-32 (2020).

247. X. H. Ning *et al.*, Moderate hypothermia (30 degrees C) maintains myocardial integrity and modifies response of cell survival proteins after reperfusion. *Am J Physiol Heart Circ Physiol* **293**, H2119-2128 (2007).

248. X.-H. Ning *et al.*, Hypothermia preserves function and signaling for mitochondrial biogenesis during subsequent ischemia. *American Journal of Physiology-Heart and Circulatory Physiology* **274**, H786-H793 (1998).

249. S. Fischer, D. Renz, M. Wiesnet, W. Schaper, G. F. Karliczek, Hypothermia abolishes hypoxia-induced hyperpermeability in brain microvessel endothelial cells. *Brain Res Mol Brain Res* **74**, 135-144 (1999).

250. E. W. Childs, K. F. Udobi, F. A. Hunter, Hypothermia reduces microvascular permeability and reactive oxygen species expression after hemorrhagic shock. *J Trauma* **58**, 271-277 (2005).

251. A. Diestel, J. Roessler, F. Berger, K. R. Schmitt, Hypothermia downregulates inflammation but enhances IL-6 secretion by stimulated endothelial cells. *Cryobiology* **57**, 216-222 (2008).

252. J. Y. Chung *et al.*, Moderate hypothermia attenuates α(1)-adrenoceptor-mediated contraction in isolated rat aorta: the role of the endothelium. *Cryobiology* **65**, 33-40 (2012).

253. D. Yang, P. Xie, S. Guo, H. Li, Induction of MAPK phosphatase-1 by hypothermia inhibits TNF-alpha-induced endothelial barrier dysfunction and apoptosis. *Cardiovasc Res* **85**, 520-529 (2010).

254. R. Tissier *et al.*, Mild hypothermia reduces per-ischemic reactive oxygen species production and preserves mitochondrial respiratory complexes. *Resuscitation* **84**, 249-255 (2013).

255. T. L. Merrill *et al.*, Myocardial tissue salvage is correlated with ischemic border region temperature at reperfusion. *Catheterization and cardiovascular interventions : official journal of the Society for Cardiac Angiography & Interventions*, (2019).

256. S. Marek-Iannucci, A. Thomas, R. A. Gottlieb, Minimal Invasive Pericardial Perfusion Model in Swine: A Translational Model for Cardiac Remodeling After Ischemia/Reperfusion Injury. *Front Physiol* **11**, 346 (2020).

257. M. C. de Waard *et al.*, Automated peritoneal lavage: an extremely rapid and safe way to induce hypothermia in post-resuscitation patients. *Critical Care* **17**, 1-8 (2013).

258. A. Abou-Chebl, G. Sung, D. Barbut, M. Torbey, Local Brain Temperature Reduction Through Intranasal Cooling With the RhinoChill Device. *Stroke* **42**, 2164-2169 (2011).

259. B. Inderbitzen *et al.*, Safety and Performance of a Novel Intravascular Catheter for Induction and Reversal of Hypothermia in a Porcine Model. *Neurosurgery* **50**, 364-370 (2002).

260. R. Y. Kwong, H. Korlakunta, Diagnostic and Prognostic Value of Cardiac Magnetic Resonance Imaging in Assessing Myocardial Viability. *Topics in Magnetic Resonance Imaging* **19**, 15-24 (2008).

261. K. Kitagawa *et al.*, Acute Myocardial Infarction: Myocardial Viability Assessment in Patients Early Thereafter—Comparison of Contrast-enhanced MR Imaging with Resting 201Tl SPECT. *Radiology* **226**, 138-144 (2003).

262. M. Gutberlet *et al.*, Myocardial viability assessment in patients with highly impaired left ventricular function: comparison of delayed enhancement, dobutamine stress MRI, end-diastolic wall thickness, and TI201-SPECT with functional recovery after revascularization. *European Radiology* **15**, 872-880 (2005).

263. P. A. Villablanca *et al.*, Therapeutic hypothermia in ST elevation myocardial infarction: a systematic review and meta-analysis of randomised control trials. *Heart* **102**, 712-719 (2016).

264. V. Talman, H. Ruskoaho, Cardiac fibrosis in myocardial infarction—from repair and remodeling to regeneration. *Cell and Tissue Research* **365**, 563-581 (2016).

265. W. W. O'Neill, Cooling as an adjunctive therapy to percutaneous intervention in patients with acute myocardial infarction (COOLMI). *Transcatheter Cardiovascular Therapeutics Session. Washington, DC, USA*, 15-19 (2003).

266. J. Shi *et al.*, Myocardial hypothermia induced after reperfusion does not prevent adverse left ventricular remodeling nor improve cardiac function. *Life Sciences*, (2019).

267. N. Torrealba, P. Aranguiz, C. Alonso, B. A. Rothermel, S. Lavandero, Mitochondria in structural and functional cardiac remodeling. *Mitochondrial Dynamics in Cardiovascular Medicine*, 277-306 (2017).

268. E. J. Benjamin *et al.*, Heart Disease and Stroke Statistics-2019 Update: A Report From the American Heart Association. *Circulation* **139**, e56-e528 (2019).

269. S. de Waha *et al.*, Prognosis after ST-elevation myocardial infarction: a study on cardiac magnetic resonance imaging versus clinical routine. *Trials* **15**, 1-9 (2014).

270. C. C. Chiueh, Iron overload, oxidative stress, and axonal dystrophy in brain disorders. Proceedings of 2000 NIH Workshop of Hallervorden-Spatz Syndrome (February 12, 2001). *Pediatric Neurology* **25**, 138-147 (2001).

271. S. M. H. Sadrzadeh, Y. Saffari, Iron and Brain Disorders. *Pathology Patterns Reviews* **121**, S64-S70 (2004).

272. A. Joerk *et al.*, Impact of heme and heme degradation products on vascular diameter in mouse visual cortex. *J Am Heart Assoc* **3**, (2014).

273. A. R. Nair, P. J. Ebenezer, Y. Saini, J. Francis, Angiotensin II-induced hypertensive renal inflammation is mediated through HMGB1-TLR4 signaling in rat tubulo-epithelial cells. *Exp Cell Res* **335**, 238-247 (2015).

274. A. R. Nair, G. S. Masson, P. J. Ebenezer, F. Del Piero, J. Francis, Role of TLR4 in lipopolysaccharide-induced acute kidney injury: protection by blueberry. *Free Radic Biol Med* **71**, 16-25 (2014).

275. O. Bondarenko *et al.*, Standardizing the definition of hyperenhancement in the quantitative assessment of infarct size and myocardial viability using delayed contrast-enhanced CMR. *Journal of Cardiovascular Magnetic Resonance* **7**, 481-485 (2005).

276. Q. Sun *et al.*, Sustained vascular endothelial growth factor delivery enhances angiogenesis and perfusion in ischemic hind limb. *Pharmaceutical research* **22**, 1110-1116 (2005).

277. N. Seiwert *et al.*, Heme oxygenase 1 protects human colonocytes against ROS formation, oxidative DNA damage and cytotoxicity induced by heme iron, but not inorganic iron. *Cell Death & Disease* **11**, 787 (2020).

278. X. J. Zhou, Z. Laszik, X. Q. Wang, F. G. Silva, N. D. Vaziri, Association of renal injury with increased oxygen free radical activity and altered nitric oxide metabolism in chronic experimental hemosiderosis. *Lab Invest* **80**, 1905-1914 (2000).

279. A. Kali, R. L. Q. Tang, A. Kumar, J. K. Min, R. Dharmakumar, Detection of acute reperfusion myocardial hemorrhage with cardiac MR imaging: T2 versus T2. *Radiology* **269**, 387-395 (2013).

280. J. P. Gnana-Prakasam *et al.*, Polarized distribution of heme transporters in retinal pigment epithelium and their regulation in the iron-overload disease hemochromatosis. *Invest Ophthalmol Vis Sci* **52**, 9279-9286 (2011).

281. S. Kumar, U. Bandyopadhyay, Free heme toxicity and its detoxification systems in human. *Toxicol Lett* **157**, 175-188 (2005).

282. Y. Akamatsu *et al.*, Heme oxygenase-1-derived carbon monoxide protects hearts from transplant associated ischemia reperfusion injury. *FASEB journal : official publication of the Federation of American Societies for Experimental Biology* **18**, 771-772 (2004).

283. C. C. Winterbourn, Toxicity of iron and hydrogen peroxide: the Fenton reaction. *Toxicol Lett* **82-83**, 969-974 (1995).

284. C. Donadee *et al.*, Nitric Oxide Scavenging by Red Blood Cell Microparticles and Cell-Free Hemoglobin as a Mechanism for the Red Cell Storage Lesion. *Circulation* **124**, 465-476 (2011).

285. C. D. Reiter *et al.*, Cell-free hemoglobin limits nitric oxide bioavailability in sickle-cell disease. *Nat Med* **8**, 1383-1389 (2002).

286. H. Drexler, E. Hablawetz, W. Lu, U. Riede, A. Christes, Effects of inhibition of nitric oxide formation on regional blood flow in experimental myocardial infarction. *Circulation* **86**, 255-262 (1992).

287. A. A. Glean *et al.*, Effects of nitrite infusion on skeletal muscle vascular control during exercise in rats with chronic heart failure. *Am J Physiol Heart Circ Physiol* **309**, H1354-1360 (2015).

288. F. Vinchi *et al.*, Hemopexin therapy improves cardiovascular function by preventing heme-induced endothelial toxicity in mouse models of hemolytic diseases. *Circulation* **127**, 1317-1329 (2013).

289. M. Giacca, S. Zacchigna, VEGF gene therapy: therapeutic angiogenesis in the clinic and beyond. *Gene Ther* **19**, 622-629 (2012).

290. A. Piga, C. Gaglioti, E. Fogliacco, F. Tricta, Comparative effects of deferiprone and deferoxamine on survival and cardiac disease in patients with thalassemia major: a retrospective analysis. *Haematologica* **88**, 489-496 (2003).

291. V. Perifanis *et al.*, comparison of effects of different long-term iron-chelation regimens on myocardial and hepatic iron concentrations assessed with T2* magnetic resonance imaging in patients with beta-thalassemia major. *Int J Hematol* **86**, 385-389 (2007).

292. V. Berdoukas *et al.*, The efficacy of iron chelator regimes in reducing cardiac and hepatic iron in patients with thalassaemia major: a clinical observational study. *J Cardiovasc Magn Reson* **11**, 20 (2009).

293. L. J. Anderson *et al.*, Comparison of effects of oral deferiprone and subcutaneous desferrioxamine on myocardial iron concentrations and ventricular function in beta-thalassaemia. *Lancet* **360**, 516-520 (2002).

294. A. Pepe *et al.*, Deferasirox, deferiprone and desferrioxamine treatment in thalassemia major patients: cardiac iron and function comparison determined by quantitative magnetic resonance imaging. *Haematologica* **96**, 41-47 (2011).

295. S. J. Duffy *et al.*, Iron Chelation Improves Endothelial Function in Patients With Coronary Artery Disease. *Circulation* **103**, 2799-2804 (2001).

296. V. Berdoukas, K. Farmaki, S. Carson, J. Wood, T. Coates, Treating thalassemia major-related iron overload: the role of deferiprone. *J Blood Med* **3**, 119-129 (2012).

297. A. Belmont, J. L. Kwiatkowski, Deferiprone for the treatment of transfusional iron overload in thalassemia. *Expert Review of Hematology* **10**, 493-503 (2017).

298. O. Shalev *et al.*, Deferiprone (L1) chelates pathologic iron deposits from membranes of intact thalassemic and sickle red blood cells both in vitro and in vivo. (1995).

299. L. De Franceschi *et al.*, Deferiprone therapy in homozygous human β-thalassemia removes erythrocyte membrane free iron and reduces KCl cotransport activity. *Journal of Laboratory and Clinical Medicine* **133**, 64-69 (1999).

300. R. Galanello, S. Campus, Deferiprone chelation therapy for thalassemia major. *Acta haematologica* **122**, 155-164 (2009).

301. D. Pennell, J. Carpenter, M. Roughton, Z. Cabantchik, On improvement in ejection fraction with iron chelation in thalassemia major and the risk of future heart failure. *Journal of Cardiovascular Magnetic Resonance* **13**, 1-9 (2011).

302. R. R. Crichton, R. J. Ward, R. C. Hider, The Efficacy of Iron Chelators for Removing Iron from Specific Brain Regions and the Pituitary-Ironing out the Brain. *Pharmaceuticals (Basel)* **12**, (2019).

303. B. P. Esposito *et al.*, Labile plasma iron in iron overload: redox activity and susceptibility to chelation. *Blood* **102**, 2670-2677 (2003).

304. H. X. Yang, P. Wang, N. N. Wang, S. D. Li, M. H. Yang, Tongxinluo Ameliorates Myocardial Ischemia-Reperfusion Injury Mainly via Activating Parkin-Mediated Mitophagy and Downregulating Ubiquitin-Proteasome System. *Chin J Integr Med* **27**, 542-550 (2021).

305. B. Ibáñez, G. Heusch, M. Ovize, F. Van de Werf, Evolving therapies for myocardial ischemia/reperfusion injury. *J Am Coll Cardiol* **65**, 1454-1471 (2015).

306. N. K. Kapur, R. H. Karas, A new shield from the double-edged sword of reperfusion in STEMI. *Eur Heart J* **36**, 3058-3060 (2015).

307. T. Nishida *et al.*, Dual Gas Treatment With Hydrogen and Carbon Monoxide Attenuates Oxidative Stress and Protects From Renal Ischemia-Reperfusion Injury. *Transplant Proc* **50**, 250-258 (2018).

308. R. N. Bhattacharjee *et al.*, CORM-401 Reduces Ischemia Reperfusion Injury in an Ex Vivo Renal Porcine Model of the Donation After Circulatory Death. *Transplantation* **102**, 1066-1074 (2018).

309. Z. Zhou *et al.*, [Protective effects of endogenous carbon monoxide against myocardial ischemia-reperfusion injury in rats]. *Sheng Li Xue Bao* **70**, 115-122 (2018).

310. L. Zhang *et al.*, Hydrogen Sulfide (H(2)S)-Releasing Compounds: Therapeutic Potential in Cardiovascular Diseases. *Front Pharmacol* **9**, 1066 (2018).

311. L. Portal, D. Morin, R. Motterlini, B. Ghaleb, S. Pons, The CO-releasing molecule CORM-3 protects adult cardiomyocytes against hypoxia-reoxygenation by modulating pH restoration. *Eur J Pharmacol* **862**, 172636 (2019).

312. K. Magierowska *et al.*, Oxidative gastric mucosal damage induced by ischemia/reperfusion and the mechanisms of its prevention by carbon monoxide-

releasing tricarbonyldichlororuthenium (II) dimer. *Free Radic Biol Med* **145**, 198-208 (2019).

313. F. Amersi *et al.*, Ex vivo exposure to carbon monoxide prevents hepatic ischemia/reperfusion injury through p38 MAP kinase pathway. *Hepatology* **35**, 815-823 (2002).

314. Y. Akamatsu *et al.*, Heme oxygenase-1-derived carbon monoxide protects hearts from transplant associated ischemia reperfusion injury. *Faseb j* **18**, 771-772 (2004).

315. J. S. Choy *et al.*, Selective Autoretroperfusion Provides Substantial Cardioprotection in Swine: Incremental Improvements With Mild Hypothermia. *JACC Basic Transl Sci* **5**, 267-278 (2020).

316. X. Chen *et al.*, Effect of propofol on myocardial ischemia/reperfusion injury in rats through JAK/STAT signaling pathway. *Eur Rev Med Pharmacol Sci* **23**, 6330-6338 (2019).

317. X. Liu *et al.*, Heme oxygenase-1 (HO-1) inhibits postmyocardial infarct remodeling and restores ventricular function. *FASEB journal : official publication of the Federation of American Societies for Experimental Biology* **20**, 207-216 (2006).

318. R. Dash *et al.*, Dose-Dependent Cardioprotection of Moderate (32C) Versus Mild (35C) Therapeutic Hypothermia in Porcine Acute Myocardial Infarction. *JACC: Cardiovascular Interventions* **11**, 195-205 (2018).

319. K. B. Kern *et al.*, Importance of Both Early Reperfusion and Therapeutic Hypothermia in Limiting Myocardial Infarct Size Post-Cardiac Arrest in a Porcine Model. *JACC: Cardiovascular Interventions* **9**, 2403-2412 (2016).

320. M. E. Farissi *et al.*, Hypothermia for Reduction of Myocardial Reperfusion Injury in Acute Myocardial Infarction: Closing the Translational Gap. *Circulation: Cardiovascular Interventions* **14**, e010326 (2021).

321. S. M. Frank, P. Satitpunwaycha, S. R. Bruce, P. Herscovitch, D. S. Goldstein, Increased myocardial perfusion and sympathoadrenal activation during mild core hypothermia in awake humans. *Clin Sci (Lond)* **104**, 503-508 (2003).

322. P. A. Arpino, D. M. Greer, Practical Pharmacologic Aspects of Therapeutic Hypothermia After Cardiac Arrest. *Pharmacotherapy: The Journal of Human Pharmacology and Drug Therapy* **28**, 102-111 (2008).

323. N. R. Ghugre *et al.*, Hemorrhage promotes inflammation and myocardial damage following acute myocardial infarction: insights from a novel preclinical model and cardiovascular magnetic resonance. *J Cardiovasc Magn Reson* **19**, 50 (2017).

324. M. Ferré-Vallverdú *et al.*, Prognostic value and clinical predictors of intramyocardial hemorrhage measured by CMR T2* sequences in STEMI. *The International Journal of Cardiovascular Imaging* **37**, 1735-1744 (2021).

325. D. Erlinge *et al.*, Therapeutic hypothermia for the treatment of acute myocardial infarction–combined analysis of the RAPID MI-ICE and the CHILL-MI trials. *Therapeutic hypothermia and temperature management* **5**, 77-84 (2015).

326. D. R. Messroghli *et al.*, Myocardial T1 mapping: Application to patients with acute and chronic myocardial infarction. *Magnetic Resonance in Medicine* **58**, 34-40 (2007).

327. H. Bulluck *et al.*, Defining left ventricular remodeling following acute ST-segment elevation myocardial infarction using cardiovascular magnetic resonance. *Journal of Cardiovascular Magnetic Resonance* **19**, 26 (2017).

328. W. R. T. Witschey *et al.*, In vivo chronic myocardial infarction characterization by spin locked cardiovascular magnetic resonance. *Journal of Cardiovascular Magnetic Resonance* **14**, 37 (2012).

329. C. Nguyen *et al.*, In vivo contrast free chronic myocardial infarction characterization using diffusion-weighted cardiovascular magnetic resonance. *Journal of Cardiovascular Magnetic Resonance* **16**, 68 (2014).